Energy & Environmental Science

Accepted Manuscript

ROYAL SOCIETY OF CHEMISTRY

www.rsc.org/ees

Energy & Environment Science

ARTICLE

ZnO Cathode Buffer Layers for Inverted Polymer Solar Cells

Zhiqiang Liang, [a,b] Qifeng Zhang,[b] Lin Jiang [a]† and Guozhong Cao[b]†

Received 00th January 20xx,
Accepted 00th January 20xx

DOI: 10.1039/x0xx00000x

www.rsc.org/

This article provides an overview on the design, fabrication and characterization of the most widely used cathode buffer layers (CBLs) constructed with pristine zinc oxide (ZnO), doped-ZnO, and ZnO-based composites as well as the surface modified ZnO-based CBLs for the improvement of power conversion efficiency (PCE) and long-term device stability of inverted polymer solar cells (PSCs). To achieve high PCE in inverted PSCs, the selection of an appropriate material to form the high quality CBL so as to optimize the electron collection and transport is particularly important. Among the different materials for CBL in inverted PSCs, ZnO has attracted most extensive research in view of its relatively high electron mobility, optical transparency, ease synthesis with versatile morphologies via low cost solution methods at low temperatures, and being environmentally stable. The research has revealed that the electronic processes at the interface between ZnO CBL and polymer active layer play an important role in determining the solar cells performance, and such processes are related to the ZnO CBL in terms of its morphology, microstructure, doping and surface modification. This review attempts to give a general review to better understand the impacts of (1) morphology, (2) thickness, (3) nanostructures, (4) doping, (5) surface modification and (6) composition/hybrids of ZnO CBLs on the solar cells performance. The fundamental understanding of the rapid progress of interfacial engineering made in PSCs would also be beneficial to the development of perovskite solar cells due to similar energy level and device structures.

1. Introduction

Harnessing the abundant and renewable solar energy has been recognized as a promising way to address the quickly growing world's energy consumption and the increasing concerns about rapid increase in green-house gas emissions from the consumption of fossil fuel as the primary energy sources. Therefore, the solar energy utilization is currently a leading research area for a CO_2-free and renewable energy supply. Many approaches have been proposed and studied extensively to harvest solar energy including solar thermal energy, photocatalytic and photo-electrochemical water splitting, and solar cells.[1-9] Among these technologies, photovoltaic technology converting sunlight directly into electricity is considered as one of the most promising and mature technologies.[7-10] Although the silicon or other inorganic semiconductor solar cells and thin-film solar cells have been the most used solar cell system because of their advantages in high efficiency and reliability, the high cost and slow energy payback time of these solar cells have limited their wide spread applications. In recent years, polymer solar cells (PSCs) have attracted extensive investigation as a potential alternative to conventional silicon-based solar cells, mainly due to their inherent advantages of being low-cost, and compatible with flexible substrate and solution-based roll-to-roll processing technique.[8, 9, 11-14] In addition, the rapid energy payback time (EPBT) and low carbon emissions are also the major motivation for PSCs in future energy marketplace.[15, 16]

Conventional PSCs device architecture consists of a bulk-heterojunction (BHJ) active layer sandwiched between a transparent conducting electrode, such as indium tin oxide (ITO) glass, and a low-work-function metal electrode (which usually uses Al material). The BHJ active layer is achieved by a blend of the p-type polymer donor and n-type fullerene acceptor materials dissolved in common solvent, and subsequent phase segregation results in the formation of two interpenetrated percolated networks during the annealing process after spin-coating. In such active layers, only excitons formed within a distance of ~20 nm from the p-type polymer donor/n-type fullerene derivative acceptor interface can reach the interface and then dissociate into free charge carriers.[13, 17-19] The design criterion for BHJ is to maximize the donor/acceptor interfacial area to provide possibly more exciton dissociation sites and form two interpenetrated continuous charge transport pathways in each material towards the corresponding electrodes.[13, 17, 18] Another outstanding merit of BHJ-based polymer solar cells is that the composite active layer can be processed from a solution in a single step, making the fabrication of devices full compatible with the roll-to-roll processing techniques.[13, 18, 20] Thus, the concept of BHJ was considered to establish the cornerstones of polymer solar cells.[21] In recent years, significant progress

[a] Institute of Functional Nano & Soft Materials Laboratory (FUNSOM), Jiangsu Key Laboratory for Carbon-Based Functional Materials & Devices, Collaborative Innovation Center of Suzhou Nano Science and Technology, Soochow University, Suzhou, Jiangsu 215123, China.
[b] Department of Materials Science and Engineering University of Washington Seattle, WA 98195-2120, USA
† Corresponding authors: Lin Jiang and Guozhong Cao.
See DOI: 10.1039/x0xx00000x

has been achieved on the improvement of the performance of PSCs.

The state of the art power conversion efficiencies (PCEs) of single junction PSCs with conventional structure exceeding 9%,[22-24] and higher than 10%[25] for tandem PSCs have been achieved in small area devices, which promises them a bright future in commercialization.

However, in spite of high PCEs, the PSCs with conventional architecture have suffer from some drawbacks that hinder the solar cells from practical application. One of the major drawbacks for the conventional structure PSCs is the lack of long-term stability when exposed to air.[26-29] This is, on one hand, because the use of a low-work-function metal (e.g., Al) as cathode, which is sensitive to air and moisture and leads to the oxidization of the cathode quickly. On the other hand, in the conventional structure PSCs, the acidic PEDOT:PSS interfacial layer directly contacts with the ITO glass and can etch the ITO resulting in a degradation of the device performance.[26-28, 30] This has inspired the emergence of inverted structure polymer solar cells, in which the nature of charge collection is reversed.[12, 31-33] Fig. 1a is a schematic showing an inverted polymer solar cell with a stacked structure of a transparent electrode (e.g., ITO, FTO and AZO), an interfacial layer named as cathode buffer layer (CBL), a BHJ active layer, an anode buffer layer (ABL) usually made of PEDOT:PSS, and a metal electrode with high-work-function such as Ag and Au. The structure of conventional PSCs is also schematically presented in Fig. 1b for comparison. It should be noted that in literature, the CBL is also named as electron selective layer (ESL), electron collection layer (ECL) or electron transport layer (ETL), and the ABL is named as hole selective layer (HSL), hole collection layer (HCL) or hole transport layer (HTL). For the sake of clarity and ease in presentation, CBL and ABL are used in this review unless specified otherwise.

In the inverted device architecture, the contact between the ITO and PEDOT:PSS is avoided, and meanwhile Al for top electrode adopted in conventional PSCs is replaced with an air stable high-work-function metal, such as Au or Ag.[31, 34] As a result, the inverted PSCs exhibit greatly improved ambient stability as compared to the PSCs with a conventional structure (Fig. 2), overcoming one big hurdle for possible widespread application of PSCs.[32, 33, 35-38] Moreover, in the case of inverted solar cells, the high-work-function metal anode, such as Ag, can be prepared with either coating or printing technology. These technologies are compatible with all solution processing and can therefore greatly simplify the fabrication process and lower the manufacturing cost of solar cells.[39-41] Another advantage of the inverted geometry is that it possesses higher flexibility in term of the design of multi-junction or tandem solar cells compared to the conventional one.[13, 25] In addition, vertical phase separation mechanism, which describes the P3HT prone to accumulate onto the electrode top and the fullerene derivative onto the bottom, also makes the inverted device configuration more advantageous compared to the normal configuration.[21, 34, 42-44] Despite the inverted PSCs have a lot of apparent merits, one shortcoming of the inverted device geometry is that the PCE is usually inferior to those of conventional PSCs in the initial stages of the study for inverted PSCs. But the study in recent years has overturned this situation and demonstrated that inverted PSCs can possess both long-term stability and high PCEs.[25, 45-50] It has been reported that, through device engineering and a use of new polymers, the state of the art PCEs of single junction inverted PSCs exceeding 10% have been achieved in small area devices, which are comparable to and even exceed the efficiencies of conventional one.[47, 49, 51-54]

The study of the high PCE, stability and roll-to-roll process have become to three major directions in polymer solar cells.[25, 30, 55, 56] The inverted PSCs seem to be the best candidate that meets the requirements for high efficiency, good stability, low cost and being compatible with the existing roll-to-roll process.[12, 34, 55, 56]

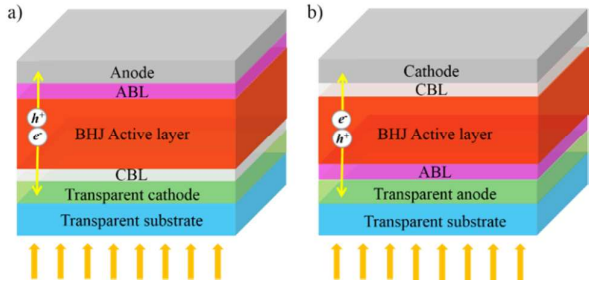

Fig. 1 Schematic illustration of device structures of (a) inverted and (b) conventional PSCs with bulk heterojunction active layer.

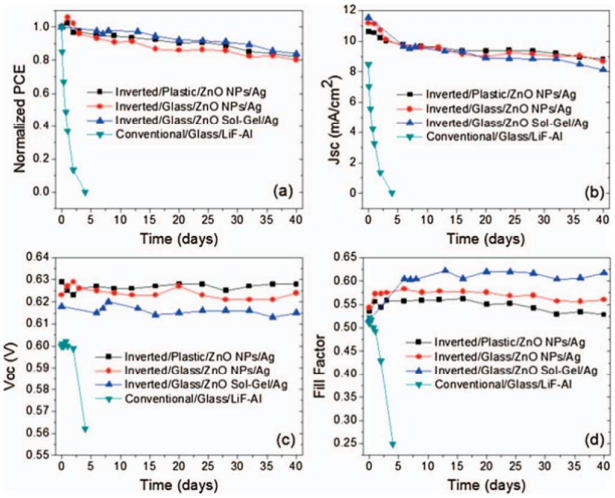

Fig. 2 Device performance of unencapsulated inverted PSCs with ZnO CBLs and conventional PSCs stored 40 days in air under ambient conditions. (a) Normalized PCE, (b) short circuit current density (J_{sc}), (c) open circuit voltage (V_{oc}), and (d) fill-factor (FF).[32]

The working mechanism of inverted PSCs can be described as the following. Under illumination, photo-generate excitons diffuse to the donor-acceptor (such as P3HT:PCBM) interface, where the excitons dissociate due to a driving force in view of the energy level difference between the donor and acceptor.

The separated electrons will diffuse through the acceptor layer and collected by CBL, and ultimately reach the cathode electrode.[37] The CBLs in inverted devices are to (1) form an electron selective and transport interlayer, (2) block the reverse holes flowing from the donor polymer to cathode, (3) adjust the energetic barrier between the active layer and the cathode, and (4) prevent the chemical or physical reaction between active layer and cathode. To achieve high power conversion efficiency in inverted polymer solar cells, the selection of an appropriate material to form the high quality CBL so as to optimize the electron collection and transport is particularly important. The key requirements for an ideal CBL include being good at electron extraction and transport, having suitable energy level that facilitates electron transport, and having high transparency, good compactness, and high stability.

Recently, the inorganic-organic organometal perovskite solar cells have emerged and acknowledged as a new promising photovoltaic technology with respect to its tremendous progress in power conversion efficiency and potentially low-cost. In the past two years, PCEs of perovskite solar cells have advanced from 15% to 19% and now exceeded 20% on the basis of both planar and mesoscopic cell configurations.[57-66] However, perovskite solar cells also face the device stability problems, and this will determine its practical applications.[57, 67-69] Similar to the polymer solar cells, it has been found that selection and modification of a suitable interface layer could substantially improve the efficiency and stability of perovskite solar cells.[68, 70-73] Therefore, the fundamental understanding of the rapid progress of interfacial engineering made in polymer solar cells would be beneficial to the development of perovskite solar cells, in addition to advance the polymer solar cell itself. Compared to the exiting photovoltaic (PV) technologies, perovskite solar cells exhibit very short energy payback time (EPBT).[74, 75] Although perovskite solar cells is the youngest number in the PV family, it may become the most environment sustainable PV technology due to its potential for high efficiency, rapid EPBT and stable performance.[74, 75]

Over the past few years, many semiconducting metal oxides (MOs) including zinc oxide (ZnO),[29, 31, 33, 37, 76, 77] zinc tin oxide (ZTO),[78] titanium sub-oxide (TiO_x),[35, 36, 79-82] aluminum oxide (Al_2O_3),[83] and niobium pentoxide (Nb_2O_5)[84] have been studied to serve as the CBL in inverted PSCs. Besides the metal oxides, several polymers, such as hydrophilic conjugated 2,7-carbazole-1,4-phenylene alternating copolymers PCP-NOH or PCP-EP,[85] cationic biopolymer poly(2-(dimethylamino)ethyl methacrylate) (PDMAEMA),[86] poly(amido amine) (PAMAM, generation 2),[86] poly(ethyleneimine) (PEI)[87] and conjugate polyelectrolyte poly [(9,9-bis(3′-(N,N-dimethylamino)propyl)-2,7-fluorene)-alt-2,7-(9,9-ioctylfluorene)] (PFN),[45, 51, 88] and PFPA1[89] have also been studied for inverted PSCs to work as efficient CBL materials. In addition, some other materials such as ZnS,[90] CdS,[91, 92] cesium carbonate (Cs_2CO_3),[93-96] $SrTiO_3$,[97] $SrTiO_3$:ZnO composite,[98] MoO_3-Al composites,[99] In_2S_3,[100, 101] ionic liquid-functionalized carbon nanoparticles (ILCNs),[102] sodium hydroxide (NaOH),[103] zwitterions,[104] amino acid (serine),[105] amino-functionalized fluorene oligomers,[106] ionic liquids (ILs),[53] and the low work function metals (such as: Al, Mg and Ca)[107] have also been investigated as CBLs in inverted PSCs. Another low work function metal, Lanthanum (La), can also serve as a cathode interlayer material for PSCs with conventional structure.[108] Graphene as a promising two-dimensional nanomaterial with outstanding electronic, optical, thermal, and mechanical properties has also been used in inverted PSCs to serve as the CBL.[109-111]

For inverted PSCs, the device performance critically relies on the sort of the CBL material and the condition of interface between the CBL and the BHJ active layer. Among the materials mentioned above, ZnO has attracted the most extensively investigated one for CBL in the inverted PSCs, mainly due to its suitable energy levels, high electron mobility, good transparency, environment stability and low cost.[13, 29, 31, 32, 37, 55, 76, 112, 113] The energy levels of ZnO (conduction band bottom and valence band top) are at around -4.4 eV and -7.8 eV, respectively. Such band positions allow ZnO to function well for electron collection and hole blocking. The relatively high electron mobility of ZnO makes it a suitable material for cathode buffer layer to reduce the charge recombination. The good transparency in the whole visible spectrum benefits lowering optical loss and the band edge cut-off of ZnO at around 375 nm can block UV light and accordingly protect the organic materials from the photo-degradation under UV light irradiation.[33, 43] For single junction inverted PSCs, the state of the art PCEs of ~10% have been achieved by using ZnO or ZnO-based CBLs.[46, 47, 49, 52, 53, 114] Another merit of ZnO as the CBL material is that it can be easily processed via a solution method with subsequent thermal treatment at relatively low temperatures. This makes the ZnO fully compatible to all solution roll-to-roll fabrication on flexible plastic substrates which is the predominant advantage of polymer solar cells.[29, 55, 115-118] Almost all of the reported inverted PSCs fabricated by roll-to-roll processing technique are based on ZnO thin layers as CBL.[40, 41, 56, 116, 119, 120] For these features and merits mentioned above, ZnO has been identified a good material to serve for the CBL in inverted PSCs.

Shirakawa *et al*. were the first group to have demonstrated the application of ZnO film as cathode interfacial layer in an organic photovoltaic cell with a stacked structure of ITO/ZnO/C60 /PAT6/Au.[17] The first inverted polymer solar cells based on a sol-gel processed ZnO thin film on ITO as the CBL and a P3HT:PCBM BHJ active layer was pioneered by White and co-workers in 2006.[31] Significant progress has been made in the past a few years in this area, with research focused mainly on the preparation method and modification of ZnO buffer layers. However, due to the use of different polymers for the construction of solar cells and different methods for the fabrication of the cathode buffer layer, it is hard to make a fair comparison of the effects of cathode buffer layer. In recent years, many papers reviewed the photovoltaic materials of active layers and electrode buffer layers, cell architectures, interfacial layers engineering, and the device operation mechanisms of polymer solar cells.[7, 8, 12-14, 19, 25, 30, 37, 44, 55, 56, 121-127] However, as one of the most extensively used CBL in

inverted PSCs, so far no paper has provided a comprehensive review on the progresses and perspectives of ZnO and ZnO based CBLs. This review article intends to fill this gap and provide a comprehensive overview on the design, fabrication, and characterization of ZnO, doped-ZnO, and ZnO-based composite CBLs as well as their surface chemistry and morphology modification for inverted PSCs. The development ZnO cathode buffer layers will make an important contribution to the fabrication of PSCs with high power conversion efficiency and long term stability at large scale for their practical applications.

2. ZnO cathode buffer layer in inverted PSCs

2.1 ZnO a good fit for CBL in inverted PSCs

In the polymer solar cells with inverted geometry, a ZnO film inserted between the BHJ active layer and cathode can function as a CBL to extract and transport electrons, and simultaneously block the reverse flow of holes from donor polymer to cathode. The good fit of ZnO as a CBL in inverted PSCs first of all originates from its suitable energy levels. Fig. 3 shows a schematic diagrams of the energy levels and the transport directions of electrons and holes in an inverted structure solar cell consisting of ZnO cathode buffer layer and P3HT: PCBM active layer. It can be seen that, on one hand, the conduction band bottom of ZnO at -4.4 eV is lower than the lowest unoccupied molecular orbital (LUMO) of fullerene derivative acceptor (for example, -3.8 eV and -3.74 eV for PCBM and ICBA, respectively), meaning that ZnO CBL can help extract and collect electrons in the fullerene derivative acceptor.[37, 128] It has been reported that the electron transport from PCBM to ZnO does not result in a significant energy loss.[31] On the other hand, the valence band top of ZnO at ~-7.8 eV is lower than the highest occupied molecular orbital (HOMO) of the polymer donor (for example, -5.0 eV for P3HT). As a result, the reverse flow of holes from the polymer donor to the ITO cathode is blocked by the great energy barrier at the P3HT/ZnO interface. This means that the ZnO CBL can prevent the generation of leakage current at the polymer/ITO interface. That is why the inverted PSCs with ZnO CBLs have been found dramatically improved photovoltaic performance compared to those without a ZnO CBL.[33, 43, 77, 129, 130]

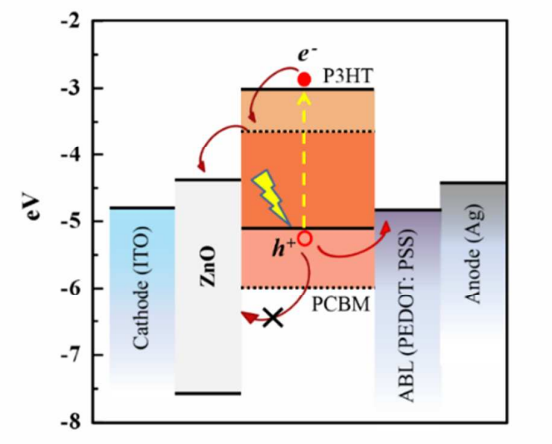

Fig. 3 Schematic illustration of the energy level and the main charge transportation of in inverted PSC with ZnO CBL and P3HT:PCBM active layer.

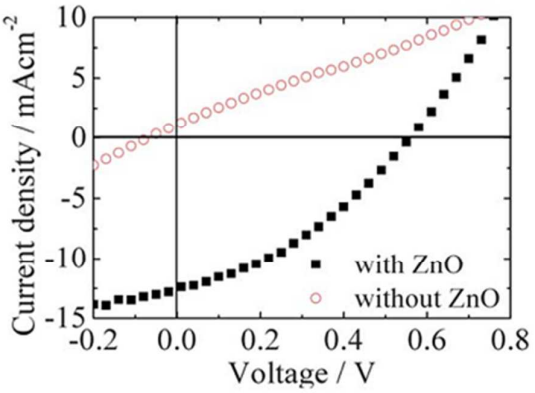

Fig. 4 The J-V curves of the inverted PSCs with and without ZnO CBL.[77]

In a study done by Liu *et al*., it was reported that the devices with and without ZnO CBL presented different shapes of the J-V curve, as shown in Fig. 4.[77] Such a difference in the J-V curve was attributed to the converse directions of charge transport, suggesting the function of ZnO CBL in transporting electrons and blocking holes.[77] Yang *et al*. have also studied inverted PSCs constructed with solution processed ZnO thin films as a CBL, PsiF-DBT:PCBM blend as BHJ active layer, a MoO_3 thin film as anode buffer layer (ABL), and an Au electrode as anode.[33] It was found that, due to the use of ZnO, the series resistance (R_S) of solar cells decreased from 56 Ω cm^2 to 13 Ω cm^2 and the shunt resistance (R_{SH}) increased from 600 Ω cm^2 to 1400 Ω cm^2 giving rise to a dramatic enhancement in the solar cell PCE, which increase from 1.67% to 3.80%. A high R_{SH} means a low current leakage or energy loss across the solar cell.[33, 131] Table 1 shows a summary of device characteristics of representative inverted PSCs with or without ZnO CBL. The values shown in brackets are obtained for the solar cells without CBL, exhibiting much lower efficiencies than those using CBL for the reason of severe charge recombination. These results are great

evidence that the ZnO films can efficiently work as a hole-blocking layer to prevent the current leakage.

2.2 Fabrication for ZnO cathode buffer layer

The performance of inverted PSCs can be significantly affected by the method used for the preparation of ZnO CBL, which influences the morphology, thickness, crystallinity, and the optical and electrical properties of the resulting CBL. Various methods have been employed for the fabrication of ZnO thin films to serve as the CBL in inverted PSCs. In general, the fabrication methods for ZnO CBLs can be grouped to: (1) solution processing, mostly sol-gel method,[29, 31, 33, 76, 132-143] (2) solution method derived from pre-fabricated ZnO NPs suspensions or aqueous ZnO hydrate,[32, 77, 119, 144-147] (3) atomic layer deposition (ALD),[129, 148-152] (4) spray pyrolysis,[43, 153, 154] (5) metal organic chemical vapor deposition (MOCVD),[155] (6) mist pyrolysis chemical vapor deposition (MPCVD),[156] (7) radio-frequency sputtering (RF),[157] (8) magnetron sputtering,[158, 159] (9) fine-channel mist-spray coating,[160] (10) chemical bath deposition (CBD),[161] and (11) electro-deposition (ED)[43]. Among these methods, the solution processing and deposition methods have been the most popular way to make ZnO CBLs for inverted PCSs, due to its high-quality, ease of preparation at relatively low temperature, without requiring any vacuum instrument and low cost.

2.2.1 ZnO CBLs fabricated with sol-gel processing

Sol-gel method through the use of a mixture of zinc acetate [$Zn(OAC)_2$] and 2-ethanolamine in methoxyethanol (MEA) as precursors is a widely used approach for the fabrication of ZnO CBL for inverted PSCs. ZnO thin films created with this method present good surface quality, excellent optical transmittances and electrical properties. Moreover, this is a low-cost process that doesn't involve any expensive and/or vacuum instruments.[29, 132, 162] In addition, the features of low temperature and solution processing make the sol-gel method compatible to roll-to-roll manufacturing for the fabrication of inverted PSCs on flexible plastic substrates, which is one of the important advantage of PSCs.[29, 55, 115]

Table 1. Non exhaustive survey of inverted PSCs with or without ZnO CBLs. The photovoltaic parameters are compared to those measured for a reference cell (values in parentheses) without the ZnO CBLs.

Device architecture	J_{sc} [mA cm^{-2}]	V_{oc} [V]	FF [%]	PCE [%]	Ref.
ITO/ZnO/P3HT:PsiF-DBT/MoO_3/Au	5.03 (4.23)	0.90 (0.81)	60 (39)	3.80 (1.67)	33
ITO/ZnO (SP)/P3HT:PCBM/WO_x/Al	10.03 (8.91)	0.48 (0.41)	53 (50)	2.56 (1.76)	43
ITO/ZnO (ED)/P3HT:PCBM/WO_x/Al	10.08 (8.91)	0.55 (0.41)	66 (50)	4.00 (1.76)	43
ITO/ZnO/P3HT:PCBM/MoO_3/Ag	11.9 (8.5)	0.59 (0.33)	0.6 (0.31)	4.18 (0.57)	129
ITO/ZnO/P3HT:PCBM/MoO_3/Au	12.05 (10.9)	0.59 (0.40)	49.8 (39.8)	3.54 (1.74)	157
ITO/ZnO/P3HT:PCBM/PEDOT:PSS/Ag	8.41 (6.86)	5.65 (4.26)	53.9 (29.2)	2.56 (0.85)	163
ITO/ZnO/PCDTBT12:$PC_{71}BM$/MoO_3/Al	9.78 (9.57)	0.98 (0.59)	57.7 (46.4)	5.53 (2.62)	130
ITO/ZnO/PTB7:PC71BM/MoO_x/Ag	14.64 (16.16)	0.75 (0.48)	64.75 (45.27)	7.11 (3.48)	48

In the sol-gel method, the post heat treatment processing is adopted to convert the spin-coated gel film to crystalline ZnO and is a factor which can significantly affect the optical and electrical property of ZnO films as well as the photovoltaic performance of the inverted PSCs. Firstly, the heat treatment temperature is required to be higher than the boiling points of the solvents (2-methoxyethanol and MEA at 125 °C and 170°C, respectively) to get the solvents completely evaporated.[162, 164] Secondly, it has been demonstrated that, when heated in air, the $Zn(OAC)_2$ begin to thermal decompose at 190 °C, its thermal decomposition completed at around 310 °C, and the formation of crystalline ZnO at the temperature between 300 °C and 400 °C. A higher annealing temperature ranging from 400-500 °C is identified as the most efficient temperature for the thermal decomposition of $Zn(OAC)_2$ to form crystalline ZnO.[165]

The electron mobility of sol-gel processed ZnO films as well as the device performance of inverted PSCs based on these ZnO films as the CBL would be promoted by improving the crystallinity of ZnO. However, there have been conflicting reports of the optimized annealing temperature of sol-gel processed ZnO CBLs for inverted PSCs in the literature.[29, 33, 38, 137, 143, 166, 167] The optimal annealing temperature reported in the literature range from 100 °C to 450 °C.[26, 30, 35, 134, 140, 161, 162] Zhang *et al*. reported that the inverted PSCs using sol-gel processed ZnO CBLs exhibit a clear improvement in the device performance with increasing the ZnO sintering temperature from 100 °C to 350 °C.[137] It was observed that the R_S of the inverted devices decreased with an increased sintering temperature and it reached a minimal value when the sintering temperature increased from 100 °C to 350 °C, as a result an improved device performance (PCE = 2.58%) was

achieved. Such a performance improvement was ascribed to the improved ZnO quality in view of a relatively high sintering temperature, which effectively promoted the electron mobility of sol-gel processed ZnO films by improving the crystallization of ZnO. However, the need of high annealing temperature above 300 °C hampers the advantage of PSCs compatible with flexible substrates, such as polyethylene terephthalate (PET), which usually cannot withstand a high temperature treatment process. Additionally, the high annealing temperature processes will also lead to the degradation of the conductivity of cathode (i.e., ITO) and thus degrades the device performance.[137, 167]

In order to overcome these constraints, the sol-gel derived ZnO CBLs annealed at relatively low temperature have been studied.[29, 33, 38, 137, 167] Sun *et al*. fabricated sol-gel derived ZnO CBLs obtained at the temperatures of 130 °C, 150 °C and 200 °C.[29] They found that the ZnO films annealed at 200 °C were able to function as an efficient electron transporting layer in inverted solar cells, leading to a PCE as high as of 6.33% for the inverted devices constructed with PCDTBT:$PC_{70}BM$ active layer. In addition, the inverted devices based on those low temperatures (130 °C, 150°C and 200 °C) annealed ZnO buffer layers exhibit a promising long-term stability. For example, the PCEs retains above 70% of its original value even after being exposed to air at room temperature for more than 30 days (without encapsulation).[29] In sharp contrast, for the unencapsulated solar cells with PCDTBT:$PC_{70}BM$ active layer and in the conventional structure, the PCE decreases significantly under same conditions.[29]

Some research revealed that the ZnO films annealed at 200 °C was amorphous instead of crystalline, and as a result their electron transporting property (~$1.3 \times 10^{-4} – 2.6 \times 10^{-5}$ $cm^2 V^{-1} s^{-1}$) is not as good as that of the crystalline ZnO (~1 $cm^2 V^{-1} s^{-1}$).[33, 38, 143] However, it seems because the electron mobility of this amorphous ZnO is comparable to that of most organic materials for PSCs, the device performance is not apparently affected by the relatively poor conduction of amorphous ZnO.[33] Through using the low temperature annealed amorphous ZnO CBL and PTB7-F20/$PC_{71}BM$ blends active layer, Park *et al*. prepared inverted PSCs and reached a J_{sc} of 13.93 mA cm^{-2}, a V_{oc} of 0.71 V, a FF of 0.65, and a PCE of 6.42%, plus long term stability.[143] Recently, Jagadamma *et al*. reported the use of sol-gel driven amorphous ZnO CBL annealed at a lower temperature (~100 °C) for inverted PSCs to minimize the degradation to flexible plastic substrates.[140] They demonstrated that the sol-gel driven amorphous ZnO layers annealed at such a low temperature delivered the solar cell performance comparable to the best devices based on ZnO films prepared at substantially higher temperature. In their results, the inverted PSCs based on this amorphous ZnO CBLs and constructed with low band-gap polymer donors on glass/flexible PET substrates show performances of: PTB7:$PC_{71}BM$ (PCE: 6.5% (glass)/5.6% (PET)) and PBDTTPD:$PC_{71}BM$ (PCE: 6.7% (glass)/5.9% (PET)).[140] More recently, Morvillo *et al*. investigated the performance of the inverted PSCs based on the sol-gel deposited ZnO CBLs annealed at different temperatures (100, 150, 200, 250 and 300 °C) for 5 or 10 min.[167] They found that the sheet resistance of the ITO increased linearly with the increasing of annealing temperatures and times, which, in turn, contributes to the reduction of the FF and the PCE of the corresponding devices. As a result, the highest PCE (7%) was achieved for the device fabricated using a ZnO CBL annealed at 150 °C for only 5 min. Therefore, recently, most of the sol-gel processed ZnO CBLs adopted heat treatment at a relative low temperature (< 200 °C) due to the comparable performance and compatible with the solution processing technique of inverted PSCs fabricated on flexible substrates.

During the post annealing process, the annealing environment, such as humidity and vacuum, can also affect the electrical property of ZnO CBL to some extent.[168] Lin *et al*. found that a thermal treatment (150 °C) of the solution processed ZnO CBLs in vacuum could help further reduce the defects and increase the electron mobility in the low temperature processed ZnO film (up to 0.36 $cm^2V^{-1}S^{-1}$), and thus improve the electron extraction in inverted PSCs.[168] Besides the annealing temperature and annealing environment, the concentration of ZnO precursor is another key factor largely affecting the quality on ZnO CBLs derived from a sol-gel route. In general, a relatively low sol concentration (~0.1-0.3 M) is more prone to lead to a ZnO film with high quality, reflecting on denser film, lower surface roughness, and higher transmittance.[38, 132, 137, 168] This is because a low sol concentration can form small nano-sized ZnO colloids and small grain sizes. As result, the inverted devices based on the dense ZnO CBLs exhibit a low reverse current and contact resistance between the ZnO layer and active layer owing to the full coverage of ITO surface and intimate contact between the ZnO and active layer, and as a result the overall R_S is reduced, giving rise to enhanced photovoltaic performance.[132, 137] On the contrary, a relatively high sol concentration (~0.5-0.75 M) is usually prone to result in a ZnO film with larger surface roughness and even voids. The rough surface and the existence of voids in ZnO buffer layers would result in an increase in the R_S, due to the inferior contact between the ZnO buffer layer and photoactive layer.[37, 132, 137] However, it has also been demonstrated that ZnO buffer layers having both dense and smooth surface and large surface area could be obtained by using a slow ramp annealing method to heat treat the wet gel film derived from ZnO sol with relatively high concentrations (i.e., 0.75 M).[138, 139] It was explained that a low heating rate in the ramp annealing process provided sufficient time for the gel particles to structurally relax and pile up, resulting in a dense and undulated film.[138, 139] More recently, it was reported that the type of ZnO precursor could also affect the property of the sol-gel processed ZnO CBL, and thus impact on the device efficiency and stability.[169] It has been reported that the inverted PSCs with ZnO layers derived from diethylzinc are more stable than the devices with ZnO layers prepared by decomposing zinc acetate under long term illumination.[169] The difference in device stability was attributed to the different chemical nature of ZnO surfaces, specifically the presence of interstitial zinc (Zn_i) defects at ZnO surface and their

subsequent interactions with the adjacent active layer. It was explained that the ZnO layers derived from diethylzinc (deZn) possessed less Zni defects than the ZnO layers deposited from zinc acetate ($Zn(OAC)_2$).[169] Overall, to achieve a high quality ZnO CBL with the solution processed sol-gel method, the type of ZnO precursor as well as the concentration, and the post heat treatment temperature and environment should be considered comprehensively.

2.2.2 ZnO CBLs derived from pre-fabricated ZnO nanoparticles suspensions or aqueous ZnO hydrate

Besides sol-gel method, another widely used solution processing method to deposit ZnO CBLs is spin-coating the pre-fabricated the ZnO nanoparticle (NP) suspensions or colloids, synthesized using a hydrolysis and condensation of zinc acetate dihydrate under low temperature.[12, 32, 77, 119, 144-147, 170] The resulting ZnO NPs demonstrated a good electron mobility (~0.066 cm^2 V^{-1} s^{-1}) even through no additional post-thermal treatment applied.[171] Hau *et al*. prepared ZnO NPs CBLs (50 nm in thickness) with dense and homogenous surface (Fig. 5) by spin-coating pre-fabricated colloidal ZnO NPs.[12, 32] They found that the inverted devices with the ZnO NPs CBL exhibited performance comparable to that of devices based on sol-gel processed dense ZnO CBL treated at high temperature (400 °C). Qin *et al*. found that there were a large number of hydroxyl (-OH) groups formed on the ZnO NPs synthesized by hydrolysis and condensation of zinc acetate dehydrate.[147] It was suggested that the surface hydroxyl groups could depredate the photoactive layer by elevating photocatalytic activity of ZnO, and hence deteriorate the device performance. Fortunately, the hydroxyl groups could be effectively detached from the ZnO NPs by annealing at a low temperature, ~150 °C.[147] The low temperature treatment and the scalable processing capability make the colloidal ZnO NPs well compatible with the solution processing technique for inverted PSCs fabricated on flexible substrates. Krebs *et al*. has successfully employed the solution processed ZnO NPs layers as CBLs for full roll-to-roll printing process to manufacture inverted PSCs with large scale.[41, 116] Recently, Spyropoulos and co-workers reported the fabrication of flexible organic tandem solar modules with PCE as high as of ~6% by using ZnO NP CBL combined high throughput roll-to-roll compatible processing.[120]

However, the ZnO NPs in suspension are not very stable and are sensitive to the moisture. Therefore, an appropriate ligand is usually required to be attached onto the NPs to stabilize them to avoid the NPs from aggregating. To prevent the aggregation of ZnO NPs and to fabricate ZnO film with a smooth surface are important for the achievement of high performance inverted PSCs.[108, 132-134, 172] Therefore, a major challenge of this method is to achieve spatial distribution of individual NPs and gain high electron mobility without high temperature annealing process.[173-175] The improvement of spatial distribution of ZnO NPs by using polymeric or organic molecules as a matrix/surfactant has been reported by several groups.[145, 173-175] However, it should be noted that the removal of surfactant material form ZnO film is required to optimize the property of ZnO CBLs as well as the device performance, due to the fact that surfactant materials may reduce the electron transport by introducing additional resistance.[173, 174] Besides the surfactant, the solvent of ZnO NP solution also plays an important role in the ZnO NP dispersion and the morphology of ZnO NPs film. Li *et al*. reported the study of the control of ZnO NP aggregations in solution by adjusting the solvent ratio (chloroform vs methanol).[172] They found that when the ratio of chloroform: methanol was 1:1 (V/V), the superior dispersity of ZnO NPs in solution and a consequent ZnO film with compact and homogeneous surface could be obtained. As a result, a remarkable PCE of 8.54% in inverted PSCs based on PTB7:$PC_{71}BM$ active layer was achieved. Besides the use of colloidal ZnO NPs, Chen *et al*. achieved ultrathin (~4 nm) ZnO CBLs by spin coating an aqueous zinc oxide hydrate ($ZnO\text{-}xH_2O$) solution.[176] They demonstrated that a post annealing temperature can be as low as 80 °C due to the low energy metal-ammine dissociation and hydroxide condensation/ dehydration chemistry. The inverted devices with the ultrathin ZnO CBLs and PCDTBT: $PC_{71}BM$ photoactive layers show a high PCE, up to 6.48 %, which is comparable to those devices based on ZnO CBLs deposited by sol-gel process using zinc acetate and annealed at 200 °C.[176]

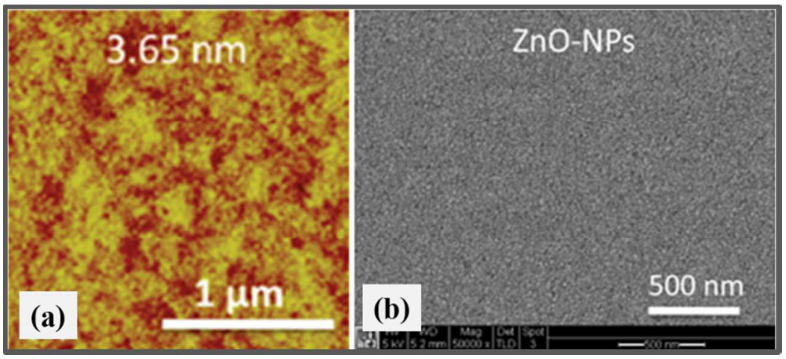

Fig. 5 (a) AFM and (b) SEM images of ZnO NPs thin films.[170]

2.2.3 ZnO CBLs fabricated by atomic layer deposition method

Besides the above-mentioned solution approaches, there are several other methods for the fabrication of ZnO CBLs, including atomic layer deposition (ALD), [129, 149-151] spray pyrolysis,[43, 153, 154] metal organic chemical vapor deposition (MOCVD),[155] mist pyrolysis chemical vapor deposition (MPCVD),[156] radio-frequency sputtering (RF),[157] magnetron sputtering,[158, 159] fine-channel mist-spray coating.[160] Among these methods, the ALD technique is regarded as a very promising approach to fabricate the ZnO CBLs for inverted PSCs in view of the capability of ALD in producing high surface quality film at relatively low temperature and controlling the film thickness precisely.[149]

Wang *et al*. deposited the ZnO CBL on the plastic substrate, ITO/PEN, by ALD method at low temperatures (45 °C and 80 °C) for flexible inverted PSCs.[129] They found that the devices with ZnO grown at 80 °C presented enhanced photovoltaic performance compared to the devices with ZnO grown at 45 °C, for the reason that the former achieved a smoother and more hydrophobic surface than the latter. The authors suggested that the smoother and more hydrophobic surface of ZnO was beneficial to the contact quality between the ZnO and active layer, thus leading to reduced series resistance and improved electron transport to the ITO electrode. It is worthy pointing out that, besides the morphology, the ALD temperature also affects the electrical properties of the grown ZnO films.[177] Chang and Tsai found that both the electron mobility and electron concentration of the ZnO CBL increased with increasing deposition temperature for the reason of increased crystallinity.[150] In their results, the best inverted device was achieved by using a ZnO CBL (60 nm in thickness) deposited at 90 °C exhibited PCE of 4.1%, high R_{SH}, and low R_S[150] An atmospheric atomic layer deposition (AALD) method was also developed to grown ZnO thin layer in atmospheric ambient to avoid the slow and vacuum-based process in conventional ALD.[151] It has been demonstrated that the AALD ZnO layers possessed compact surface, high electron mobility (3.4 ± 0.1 cm^2 Vs^{-1}) and good transmittance to visible light. As a result, the inverted BHJ P3HT:PCBM PSCs with AALD ZnO CBLs exhibited a PCE of 3.6% and good device stability in air. Compared with the conventional ALD route, such an AALD method allows the ZnO layer to be deposited more rapidly in air, and thus has higher potential for implementing in a throughput roll-to-roll process.

2.3 The impacts of the morphology of ZnO CBL on the performance of inverted PSCs

The photovoltaic performance of the inverted PSCs depends critically on the electrical property of the interface between ZnO CBL and active layer. The condition of interface is largely related to the contact quality and the contact area.[13, 37, 132, 178] Therefore, control of the morphology of ZnO CBL is an important aspect to tune the contact quality so as to achieve the full potential of inverted PSCs.

In a work performed by Liang *et al*.,[132] ZnO CBL was prepared with a sol-gel method and its morphology was controlled through adjusting the concentration of precursor sol. Fig. 6a through 6f exemplify the morphology change when the concentration of precursor sol changes from 0.05 to 1 M. The PCE of 3.3% was obtained for the device with P3HT:PCBM active layer and based on a dense and homogenous ZnO film driven from 0.1 M sol (Fig. 6c); such an efficiency is 32% higher than that for the device made with a rough ZnO film derive from a 1 M sol. The PCE enhancement arises from the higher FF while J_{sc} only increases slightly and the V_{oc} remains almost unchanged. R_S, series resistance, was found to increase with increasing the surface roughness and the content of voids in ZnO film. According to these experimental observations, Liang *et al*. suggested that the dense ZnO CBL with homogenous surface allowed the formation of an intimate contact between the ZnO CBL and the BHJ photoactive layer, however a rough surface including voids led to inferior contact and an increase in the contact resistance.[132] In addition, the uniform coverage of ZnO CBL derive from 0.1 M sol is crucial to separating the ITO cathode from contacting with the active layer, and blocking the reverse flow of holes from active layer to ITO electrode. These results demonstrated that the ZnO layer with dense and homogenous surface benefited to establishing a better contact between the ZnO and the active layer, resulting in the low R_S of the device.

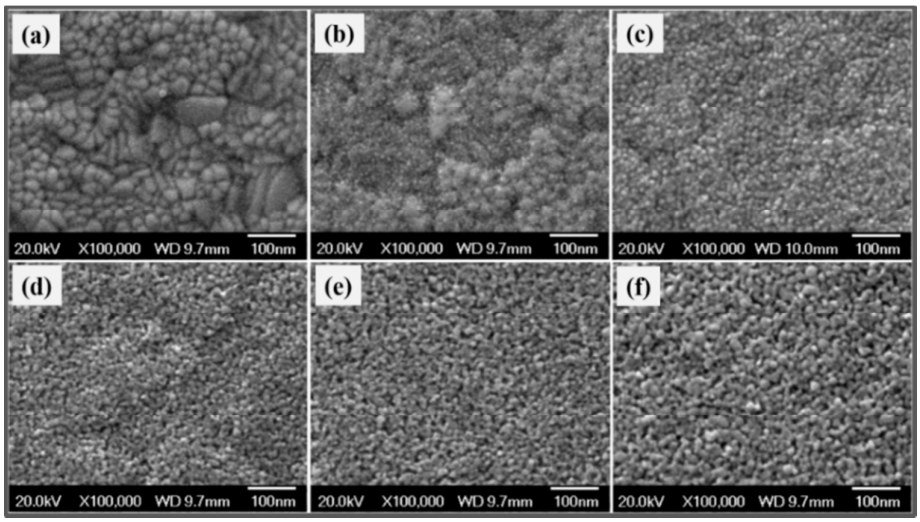

Fig. 6 The SEM images of ZnO layers derived from sol concentrations of (a) 0.02, (b) 0.05, (c) 0.1, (d) 0.3, (e) 0.6, and (f) 1 M, respectively.[132]

Besides the compactness, the surface area of ZnO CBL, which is mainly determined by the morphology, is another important issue that impacts the device performance by affecting the interfacial area between the CBL and active layer and therefore affecting the electron collection efficiency.[43, 138, 139, 152] Sekine *et al*. firstly reported the use of a unique nano-ridge (also named as nano-ripple) ZnO films having both large surface area and dense surface in inverted PSCs to serve as a CBL (Fig. 7a).[139] By adopting sol-gel processing and using a ramp annealing method at a rate of 50 °C/min from room temperature to 275 °C, they fabricated the nano-ridge of ZnO films with peak height around 120 nm and valley to valley distance of about 500 nm, as shown in Fig. 7b and 7c.[139] It was suggested that the low heating rate of the ramp annealing method provided sufficient time for the gel particles to structurally relax and pile up, resulting in a dense and undulated film.[139] In their results, the inverted solar cells fabricated based on nano-ridge films showed an average PCE of 3.87 %, while the devices with planar films only showed an efficiency of 3.06%. The enhancement was concluded to low leakage current due to the improvement in the electron collection efficiency and hole blocking capability of the nano-ridge film, resulting in higher FF, while the V_{oc} and J_{sc} were found to remain almost unchanged. The better charge extraction was thought to result from the large surface area of the ZnO nano-ridge film, which makes the device possess large ZnO/BHJ active layer interfacial area for electron collection and shortens the travelling distance of charges. Meanwhile, the ZnO nano-ridge film is also very dense, making it effective in blocking the hole from transporting from active layer to ITO cathode, and thus reducing the charge recombination and leading to a low leakage current.

To meet the full potential of ZnO nano-ripple CBLs for high performance inverted PSCs, the ripple size and density should be controlled. By adding ZnO nanoparticles in zinc acetate solutions and using a ramp annealing method, Lim *et al*. prepared ZnO nano-ripple films with controlled ripple size and density (Fig. 8).[138] It has been found that the surface structure of ZnO nanoripples with ~70 nm high nanoripples gives the highest PCE ~3.2%. They demonstrated that the homogenous surface and a higher contact area between ZnO and active layer contributed to the enhanced photovoltaic performance of the inverted PSC. Besides adding ZnO NPs, it has been found that the ripple morphology can also be tuned via controlling the concentration of the $Zn(OAC)_2$ sol-gel solution, annealing ramp rate, and the spin-coating parameters.[140, 143, 179-181] This is because the surface morphology of the sol-gel derived ZnO thin films depends largely on the solvent drying kinetics.[143]

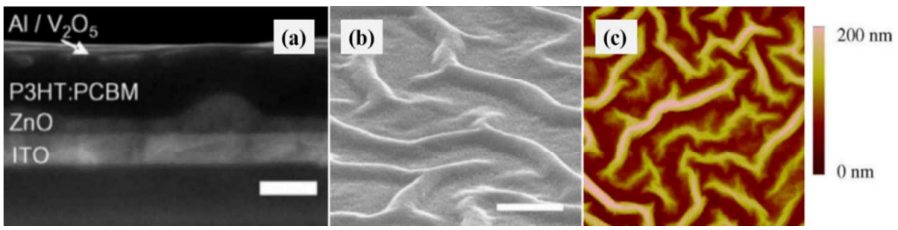

Fig. 7 (a) Cross sectional SEM image of the inverted PSC, scale bar: 200 nm and (b) SEM image of ZnO nano-ridge film, scale bar: 500 nm, and (c) AFM image of ZnO nano-ridge film showing a 5 um × 5 um surface area.[139]

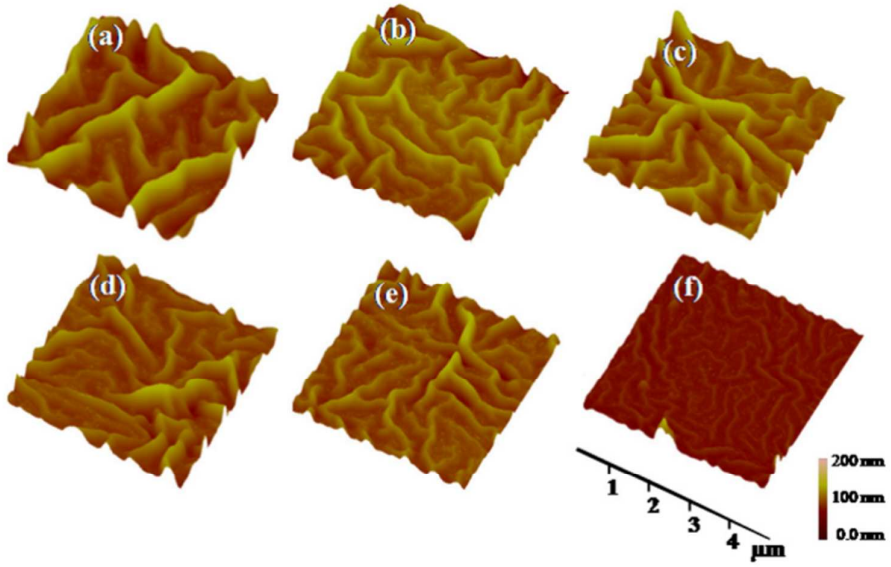

Fig. 8 AFM images of (a) ZnO layer was spin-coated using bare zinc sol. (b-f) ZnO layers were spin-coated using mixtures of ZnO nanoparticles and ZnO sol. Amount of ZnO nanoparticles added to 21 ml of ZnO sol was 0.25, 1, 3, 5 and 10 mg ZnO NPs for b-f, respectively. All of the ZnO layers were heated to 350 °C with a heating rate of 23 °C/min.[138]

Although many reports demonstrated that the ripple morphology of ZnO CBLs could result in a high contact area between the ZnO and active layer and thus enhanced the solar cell performance, there are some other reports show that the ripple ZnO CBLs with a large surface area however harm the device performance compared to the smooth ZnO layers.[140, 180] Ma *et al*. reported that nano-ripple ZnO CBLs with a high surface roughness could lead to high surface energy and a small donor/acceptor (D/A) interfacial area in the active layer deposited on the top of ZnO CBLs, and thus lower the J_{sc}.[180] In addition, it has been suggested that the large surface area of ZnO CBLs could also result in more trap-assisted recombination at the active layer/ZnO interface compared to the case of smooth ZnO CBL, and accordingly reduces the FF of solar cell. As a result, the best inverted PSCs was produced with the smoothest ZnO layer which gives the largest D/A interfacial area, and lowest ZnO/active layer interfacial area.[180] The different or even contrary effect of the large surface area of nano-ripple ZnO CBLs on the device performance may because the dominant factors influencing on the device performance, such as surface area, surface energy and surface defect, are different in different researches. Therefore, to fully achieve the potential of the nano-ripple ZnO CBLs possessing a large surface area, the surface defects of the nano-ripple ZnO should be passivated and the surface energy should be optimized.

Besides the 3 D ZnO nano-ridge films, there are several other ZnO films with large surface area fabricated to serve as CBL in inverted PSCs. Schumann *et al*. reported the preparation of ZnO CBLs using spry-pyrolysis (SP) and electro-deposition (ED) methods achieved different surface morphologies.[43] In their work, interfacial area between the ZnO and BHJ active layer was adjusted by controlling the surface roughness of ZnO CBL. They demonstrated that the J_{sc} increased with increasing the ZnO/BHJ active layer contact area which provided larger interface for electron extraction and transport. It should be noted that, in Schumann' work, the gaps in ZnO films seem to be wide enough and allow the blend of polymer/fullerene to infiltrate easily and thus obtain an intimated contact. Shin *et al*. fabricated ZnO CBL with large surface area by utilizing a mist pyrolysis chemical vapor deposition (MPCVD) method at a low temperature of 180 °C.[156] It was also demonstrated that a large ZnO CBL surface area might enlarge the interfacial area between the active layer and ZnO CBL, leading to an effective increase in the number of electrons transferred from the active layer to the ZnO CBL. From these reports, we can conclude that the morphology of ZnO CBL for inverted PSCs should meet the following requirements: (i) having dense and homogenous surface, (ii) being able to provide large surface area, and (iii) allowing the polymers to well contact with ZnO layer.

2.4 The effects of thickness of ZnO CBL on the performance of inverted PSCs

The thickness of ZnO CBL can affect the device performance by changing the optical transmittance, electrical conduction, and even work function of CBL, and thus impose a profound impact on the photovoltaic performance of the inverted PSCs. Stubhan *et al*. reported that increasing the thickness of ZnO CBLs from 30 to 126 nm could result in a drop of solar cell PCE from 2.5% to 1.5%.[163] It was explained that the efficiency decrease arose from the low conduction of thick ZnO CBL, which resulted in an increase of the series resistance (R_S) from 1 Ω cm^2 to 3.2 Ω cm^2. Cheun *et al*. have also studied the effects of the thickness of ZnO CBL by varying the thicknesses from 0.1

to 100 nm using an atomic layer deposition (ALD) technique.[149] They demonstrated that the device performance strongly depended on the thickness of ZnO CBL and there was a critical value for the thickness, which was around 10 nm. For ZnO CBL with thickness below this critical value the device demonstrated poor performance and the current–voltage (J–V) curves presented an "s-shaped" kink. For devices with ZnO layers from 10 nm and up to 100 nm in thickness, the "S-shaped" kink completely disappeared, and the thickness difference of ZnO CBL only caused a little variation in the PCE and FF. Such a "S-shaped" J-V curve was suggested to be a result of the low conductivity of such an ultra-thin ZnO layers, which had large surface-to-bulk ratio and might cause considerable defects at grain boundaries; these defects act as electron traps reducing the electrical conduction of the CBL.[41, 149] Recently, a number of studies have ascribed the low conductivity of ZnO layers to the presence of oxygen at the grain boundaries or surface.[41, 128, 182, 183] Similar phenomenon of "S-shaped" kink in J-V curve in inverted devices with ultrathin ZnO CBL (several nanometers) has been also found in Liang's[132] and Sharma's[180] work. In addition, the film thickness and the preparation method are two main factors affecting the coverage of ZnO buffer layer. A full and conformal coverage of ZnO layer is crucial to separate the cathode from the active layer, and block the reverse flow of holes from active layer to cathode.[132, 140, 184, 185] For the ZnO buffer layer derived from sol-gel method, it has been found that a very thin ZnO layer (a few nanometers in thickness) is difficult to achieve a full coverage on the ITO surface, and thus leaving a portion of uncovered ITO in direct contact with the active layer forming current leakage pathways.[132, 140, 185] Therefore, for ZnO buffer layers derived from sol-gel method, a certain thickness (around ten nanometres) is necessary to obtain a full coverage on cathode.

Cheun *et al*. found that, when the thickness of ZnO layers increased form 10 nm to 100 nm, similar grain sizes and surface morphology were observed, resulting in little variation in the device performance.[149] More recently, Hu *et al*. fabricated ZnO CBLs with varying thicknesses (from 0 to 1500 nm) and different surface morphology and work function.[155] They found that, when using a P3HT:PCBM active layer, the optimized inverted device with ZnO thickness of 80 nm showed a PCE of 2.93% using a P3HT:PCBM active layer. Based on the UPS spectra, Loser *et al*. found that both the valence band (VB) and conduction band (CB) shifted slightly when the thickness of ZnO layer increased from 3.0 to 42 nm.[186] In their results, the device performance only slightly varies as the ZnO thickness changes. Overall, a few tens of nanometers of ZnO layer is suitable to obtain uniform and dense surface so as to fully cover the cathode surface and completely separate the cathode from contacting with active layer and thus blocking the reverse hole flow, while not harm its electrical properties, transmittance, and mechanical robustness. It has been demonstrated that the inverted PSCs with different thickness of ZnO CBLs exhibit good long-term device stability, which is much better than that of the inverted PSCs without ZnO CBLs as well as that of various conventional PSCs.[38]

Transmittance of CBL is another important factor that affects the device performance by influencing the light harvest of the BHJ photoactive layer.[76, 132, 135, 156] In order to obtain a high device performance, the light absorption of active layer should be maximized. In inverted PSCs, incident light comes from the transparent cathode side (i.e., ITO or FTO) where the CBL was prepared on. Therefore, CBL with high transmittance in visible region is important in order to make the active layer gain high optical absorption of active layer. The transmittance of ZnO films not only depends on the film thickness, but is also affected by the crystal size, defects and crystallinity, which are related to the preparation methods and post-treatment parameters.[187-189] High quality ZnO thin films possess an excellent transparency in the whole visible range and give rise to minimize optical losses. Through an optimization of the heat treatment process, Liang *et al*. fabricated high transparent ZnO layers on ITO cathode with the thickness ranging from several nm to ~55 nm using a sol-gel process.[132] They found that the transmittance of ITO/ZnO layers increased with increasing the ZnO thickness, and is even higher than the bare ITO when the ZnO thickness is over 10 nm (Fig. 9). The transmittance enhancement of ITO/ZnO layers was attributed to the antireflection effects caused by the ZnO coating on the surface of the ITO substrates, originating from the good transparency and appropriate refractive index (n ~2) of ZnO film.[38, 141, 190] Therefore, the high transmittances of the ITO/ZnO layers will certainly benefits to the light absorption of active layer in inverted PSCs. In addition, in Fig. 9, it can be seen that the sharp absorption edge of the transmittance spectra of ZnO modified ITO exhibits a gradual red shift toward ~380 nm (corresponding to energy gap, ~3.2 eV of ZnO) with increasing the ZnO film thickness.[132, 141, 142] The band edge cut-off of ZnO at ~380 nm can help to block the UV light and thus protect the organic materials from the photo-degradation induced by UV light.[33, 43]

In Liang's work, a new parameter, "relative optical transmittance" (T_R), was put forward to quantify the overall effect of the transmittance of ZnO CBLs on the optical absorption of the given photoactive layer in inverted PSCs. The T_R were calculated using the following formula:[132]

$$T_R = \frac{\int_{\lambda_2}^{\lambda_1} \mathrm{I}_\lambda t_\lambda d\lambda}{\int_{\lambda_2}^{\lambda_1} \mathrm{I}_\lambda d\lambda}$$

Where t_λ is the measured transmittance spectra of ITO/ZnO buffer layer at λ wavelength, I_λ is the measured absorption spectra intensity of active layer at λ wavelength, the $\lambda_1 \sim \lambda_2$ is the measurement arrange, usually corresponding to 300 ~900 nm.

According to the definition of "relative optical transmittance", the T_R reflects the influence of ZnO CBL transmittance on the optical-absorption of active layer. The higher T_R means less optical loss and higher optical-absorption of photo-active layer, leading to the better device performance. In Liang's work, although the transmittance of ITO/ZnO CBLs decreased at UV and increased at the

wavelength around 450 nm with increasing the thickness of ZnO films, the calculated T_R presented very small variation.[132] This indicates that the change of the transmittance of ZnO CBL in their work just makes a negligible impact on the light harvest of photo-active layer and device performance. In other words, the light harvest and the device performance are only affected when there is an obvious change in the transmittance of ZnO CBLs. Kyaw *et al*. reported that the improvement in optical transmittance of ZnO CBLs led to an increase in the J_{sc} of devices from 5.986 to 8.858 mA cm^{-2} without sacrificing the V_{oc} and FF of the solar cell.[76] Recently, it has been demonstrated that the light-absorption of active layer can also be enhanced by ZnO nano-ripple structure due to its good light-scattering property, which contribute to increasing the J_{sc} of device.[179, 191, 192] From these results, we can see that the charge extraction at the ZnO/active layer interface and the photovoltaic performance of the inverted devices are a combined effect relating to both the thickness and morphology of ZnO layer.

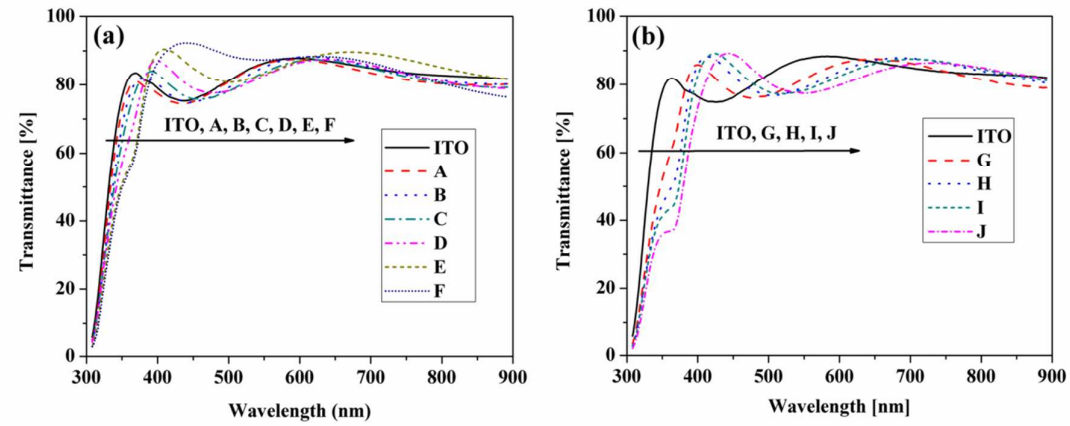

Fig. 9 The transmittance spectra of bare ITO and ITO coated with ZnO layers. (a) ZnO layers derived from A) 0.02, B) 0.05, C) 0.1, D) 0.3, E) 0.6 and F) 1 M sol, respectively; (b) ZnO CBLs derived from 0.1 M sol and by spinning (G) 3, H) 5, I) 7 and J) 10 times, respectively.[132]

3. Doping of ZnO CBLs in inverted polymer solar cells

In inverted PSCs, the thickness of ZnO CBLs is typically only a few tens of nanometers in order to ensure good conductivity so as to reduce the serial resistance and improve device performance.[38, 163] However, such a thin CBL makes the devices suffer from low mechanical robustness and reduced protective properties against chemical or physical reaction between the active layer and the electrode.[163, 193] Therefore, such a thin ZnO CBL imposes a challenge for the manufacturing of PSCs with scalable processes, such as the roll-to-roll manufacturing.[47, 163, 193] Doping is an efficient way to enhance the conductivity of ZnO so as to overcome the thickness limitation. Through doping, an increase in the electrical conductivity of ZnO CBL and photovoltaic performance of inverted PSCs has been observed.[163, 193-198] The group-III elements, such as boron (B),[155] aluminum (Al),[163, 193, 196, 198-200] gallium (Ga)[194, 201] and indium (In)[195] have been intensively investigated for the doping of ZnO CBLs. It was explained that the group-III elements could work as an n-type dopant for ZnO to replace Zn sites and generate free electrons. Besides aluminium and the group III elements, the group-II elements (alkaline earth), such as magnesium (Mg), strontium (Sr) and barium (Ba) doped ZnO (named as MZO, ZnSrO and ZnBaO, respectively) layers also have been introduced into inverted PSCs.[48, 202] Besides the metals, the fullerene derivatives have been used to dope ZnO for forming an efficient CBL in inverted PSCs.[49, 114] The photovoltaic performance of inverted devices based on these doped ZnO CBLs in literature is summarized in Table 2.

Table 2. Non exhaustive survey of inverted PSCs including a doped ZnO CBLs. The photovoltaic parameters are compared to those measured for a reference cell (values in parentheses), when available, based on pristine ZnO CBL.

Device architecture	J_{sc} [mA cm^{-2}]	V_{oc} [V]	FF [%]	PCE [%]	Ref.
ITO/AZO/P3HT:PCBM/PEDOT:PSS/Ag	8.36 (8.41)	0.569 (0.565)	50.8 (53.9)	2.42 (2.56)	163

ITO/AZO/P3HT:PCBM/PEDOT:PSS/Ag	8.97 (8.33)	0.54 (0.56)	55.0 (56.5)	2.65 (2.62)	[193]
ITO/AZO/P3HT:PCBM/NiO_x/Ag	6.78		38	1.36	[199]
ITO/AZO-NP/P3HT:PCBM/PEDOT:PSS/Ag	9.23	0.602	51.9	2.88	[203]
ITO/AZO/P3HT:PCBM/WO_3/Al	10.22	0.56	48.81	2.79	[200]
ITO/AZO/P3HT:PCBM/PEDOT:PSS/Ag	11.02 (10.73)	0.59 (0.58)	58.40 (53.73)	3.78 (3.32)	[204]
ITO/AZO(flat)/P3HT:PCBM/MoO_3/Ag	9.21	0.61	42.3	2.38	[192]
ITO/AZO(textured)/P3HT:PCBM/MoO_3/Ag	10.74	0.60	42.2	2.72	[192]
ITO/AZO/P3HT:PC_{60}BM/MoO_x/Ag	8.7	0.61	68.3	3.54	[47]
ITO/AZO/PBDTTPD:PC_{70}BM/MoO_x/Ag	12.5	0.87	62	6.7	[47]
ITO/AZO/PBDTTT-C-T:PC_{70}BM/MoO_x/Ag	16.0	0.76	66	7.6	[47]
ITO/AZO/ PBDTTT-C-T-EFT:PC_{70}BM/MoO_x/Ag	17.7	0.80	70.7	9.94	[47]
ITO/AZO/PTB7:PC_{70}BM/MoO_x/Ag	17.1 (16.9)	0.74 (0.73)	70.6 (66.6)	8.86 (8.24)	[47]
FTO/IZO/P3HT:PCBM/MoO_3/Ag	9.935 (8.392)	0.605 (0.613)	55 (57)	3.30 (2.94)	[195]
ITO/InZnO/PTB7-Th:PC_{71}BM/MoO_3/Ag	16.32 (15.32)	0.79 (0.79)	70.0 (67.1)	9.03 (8.12)	[49]
ITO/InZnO-BisC60/PTB7-Th:PC_{71}BM/MoO_3/Ag	17.24	0.80	74.1	10.22	[49]
ITO/GZO/P3HT:PCBM/MoO_3/Au	11.7 (6.3)	0.42 (0.41)	39.7 (35.7)	1.95 (0.92)	[194]
ITO/GZO/PCDTBT:PC_{71}BM/MoO_3/Al	10.46 (8.85)	0.90 (0.86)	59.03 (50.27)	5.56 (3.72)	[201]
ITO/GZO/PTB7:PC_{71}BM/MoO_3/Al	14.96 (14.14)	0.75 (0.74)	64.95 (50.44)	7.34 (5.31)	[201]
ITO/BZO/P3HT:PCBM/MoO_3/Al	11.31 (8.95)	0.538 (0.565)	54 (58)	3.26 (2.93)	[155]
ITO/ZMO/PTB7:PC_{71}BM/MoO_3/Ag	16.78 (14.64)	0.74 (0.75)	66.99 (64.75)	8.31 (7.11)	[48]
ITO/MgZnO/P3HT:PCBM/MoO_3/Ag	9.7 (9.2)	0.577 (0.515)	56.8 (44.9)	3.17 (2.13)	[204]
ITO/MgZnO/P3HT:ICBA/MoO_3/Ag	9.9 (9.6)	0.828 (0.727)	67.0 (55.5)	5.48 (3.88)	[204]
ITO/ZnO-C60/PTB7:PC_{71}BM/MoO_3/Ag	15.41 (13.75)	0.73 (0.70)	73.0 (69.0)	8.21 (6.65)	[114]
ITO/ZnO-C60/PTB7-Th:PC_{71}BM/MoO_3/Ag	15.73 (14.02)	0.80 (0.79)	74.3 (69.1)	9.35 (7.64)	[114]
ITO/ZnO-BisC60/PTB7-Th:PC_{71}BM/MoO_3/Ag	16.88 (15.32)	0.79 (0.79)	72.0 (67.1)	9.60 (8.12)	[49]

Among the various doping methods, aluminium doping is a well-known approach to enhance the conductivity of ZnO layer for inverted PSCs. This seems to be because the doping of ZnO with aluminium can be easily processed and the aluminium-doped ZnO (AZO) possesses better electrical properties than that of intrinsic ZnO (i-ZnO) reference.[163, 193] It has been reported that the inflection (S-shaped) I-V curve of inverted PSCs could be removed by introducing an AZO CBL.[196-198] Stubhan *et al*. and co-workers studied the thickness dependence of the performance of inverted PSCs based on both i-ZnO and AZO CBLs with thicknesses from ~30 to 120 nm.[163, 193] They demonstrated that an increase of the thickness of AZO CBL from ~30 to more than 100 nm didn't hamper the solar cell performance, while the devices based on 100 nm i-ZnO films suffered from severely decreased FF, V_{oc} and PCE due to an increase in the series resistance. Considering that a thick CBL has relatively good mechanical strength robust which benefits the inverted devices to be fabricated using a roll-to-roll method, the authors suggested that the doping of ZnO with aluminium opens the possibility to incorporate a thick CBL into the inverted devices without sacrificing their efficiency. More recently, based on a facial and low temperature (125 °C) solution processed Al doped ZnO electron accepting/hole blocking layer, Jagadamma *et al*. reached high performance inverted PSCs yielding a remarkable PCE in excess of 10% on glass substrates and 8% on plastic substrates.[47] They found that the average PCE of inverted devices using PTB7: PC_{70}BM active layer decreased marginally from 8.8% to 8.1%, while the thickness of AZO CBLs increased from 22 nm to 75 nm. The very slight decrease of the device performance with increasing the AZO thickness indicates that relative thick AZO can serve as an efficient CBL material for inverted PSCs. A thicker CBL with better mechanical strength is more suitable to the manufacturing of PSCs by scalable processes, such as the roll-to-roll manufacturing.[47, 163, 193]

For the inverted PSCs with AZO CBLs, it is worth noting that the device performances are strongly affected by the crystallinity and stoichiometry of AZO.[193, 204] This is because the electronic properties of AZO CBLs, such as work function, conductivity, mobility as well as surface states, are massively

determined by the stoichiometry of AZO.[154,164] Tsai and co-workers have investigated the effects of Al content (from 0 to 12 mol. %) on the electronic properties of AZO layers and device performances of inverted PSCs with structure of ITO/AZO/P3HT:PCBM/PEDOT:PSS/Ag (Fig. 10a).[204] They found that the carrier concentration, mobility and resistivity of AZO thin films strongly depended on Al molar ratio (Fig. 11), which furtherly impacted on the performance of inverted devices with the AZO CBLs. In their results, to achieve the best device performance, the optimum Al content of AZO CBLs is 6 mol. %. Compared the devices based on pure ZnO layers, the device with optimum AZO CBL exhibits highest PCE of 3.78%, enhanced by ~13.9% via improving J_{sc} form 10.73 to 11.12 mA cm^{-2} and FF from 53.7% to 60.8%.[204] At the optimum Al doping concentration, the authors demonstrated that the band structure of ZnO was modified with an upward energy shift in the Fermi level (Fig. 10b), which facilitates the electron collection and can also serves as an efficient hole blocking layer. It is believed that the tunable band-gap combine with the increased carrier concentration and conductivity of AZO films via Al doping, and enhanced optical absorption of P3HT are the reasons of enhanced device performance.

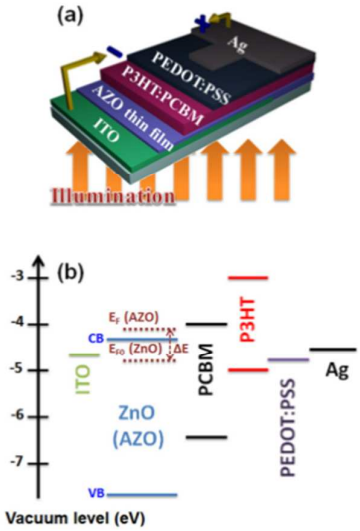

Fig. 10 (a) Schematic diagram of inverted device structure with AZO CBL, (b) band diagram of devices with pristine ZnO or AZO CBL.[204]

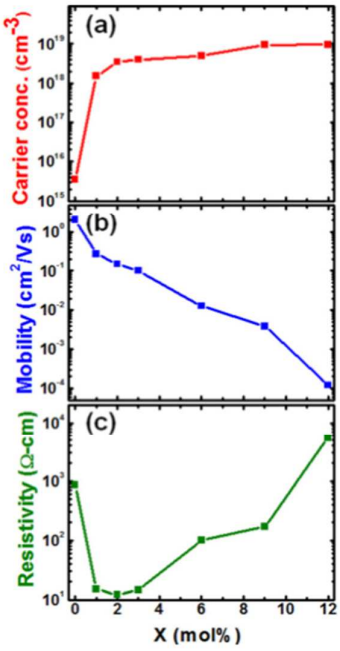

Fig. 11 (a) Carrier concentration, (b) mobility, and (c) resistivity of $A_xZn_{1-x}O$ (AZO) thin layers as a function of Al content (X, molar ratio).[204]

Doping ZnO with the group-III elements such as boron (B), gallium (Ga), or indium (In) for doping ZnO CBLs, is another effective way to improve the performance of inverted PSCs.[155, 194, 195, 201] Kyaw *et al*. investigated the correlation between the device performance and the indium contents of the sol-gel derived indium-doped ZnO (IZO) CBL in inverted PSCs.[195] Compared to the device with i-ZnO CBL, the photovoltaic performance of the devices using appropriately doped IZO CBL, especially in term of the J_{sc}, were enhanced, due to a combined effect of improvement in charge collection and higher optical transmittance of the electrode/IZO buffer layer stack. The device with 1 at% IZO CBL showed maximum PCE of 3.3% compared to the PCE of 2.94% for the device with i-ZnO CBL. Gallium (Ga) has also been used as a dopant to enhance the electrical conductivity of ZnO CBL. Shin *et al*. investigated the Ga-doped ZnO (GZO) CBL for the inverted PSCs.[194] By employing a GZO CBL, the PCE of the fabricated devices was improved by about 110% compared to the devices with i-ZnO CBL, which was ascribed to the higher electron conductivity and smooth surface morphology of the ZnO film with Ga doping.

The doping of ZnO with the group-II elements (alkaline earth), such as magnesium (Mg), strontium (Sr) and barium (Ba), doped ZnO (named as MZO, ZnSrO and ZnBaO, respectively) films have also been studied for inverted PSCs to serve as CBLs.[48, 202] Pachoumi *et al*. reported an improved performance and stability of inverted PSCs by employing the sol-gel processed amorphous Sr and Ba doped ZnO CBLs prepared at relatively low temperature.[202] The inverted PSCs based on Sr and Ba doped ZnO CBLs exhibited higher performance and better stability than the devices with pure ZnO CBLs. In addition, the commonly requirement of light soaking for reaching a maximum photovoltaic performance of inverted device based on i-ZnO CBLs was successfully circumvented. The improvements of device performance were attributed to the doping of ZnO with Sr or Ba reducing the electron trapping on the surface associated with oxygen absorption. The authors suggested that the Sr or Ba doping could effectively suppression/reduction of the oxygen adsorption at mobile oxygen vacancy sites on the ZnO surface.[202]

For doped ZnO CBLs, the band gap structure is a key parameter that could affect the device performance. The band gap and energy level dependence on the doping content enables researchers to adjust the optical and electrical properties of the doped ZnO CBLs for achieving better device performance.[48, 193, 199] For example, it is well established that the substitutional doping of Mg^{2+} into the Zn site leads to an increase in the bandgap of ZnO.[48, 205, 206] By using Mg doped ZnO (ZMO) CBLs Yin *et al*. fabricated inverted PSCs with high performance, as shown in Fig. 12a).[48] They developed a solution processed ZMO CBL with tunable band gap and energy levels (Fig. 12b), good optical transmittance and electron transporting abilities. With an increase of the Mg content (x = 0.1 - 0.6), the CB edge value of the ZMO CBLs are finely adjusted in the range of ~-4.3 – -3.9 eV (Inset in Fig. 12c) to approach the LUMO of $PC_{71}BM$. The corresponding band gap of ZMO films increased from 3.3 to 3.7 eV, which was confirmed by the gradual blue shift of the fundamental absorption edge as the Mg content increases (Fig. 12c). A favorable CB level of ZnO matching well with the $PC_{71}BM$ acceptor would improve the electron extraction/transportation in inverted devices. The electron mobility of the ZMO films was found close to that of pure ZnO film, which is in favor of electron extraction/transportation in the inverted PSCs. Moreover, ZMO layers also exhibit a more hydrophobic surface than ZnO, benefiting to forming high quality contact between the organic active layer and the inorganic metal oxide CBLs. As a result, by incorporating the optimized ZMO layers derived form a 0.2 M precursor solution, the inverted PSCs with structure ITO/ZMO/PTB7:$PC_{71}BM$/MoO_3/Ag exhibit a preferable PCEs exceeding 8% (up to 8.31-8.35%, as shown in Fig. 12d), which are much higher than those of devices with an i-ZnO CBL (PCE = 7.1%) under the same conditions.[48] Macleod and co-workers have also reported an improved PCE in inverted PSCs when a sol-gel processed Mg-ZnO is used in place of ZnO as CBLs.[206] It has been found that, as the Mg content increased, the FF and V_{oc} increased substantially for both the devices based on P3HT:PCBM and P3HT:ICBA systems. The maximum PCEs were achieved when the Mg content in the precursor was 10 mol. %, and subsequently decreased for higher Mg content due to decay in the J_{sc}. They have also found that the increase in Mg content led to a decrease in the work function and an increase in the bandgap. The increased bandgap in Mg-ZnO is ascribed to a downshift in the valence band maximum, rather than an upshift in the conduction band minimum. The improved device performances were partially ascribed to the reduced recombination caused by substituting of the Zn with Mg. However, it has been suggested that the mechanisms for the improvement of inverted devices with Mg doped ZnO CBLs remain an open question.[206] More systematic investigation needs to be done to elucidate the dominating factors with regard to the improvement in the performance of inverted PSCs when using Mg-ZnO CBL.

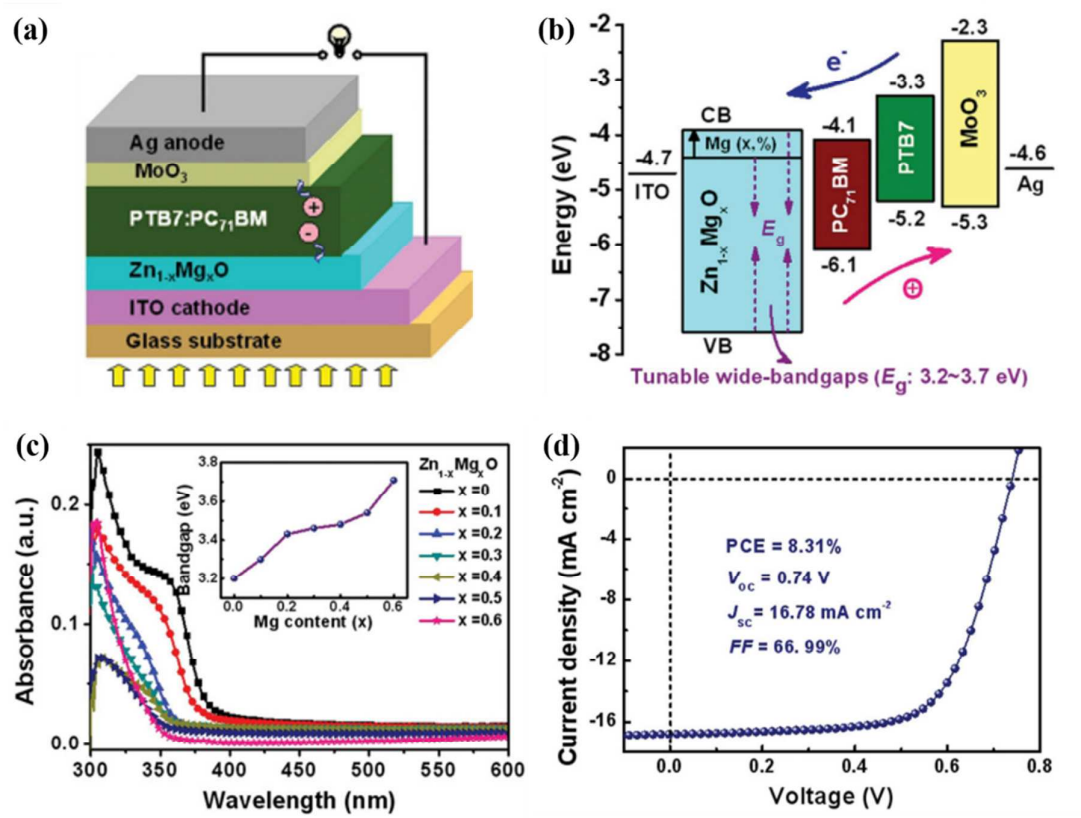

Fig. 12 (a) Schematic illustration of device structure with ZnMgO CBL. (b) Energy levels of the components in the inverted PSCs with various ZMO CBLs. (c) Optical absorption spectra of ZMO films. The inset shows an increase in the bandgap of ZMO films with the increasing of Mg content (x). (d) J-V curve of the device with the ZMO (x = 0.3) CBL.[48]

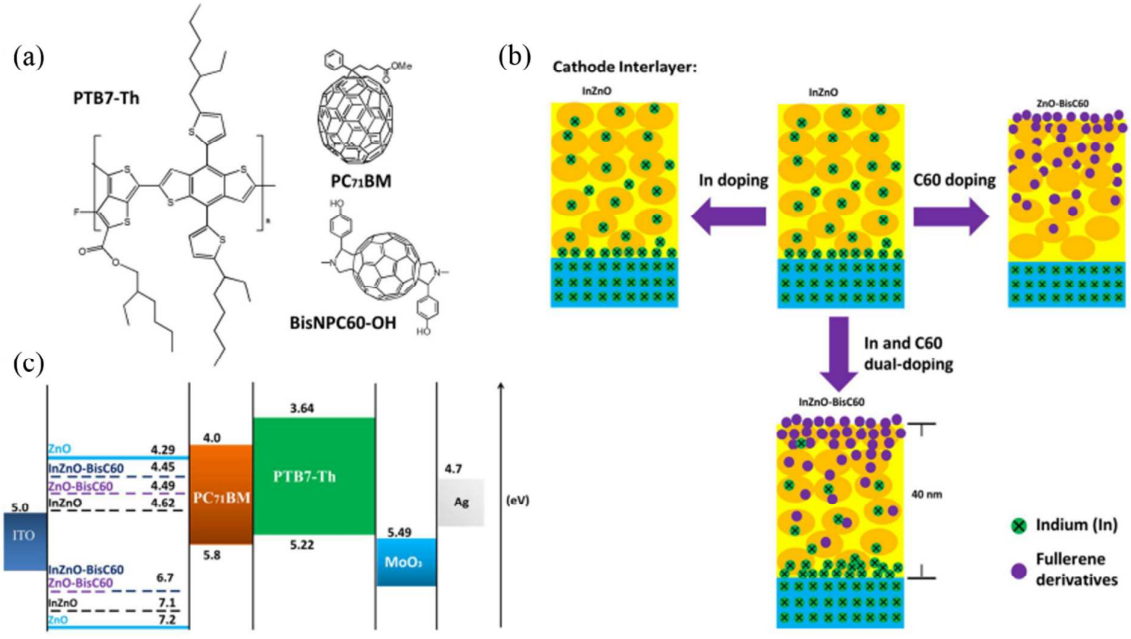

Fig. 13 (a) Chemical structures of PTB7-Th, $PC_{71}BM$ and BisNPC60-OH, (b) Schematic illustration of the proposed cathode interlayer from XPS depth profile; (c) Energy levels diagram for ZnO, InZnO, ZnO-BisC60 and InZnO-BisC60 determined from ultraviolet photoelectron spectroscopy (UPS) and UV-Vis results and for all the components in the inverted PSCs.[49]

Besides the above mentioned metals, fullerene derivatives have also been used to dope ZnO for forming high quality CBL in inverted PSCs.[49, 114] Liao *et al*. reported a fullerene derivative doped ZnO (ZnO-C60) nanofilm as the CBL of inverted PSCs.[114] For the inverted device with ZnO-C60 CBL, the PCE was remarkably improved from 7.64% to 9.35% for PTB7-th:$PC_{71}BM$ active layer, from 6.65% to 8.21% for PTB7:$PC_{71}BM$, and from 5.26% to 6.60% for P3HT:ICBA, compared to the devices with pristine ZnO CBL. It has been demonstrated that the ZnO-C60 CBL can enhance the electron collection by producing a fullerene derivative rich cathode surface and promote electron conduction at the interface and in the bulk of ZnO-C60. The high content of fullerene at the surface of ZnO-C60 CBL offers a better contact to the fullerene derivative in the active layer, and thus facilitate electron collection. In another work also done by Liao *et al*., a dual-doped ZnO with Indium and fullerene derivative (BisNPC60-OH) were fabricated by sol-gel processing and applied as CBL in inverted PSCs (Fig. 13).[49] They found that this dual doped ZnO, InZnO-BisC60, buffer layer showed dual and opposite gradient dopant concentration profiles, being rich in fullerene derivative at the cathode surface in contact with active layer and rich in Indium at the cathode surface in contact with the ITO surface (Fig. 13b). For the InZnO-BisC60 film, the surface conductivity was improved by a factor of 270 (from 0.015 to 4.06 S cm^{-1}), and the electron mobility was enhanced by a factor of 132 (from 8.25×10^{-5} to 1.09×10^{-2} cm^2 V^{-1} s^{-1}). As a result, with this InZnO-BisC60 film as CBL, the PTB7-Th-$PC_{71}BM$ inverted device exhibited a preferable PCE, 10.31%, significantly higher than the 8.25% for pristine ZnO.

4. One dimensional ZnO nanostructures for inverted polymer solar cells

For polymer solar cells, the bulk-heterojunction (BHJ) active layer was considered to establish the cornerstones of device with high performance. This is because the structure of BHJ can maximize the donor/acceptor interfacial area to provide possibly more exciton dissociation sites and form continuous pathways for the transport of electrons and holes.[13, 18, 21] However, there are still some shortcomings of BHJ active layer that limit the photovoltaic performance of polymer solar cells. One of the limitations is that the very thin thickness of the BHJ active layer leads to low optical absorption and thus non-ideal device performance.[207-209] The use of very thin active layer is, on one hand, because the photo-generated charges in active layer need to transport in the percolation network of the polymer donor and the accepter, and on the other hand the carrier mobility in polymers is relatively low.[207, 210] The charge recombination in a thick active layer will increase because of an increase in the diffusion length of carriers, leading to the device performance decrease. Thus, the optimal thickness of active layer is determined by a trade-off between maximize the optical absorption and meanwhile allow the charges transport efficiently from BHJ active layer to electrode. It has reported that an optimal active layer thickness is typically about only ~100-200 nm.[186, 207-209]

Research effort on the methods of light absorption enhancement has been driven by these limitations, including using photonic crystals,[211] plasmonic enhancement,[212-215] and textures.[216, 217] Besides the methods mentioned above, another way to enhance the light harvest of photoactive layer is to increase the effective thickness of photoactive layer and meanwhile avoid the increase of charge recombination in the case of a thick active layer.[218, 219] To increase the effective thickness of photoactive layer, the use of a vertical aligned one dimensional (1 D) ZnO nanostructure in PSCs to provide a direct electron transport pathways so as to enhance charge carrier collection and transport has been investigated.[214, 215] Fig. 14 shows a schematic diagram of inverted PSCs with 1 D ZnO nanostructure. In the case of inverted PSC with ZnO nanorods (NRs), after the charge separation at the polymer and fullerene interface, the photo-generated electrons at LUMO level of fullerene transfer to the conduction band of ZnO. Then, the electrons quickly move to cathode electrode along the ZnO NRs, in view of high electron mobility of ZnO NRs (~15 cm^2 s^{-1} V^{-1} along c-axis)[220] which is several orders of magnitude higher than what are typically found in most of organic semiconducting materials.[7, 218, 221] For the devices with ZnO NRs, the average distance from the generation sites of charge carriers to the surface of ZnO electron collection layer would be shorter than that in the solar cells without ZnO NRs, and as a result the charges recombination can be effectively reduced.[218, 222] To date, 1 D ZnO nanostructures, such as nanorods (NRs),[218, 221, 223-231] nanowires (NWs),[222, 232-234] nanofibers (NFs),[235] and nanopillars,[236, 237] and 2 D vertical aligned nanowall arrays, [231, 238] combined with dense ZnO films have been employed to fabricate the inverted PSCs. Table 3 summarizes the photovoltaic parameters of inverted devices using of 1D ZnO nanostructures. Fig. 15 presents the SEM images of several typically vertical aligned 1 D ZnO nanowires used in inverted PSCs.

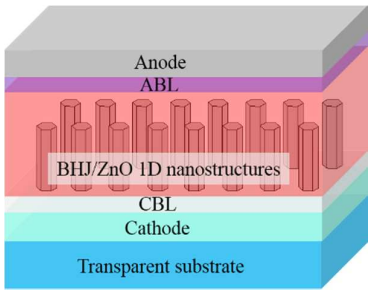

Fig. 14 Schematic diagram of inverted PSC structure with 1 D ZnO nanorods.

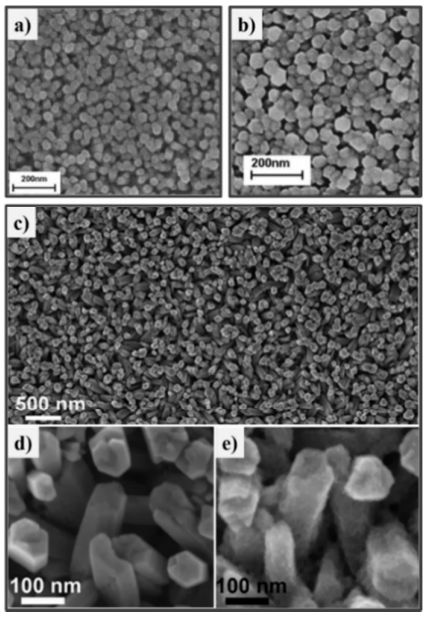

Fig. 15 SEM images of 1 D ZnO nanostructures employed in inverted PSCs. (a) Top view of ZnO nanorods.[227] (b) Hydrothermal two-growth ZnO nanorods.[239] FE-SEM micrographs of (c) ZnO nanowires and magnified views of (d) as-electrodeposited and (e) ZnO nanoparticles modified ZnO nanowires.[233]

Table 3. Non exhaustive survey of photovoltaic parameters of inverted PSCs including a 1 D ZnO nanostructure. The photovoltaic parameters are compared to those measured for a reference cell (values in parentheses), when available, without the 1D ZnO nanostructure layer.

Device architecture	J_{sc} [mA cm^{-2}]	V_{oc} [V]	FF [%]	PCE [%]	Ref.
ITO/ZnO NF/P3HT:PCBM/Ag	10.00	0.475	43	2.0	235
ITO/ZnO NR/P3HT:PCBM/Ag	9.60 (9.0)	0.57 (0.52)	50 (38)	2.7 (1.8)	218
ITO/ZnO NR/PCBM:P3HT/VOx/Ag	10.4 (10.6)	0.58 (0.57)	65 (50)	3.9 (3.0)	223
ITO/ZnO NR/PCBM:P3HT/Ag	11.7	0.53	58	3.58	219
ITO/ZnO NR/P3HT:PCBM/Ag	6.62	0.36	49	1.16	224
ITO/ZnO NR-N719/P3HT:PCBM/Ag	8.89	0.57	41	2.00	224
ITO/ZnO (Buffer layer)/ZnO NR/P3HT:PCBM/Ag	14.99 (9.59)	0.48 (0.49)	34 (35)	2.44 (1.64)	225
ITO/ZnO NR/P3HT:PCBM/PEDOT:PSS/Ag	6.28	0.432	44.76	1.19	226
ITO/ZnO NR/P3HT:PCBM/Ag	10.13	0.51	45	2.35	227
ITO/ZnO NR-PCBM/P3HT:PCBM/Ag	11.67	0.55	50	3.2	227
ITO/AZO/ZnO NW/P3HT:PCBM/PEDOT:PSS/Ag	10.02	0.55	53	2.94	232
ITO/ZnO NR/P3HT:PCBM/MoO_x/Au	9.917	0.266	37.126	0.979	228

	(3.250)	(0.220)	(36.212)	(0.259)	
FTO/ZnO nanopillars/P3HT:PCBM/Ag	7.29	0.40	35	1.02	236
	(5.46)	(0.25)	(27)	(0.37)	
ITO/ZnO NW + ZnO NPs/P3HT:PCBM/MoO_3/Ag	13.75	0.57	52	4.1	233
	(9.48)	(0.56)	(64)	(3.41)	
ITO/ZnO NR/P3HT:PCBM/MoO_3/Al	9.02	0.555	44.2	2.15	221
ITO/ZnO NR/P3HT:PCBM/MoO_3/Ag	5.70	0.509	38	1.11	229
ITO/ZnO NR/P3HT:PCBM:x-3-HF/Ag	11.56	0.59	44.63	3.05	230
FTO/ZnO nanopillars/P3HT:PCBM/MoO_3/Ag	8.55	0.44	45	1.71	237
	(5.46)	(0.25)	(27)	(0.37)	
ITO/ZnO NW/P3HT:PCBM/MoO_3/Ag	9.4	0.55	66.1	3.5	222
	(9.1)	(0.54)	(59.7)	(2.9)	
ITO/ZnO NR/P3HT:ICBA/PEDOT:PSS/Ag	8.34	0.793	61.12	4.04	231
	(7.73)	(0.802)	(61.42)	(3.80)	
ITO/ZnO NR/PBDTTT-C-T:$PC_{71}BM$/MoO_x/Ag	18.4	0.733	58.0	7.80	239
	(13.5)	(0.788)	(50.6)	(5.40)	
ITO/ZnO NR/PTB7:$PC_{71}BM$/MoO_x/Ag	16.5	0.709	66.7	7.80	239
	(16.0)	(0.708)	(63.7)	(7.24)	

Olson *et al*. demonstrated for the first time that the inverted PSCs fabricated with the blend of a P3HT:PCBM and 1 D ZnO nanostructure prepared with a solution method, and a PCE of 2.03 % was obtained.[235] Kazuko *et al*. investigated the effect of the length of ZnO NRs on the performance of inverted PSCs.[218] They found that the PCE and FF of devices were improved from 1.8% and 0.38 to 2.7% and 0.50, respectively, while the I_{sc} and V_{oc} remained almost constant when the length of ZnO nanorods increased from 0 to 350 nm. The improvement in PEC was mainly ascribed to the enhancement in FF, resulting from introducing ZnO nanorods as direct pathways for more efficient electron transport and collection. It has been demonstrated that the ZnO NR array in ZnO NR/P3HT:PCBM system mainly works as electron collector/transport pathway, rather than an accepter material to form heterojunctions with the donor polymer in view of much larger interface between the P3HT and PCBM than the interface between the P3HT and ZnO NR.[77, 218, 240] In conventional and inverted PSCs, holes are also commonly limiting charge carrier. Although ZnO nanorods may not improve the hole transport, the extraction and transport away of electrons would reduce the probability of electron-hole recombination.

In order to fully achieve the potential of 1 D ZnO nanostructures in inverted PSCs, an electrical coherence at the organic photoactive layer and ZnO interface needs to be provided. Therefore, the infiltration of polymer into the space between ZnO NRs is a critical issue that greatly affects the devices performance. Several methods have been developed to improve the contact between the active layer and ZnO nanostructures, including surface modification of ZnO nanostructures and optimizing the post-treatment processes.[219, 227, 231, 233] Fig. 16 shows the SEM images of the cross-section of inverted devices with the ZnO nanowire arrays with or without surface modification. Obviously, the surface modification of ZnO NPs effectively improved the infiltration of polymer and fullerene blend into the space of ZnO NRs.

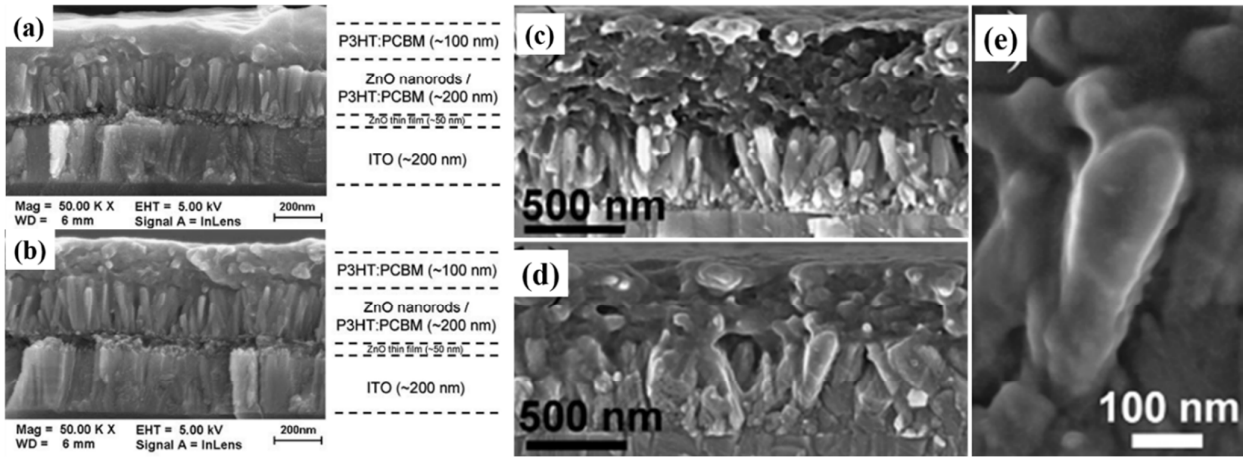

Fig. 16 Cross-sectional SEM images of inverted devices (a) with and (b) without fullerene interlayer.[227] Cross-sectional FE-SEM micrographs of inverted devices with (c) unmodified ZnO nanowires, (d) ZnO NPs modified ZnO nanowires, and (e) the higher magnification view of the ZnO nanowires well covered by the P3HT:PCBM blend.[233]

Chou *et al*. reported that the device performance of inverted PSCs with ZnO NRs could be improved by increasing the polymer solidification time.[219] They suggested that the increase of polymer solidification time made the polymer chains have enough time to self-organize, leading to the enhanced crystallinity of polymer and improved infiltration of photoactive layer into ZnO NPs space. For the inverted device with the active layer up to 400 nm in thickness, the PCE of the device was improved to 3.58% as a result of enhanced FF (58%).[219] Thitima *et al*. reported that the performance of inverted PSCs could also be improved by modifying the surface of ZnO nanostructure with N719 dye.[224] The dye interlayer covered on the surface of ZnO was thought to serve as a mediator to improve the electron transportation and injection from polymer to ZnO. Huang *et al*. reported that the solution-processed PCBM interlayer could efficiently modify ZnO NRs and accordingly enhance the PCE from 2.35% to 3.2%.[227] They demonstrated that the PCBM interlayer enhanced the infiltration of the photoactive layer into the intervals between ZnO NRs (Fig. 16b) and may facilitate the self-organization of polymer.

Ajuria *et al*. investigated the functionalization of the ZnO nanowires (NW) surface with ZnO nanoparticles (NPs) with the consideration to improve the contact between ZnO and P3HT:PCBM active layer.[233] It was found that, by modifying the ZnO NW array with a thin layer of ZnO NPs by immersing in a ZnO colloidal suspension, improved P3HT:PCBM blend penetration was achieved (Fig. 16d and 16e). A PCE as high as 4.1 % was obtained for the inverted device based on ZnO NP-coated NWs and commercial P3HT:PCBM blend active layer. The ZnO NP modification was found to contribute to enhancing the exciton dissociation and increasing the charge lifetime by reducing charge recombination. More recently, Ho *et al*. fabricated ZnO NRs with controlled density and length by using a two-growth hydrothermal method (as shown in Fig. 15 b).[239] Compared to the devices made with planar ZnO films, the PCEs of devices with the two-growth ZnO NRs are enhanced from 5.40% to 7.80% and from 7.24% to 8.01% for PBDTTT-C-T:$PC_{71}BM$ and PTB7:$PC_{71}BM$ active layer, respectively. The improved device performances were ascribed to the morphology of two-growth ZnO NRs, which helps to achieve deeper and superior infiltration of organic active layer.[239] From these results, we can conclude that, for 1 D ZnO nanostructures applied in inverted PSCs, their length, density, surface morphology, and surface modification are key parameters that will significantly affect the penetration of polymer and fullerene blend and thereby affect the device performance.

5. Surface modification of ZnO CBL

The performance of polymer solar cells is critically dependent on the properties of each layer and the interfacial contacts. For ZnO CBLs, without interface engineering, the inorganic ZnO CBL and surface defects may lead to a poor interfacial contact with the polymer based active layer and, thus, result in a poor electron extraction, which is one of the main reasons leading to relatively high charge recombination and series resistance (R_S).[241, 242] Especially, in the case of ZnO CBLs prepared with widely used sol-gel processing or colloidal nanocrystals, the low-temperature and solution process often lead to a high densities of surface defects, such as dangling bonds, surface groups and charged oxygen molecules.[41, 128, 196, 243] Such surface defects can act as recombination centres for photogenerated charge carriers, decreasing the photocurrent and power conversion efficiency as well as the device stability. It has been demonstrated that the deteriorated electrical properties at the interface between ZnO CBLs and organic active layers are caused by incompatible chemical interfaces and the formation of electron trapping states on the surface of ZnO layers.[244] A phenomenon commonly observed on the J-V curve of inverted PSCs when employing ZnO CBLs is the appearance of an inflection point, i.e. the so-called "s-shape" kink feature. It is believed to be due to the accumulation of charges at the ZnO/active layer interface.[145, 149, 198, 202] Therefore, appropriate electrical contacts at interfaces between ZnO CBLs and BHJ active layers are highly desirable and essential to achieve high power conversion efficiency and good stability of inverted PSCs. In this regard, many studies have focused on engineering the surface of ZnO CBLs to reduce the R_S of solar cells through improving the interfacial electrical properties, better aligning energy-level and controlling the surface energy. There have been several efficient surface engineering methods to modify the surface of ZnO CBLs, such as ultraviolet (UV) [41, 133, 145, 149, 183, 198, 202] or UV-ozone treatment,[145, 173] thermal and vacuum treatment,[168] and incorporation of surface modification interlayer, such as the self-assembled monolayers (SAMs).[170, 245-248]

5.1 UV illumination treatment of ZnO CBLs

UV or UV-containing light illumination treatment, also known as "light-soaking", is a common way to improve the electrical characteristics and optimize optimum photovoltaic performance of inverted devices with ZnO CBLs.[41, 133, 145, 149, 183, 198, 202] UV illumination can passivate the defects states, such as the negatively charged oxygen molecules trapped at the grain boundaries and surface, and thus remove electron extraction barrier and reduce carrier recombination at ZnO/photoactive layer interface.[41, 128, 196] The metal-oxide/organic active layer interface is identified as the reason of the S-shaped J-V curve due to an electron extraction barrier.[182, 183, 198] Under the dark condition, electrons in the conduction band of ZnO layer are trapped by the chemisorption of O_2 molecules (Fig. 17a, step (1)), and therefore forming a depletion layer and band bending next to the surface (Fig. 17a, step (2)).[182, 183] It has been suggested that both the depletion layer and the band bending can result in the formation of a barrier for the electron injection and extraction at the ZnO/BHJ active layer interface and are more pronounced in the case of small ZnO nanocrystals with a high surface-area-to volume ratio. Upon UV illumination, the electron-hole pairs are generated in ZnO,

leading to neutralization of O_2 species and desorption of oxygen from ZnO surface, as shown in Fig. 17a, step (3), (4) and (5).[182] The desorption of O_2 from ZnO surface reduces the electron traps, and thus increases the concentration of mobile electrons.[183] As a result, the inflection point problem (S-shaped), on J-V curve of the inverted devices incorporating ZnO CBLs could be solved by exposing the cells to UV illumination, leading to the device performances improvement (Fig. 17b).[41] The UV-ozone (UVO) treatment has also been investigated to modify ZnO CBLs.[145, 173] Chen *et al*. found that the UVO treatment of ZnO NPs films could effectively passivate the defect states leading to longer carrier life time of devices compared to the devices treated with UV light soaking.[145] By reducing the interfacial recombination via UVO treatment and employing high performance PDTG-TPD: $PC_{71}BM$ active layer, the inverted PSCs with PCEs exceeding 8% were achieved. According to the PL measurement, it was proposed that the passivation mechanism under UVO treatment of ZnO films is correlated with the reduction of oxygen vacancies (V_O) in both the surface and bulk due to the penetration of oxygen in the porosity NPs films. As a result, the defect passivation in ZnO NPs layers can help to reduce the carrier recombination at the ZnO/active layer interface, and thus enhance the device performances.[145] However, the UV exposure approach is limited in the case when the devices are based on substrates with low UV transmittance, UV blocking filters or UV to VIS down-conversion concepts.[198] Many active organic donor polymers must be protected from being exposed to UV light so as to achieve a reasonable device stability.[55, 198, 249] In order to alleviate the requirement for UV illumination, surface modification methods and the use of doped-ZnO CBLs are developed to improve the electronic property of ZnO CBLs and the contact property of ZnO/organic active layer interface.

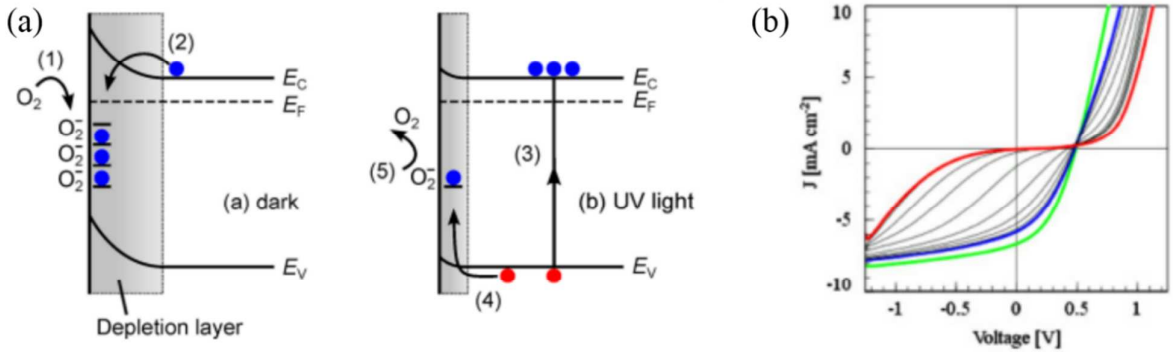

Fig. 17 (a) Schematic view of the oxygen absorption and desorption process in n-type ZnO layer in the dark (left) and UV illumination (right).[182] (b) The evolution of J-V curves over time during UV illumination for a single inverted PSC with ZnO NPs layer.[41]

5.2 Fullerene based interlayer modification of ZnO CBLs

Modifying ZnO CBLs with a functional interlayer derived from fullerene derivatives (C60-SAM),[50, 170, 203, 245, 247, 248, 250] conjugated polyelectrolyte (CPE)[251, 252] and poly(ethyleneimine) (PEI)[87] is another representative method to enhance the electrical properties of ZnO/BHJ active layer interface as well as the performance of inverted PSCs. Among these interfacial modification materials, fullerene derivatives (C60-SAM), which are very effective in acting as interlayer for the modification of ZnO CBL in inverted PSCs, are the most extensively investigated interfacial modification materials. Fig. 18 shows several cross-section schematics of the inverted devices with fullerene derivatives modified ZnO CBLs. The improvement of photovoltaic parameters of inverted devices using surface modified ZnO CBLs with fullerene derivatives (C60-SAM) is summarized in Table 4.

Energy & Environment Science

ARTICLE

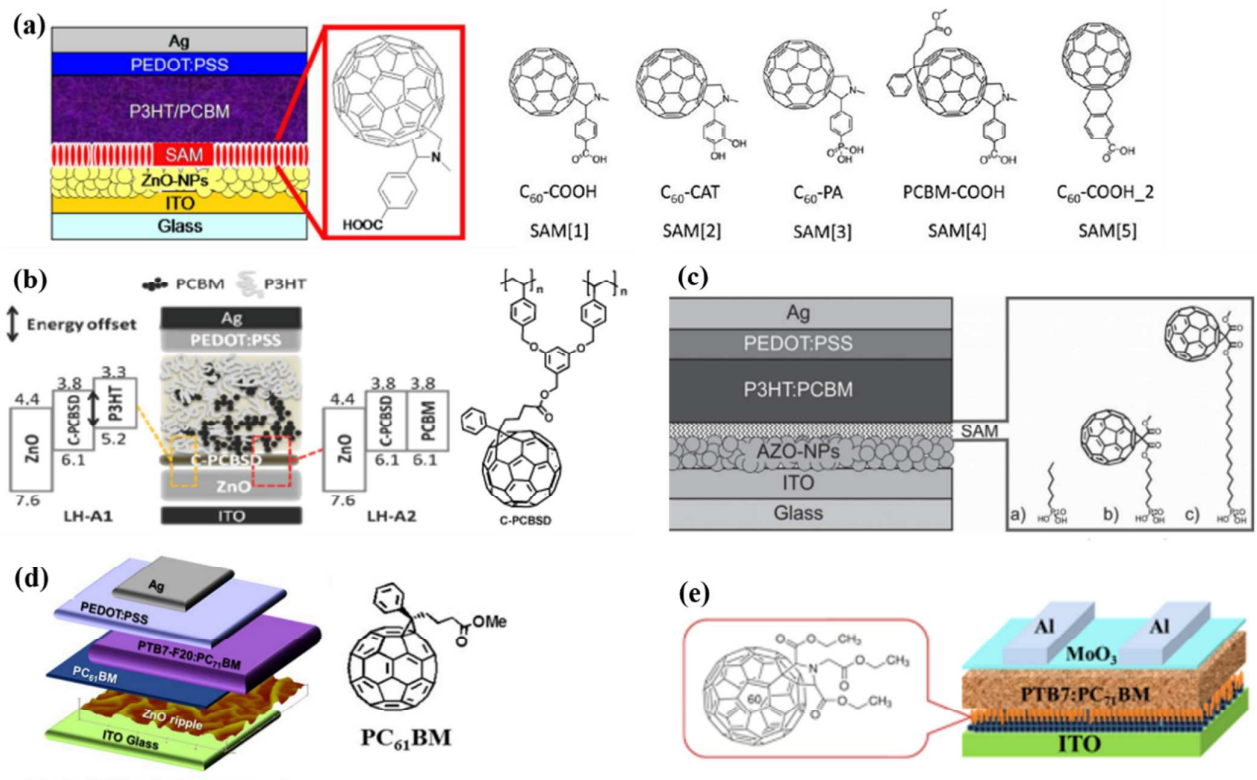

Fig. 18 Schematic illustrations of device structures and chemical structures of ZnO surface modification fullerene based interlayers including (a) fullerene self-assembled monolayer (C60-based SAM) modifiers containing different anchoring groups,[170, 245] (b) cross-linked fullerene (C-PCBSD) interlayer,[247] (c) hosphonic acid anchored C60 SAMs,[203] (d) $PC_{61}BM$[248] and (e) C60 pyrrolidine tris-acid ethylester (PyC60).[50]

Table 4. Non exhaustive survey of inverted PSCs including modified ZnO CBLs with fullerene derivatives (C60-SAM). The photovoltaic parameters are compared to those measured for a reference cell (values in parentheses), when available, made with a pristine ZnO CBL.

Device architecture	J_{sc} [mA cm^{-2}]	V_{oc} [V]	FF [%]	PCE [%]	Ref.
ITO/ZnO/SAM/PCBM:P3HT/PEDOT:PSS/Ag	12.0 (10.8)	0.63 (0.63)	60.6 (55.4)	4.54 (3.74)	245
ITO/ZnO/C60-SAM/P3HT:PCBM/Ag	10.25	0.62	66.6	4.20	144
ITO/ZnO/C60-COOH/PCBM:P3HT/PEDOT:PSS/Ag	11.12 (10.07)	0.61 (0.60)	64.0 (57.7)	4.36 (3.47)	170
ITO/ZnO/C60-CAT/PCBM:P3HT/PEDOT:PSS/Ag	10.86	0.61	62.4	4.13	170
ITO/ZnO/C60-PA/PCBM:P3HT/PEDOT:PSS/Ag	10.27	0.62	62.6	3.96	170
ITO/ZnO/ PCBM-COOH/PCBM:P3HT/PEDOT:PSS/Ag	10.85	0.62	63.6	4.24	170
ITO/ZnO/C60-COOH_2/PCBM:P3HT/PEDOT:PSS/Ag	11.26	0.61	62.4	4.30	170
ITO/ZnO/C-PCBSD/P3HT:PCBM/PEDOT:PSS/Ag	12.8 (11.6)	0.60 (0.58)	58 (52)	4.4 (3.5)	247
ITO/ZnO/C-PCBSD/ICBA:P3HT/PEDOT:PSS/Ag	12.4 (10.6)	0.84 (0.82)	60 (55)	6.22 (4.81)	250
ITO/AZO-C6-C60/P3HT:PCBM/PEDOT:PSS/Ag	9.92	0.583	57.4	3.32	203

	(9.23)	(0.602)	(51.9)	(2.88)	
ITO/ZnO/PyC60/PTB7:$PC_{71}BM$/MoO_3/Al	16.04	0.753	72.5	8.62	50
	(16.11)	(0.740)	(68.5)	(7.92)	
ITO/ZnO-PC61BM/PTB7-F20:PC71BM/PEDOT:PSS/Ag	17.042	0.684	66.0	7.698	248
	(14.783)	(0.693)	(63.1)	(6.475)	

The C60-SAMs can be easily processed to form a modification layer on the surface of ZnO CBLs through either a solution immersion technique or solution-based spin-coating method. Jen group developed a series of C60-based SAM modifiers containing different anchoring groups (catechol, carboxylic acid, and phosphonic acid), linkage location, and functionalization (Fig. 18a).[170, 245] They found that these C60-SAMs functional layers could help to reduce the charge recombination at the ZnO/active layer interface, improve the morphology of the active layer, and enhance the charge selectivity, leading to high FF and J_{sc}. For instance, an average PCE of 4.5% (with the highest PCE of 4.9%) was achieved for the devices with C60-SAMs (SAMs [1], shown in Fig 18a) modified ZnO CBL surface; such an efficiency is over 20% higher than those unmodified devices. Cheng *et al*. synthesized a PCBM-based and cross-linked n-type interlayer (C-PCBSD) (Fig. 18b) for the modification of ZnO CBL.[247, 250] This C-PCBSD interlayer was considered to have several positive impacts on the interfaces of the active layer, including improved exciton dissociation efficiency, reduced charge recombination, decreased interface contact resistance, and introduced vertical phase separation to reduce the bulk resistance of the active layer as well as passivating the local shunts of the ZnO CBL interface.[247, 250] As shown in Fig. 18b, the authors suggested that, firstly, the C-PCBSD interlayer provided an extra P3HT/C-PCBSD interface area for ultrafast excitons dissociation; secondly, the LUMO energy level of C-PCBSD (3.8 eV) was located between the LUMO of P3HT (3.3 eV) and the conduction band of ZnO (4.4 eV), which makes the electrons can be efficiently transported from active layer to ZnO through C-PCBSD as an energetically favorable downhill pathway.[247] As a result, the inverted devices based on C-PCBSD modified ZnO CBL with P3HT:PCBM blend active layer gained an improvement in J_{sc} from 11.6 mA cm^{-2} to 12.8 mA cm^{-2}, and exhibited PCE as high as 4.4%, which is much higher than 3.5% for a reference device with unmodified ZnO CBL.[247] An impressive high PCE of 6.2% has been achieved through introducing C-PCBSD modified ZnO CBL into inverted device based on ICBA: P3HT blend active layer, leading to a 29% enhancement compared to the device with un-modified ZnO CBL.[250] The improved device photovoltaic performance in terms of J_{sc} and FF of the devices with C-PCBSD modified ZnO CBL was attributed to high shunt resistance (R_{SH}) and low series resistance (R_S) due to the decreased contact resistance and increased electron collection efficiency at the ZnO/C-PCBSD interface. Besides high PCE, the devices with C-PCBSD modified ZnO CBL also demonstrated a good device stability in air without encapsulation. In their results, the PCE of the unencapsulated devices with P3HT:PCBM active layer and based on bare ZnO CBL retained 80% of its original value after being stored in ambient condition for 35 days. In contrast, the device based on C-PCBSD modified ZnO CBL exhibited a better long-term stability, retained above 85% of its original value under the same conditions.[247] In sharp contrast, the device with conventional structure (ITO/PEDOT:PSS/PCBM:P3HT/Ca/Al) and without encapsulation suffer a rapid decay in just two days. It was suggested that the coverage of three-dimensional C-PCBSD network on ZnO buffer layer might have passivated the hot spots generated in ZnO CBLs to suppress the leakage current, and thus improved the device lifetime.[247, 250]

Stubhan *et al*. investigated the modification of AZO buffer layer with phosphonic acid anchored SAMs (as illustrated in Fig. 18c).[203] They demonstrated that the phosphonic acid anchored SAM decorated AZO could increase R_{SH} and decrease the R_S of the device duo to the improved charge transfer from the PCBM to AZO. The average PCE had been improved by approximately 15% from 2.9% to 3.3%. More recently, Cho *et al*. demonstrated that the PCBM itself could serve as an interfacial modification material (Fig. 18d).[248] They suggested that the PCBM layer between ZnO and BHJ active layer can effective quench electron-hole recombination by reducing trapped charges at ZnO surface, which resulted in a 16% increase in the PCE (up to 7.7%) compared to devices without an additional PCBM layer. The C60-based modifiers with weaker acids have been also explored to modifying ZnO CBL.[50, 170, 245] It has been found that the modifiers with ester units exhibit much weaker acidity and better affinity to ZnO surface.[170] Li *et al*. developed a C60 pyrrolidine tris-acid ethylester (PyC60) with three ester groups to modified ZnO CBL (Fig. 18e).[50] By using this PyC60 upper layer modified ZnO NPs film as the CBL, high efficiency (average PCE of 8.62%) inverted PCSs based on photoactive layer of PTB7: $PC_{71}BM$ blend were achieved. The authors demonstrated that the PyC60 improves the morphology quality of ZnO/ PyC60 film by filling in the voids of ZnO layer and partly passivating the defects of ZnO NPs. It was indicated that the PyC60 could also improve the interfacial contact between the ZnO and active layer, lowering the electron injection barrier. As a result, the ZnO/ PyC60 CBL effectively decreased R_S and interfacial charge recombination, and increased electron injection and collection efficiency in the inverted PSCs.[50]

5.3 Non fullerene based interlayer modification of ZnO CBLs

Non-fullerene based interlayer, such as: mixed SAM,[242] poly(ethylene oxide) (PEO),[175] poly(ethyleneimine) (PEI),[87] ruthenium dye N719,[200] conjugated polyelectrolyte (CPE),[251, 252] HfO_2,[150] Ionic liquids (Ils)[53] and ultrathin metal oxides layers[136, 152, 253, 254] layers have also been studied to modify ZnO CBLs for further improving the performance of inverted PSCs. The improvement of photovoltaic parameters of inverted devices by using non-fullerene based interlayer modified ZnO CBLs in literature are summarized in Table 5.

Bulliard *et al*. reported a mixed SAM to control the surface energy of the ZnO buffer layer.[242] They found that, through changing the surface composition of the two different SAMs (Fig. 19a), the surface energies of the ZnO CBL were tuned over a wide range of values (between 40 mN m^{-1} and 70 mN m^{-1}) with negligible changes in its work function.[242] They suggested that a surface treatment to obtain an intermediate surface energy above the neutral range favors the competition between lateral and vertical phase separation, resulting in morphology with desirable domain size. By tuning the surface energy of ZnO CBLs in a given range, the PCE increased from 3.27% to 3.70%. Yoo *et al*., developed several SAMs derived from benzoic acid or benzoyl chloride to tune the work function and surface properties of ZnO CBLs.[255, 256] It was demonstrated that the benzoic acid interlayer could form a favorable interface dipole at the interface between the ZnO and active layer, thus to passivate the ZnO surface traps and accordingly reduce the work function and facilitate electron transport.

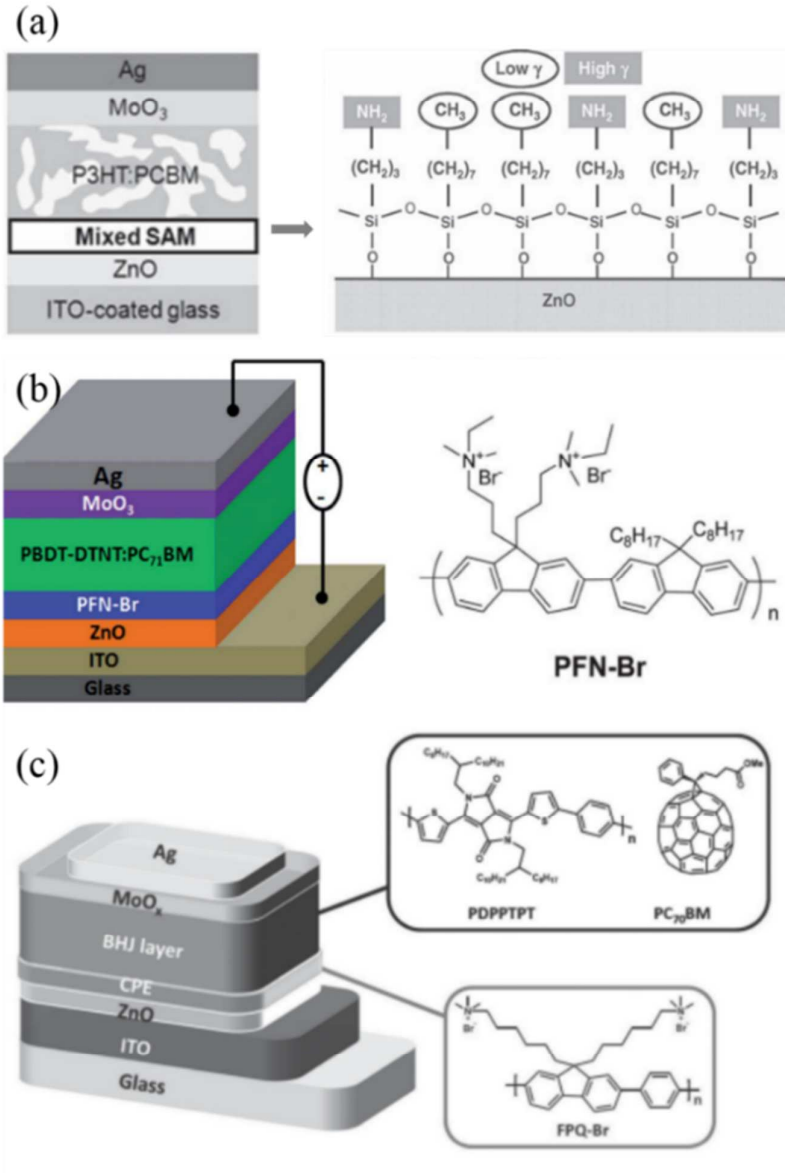

Fig. 19 Schematic illustrations of inverted device structures and chemical structures of ZnO surface modification materials including (a) mixed SAM, (b) poly [(9,9-bis(3'-(N,N-dimethylamino)propyl)-2,7-fluorene)-alt-2,7-(9,9-dioctylfluorene)] (PFN-Br),[252] and (c) bromide counterions (FPQ-Br)[251]

Table 5. Non exhaustive survey of inverted polymer solar cells including modified ZnO CBLs with non-fullerene based interlayers. The photovoltaic parameters are compared to those measured for a reference cell (values in parentheses), when available, made with a pristine ZnO CBL.

Device architecture	J_{sc} [mA cm^{-2}]	V_{oc} [V]	FF [%]	PCE [%]	Ref.
ITO/ZnO/Mixed-SAM/P3HT:PCBM/MoO_3/Ag	9.65	—	—	3.70	242
ITO/ZnO/TiO_2/P3HT:PCBM/Ag	9.81	0.58	46	2.65	136
	(9.04)	(0.59)	(47)	(2.53)	
ITO/ZnO/P3HT:PCBM/PEDOT:PSS/Au	11.89	0.59	64.1	4.5	150
	(11.14)	(0.59)	(61.8)	(4.1)	
ITO/ZnO/PFN-Br/PBDT-DTNT:PC_{71}BM/MoO_3/Ag	17.4	0.75	61	8.4	252
	(15.2)	(0.69)	(55)	(6.1)	
ITO/ZnO/Cs_2CO_3/P3HT:PCBM/MoO_x/Al	11.27	0.58	65.2	4.26	253
	(10.83)	(0.56)	(61.7)	(3.74)	
ITO/ZnO-Al/N719/P3HT:PCBM/WO_3/Al	10.46	0.61	60.00	3.83	200
	(10.22)	(0.56)	(48.81)	(2.79)	
ITO/ZnO/PEO/TQ1:PC_{71}BM/MoO_3/Ag	9.6	0.877	67	5.64	175
	(8.69)	(0.864)	(60)	(4.50)	
ITO/ZnO-ALD-ZnO/PTB7-F20:PC_{71}BM/PEDOT:PSS/Ag	17.9	0.672	65.9	7.96	152
	(16.9)	(0.679)	(66.5)	(7.66)	
ITO/ZnO/PEO/PDPPTPT:PC_{70}BM/MoO_3/Ag	14.5	0.78	62	7.04	251
	(13.4)	(0.78)	(63)	(6.37)	
ITO/ZnO/DPA-BA/P3HT:PCBM/MoO_3/Ag	8.34	0.61	54.6	2.78	255
ITO/ZnO/Cz-BA/P3HT:PCBM/MoO_3/Ag	8.29	0.62	56.1	2.88	255
	(7.83)	(0.60)	(53.0)	(2.49)	
ITO/ZnO/BBC/P3HT:PCBM/WO_3/Ag	9.00	0.58	55.6	2.90	256
	(8.63)	(0.58)	(50.2)	(2.51)	
ITO/ZnO/PEI/PTB7:PC_{71}BM/MoO_3/Al	17.19	0.73	69.6	8.76	87
	(16.00)	(0.71)	(62.0)	(6.99)	
ITO/ZnO/EDT/P3HT:PC_{61}BM/MoO_3/Ag	11.88	0.61	71	4.8	243
	(11.24)	(0.59)	(63)	(3.8)	
ITO/ZnO/[BMIM]BF4/PTB7:PC_{71}BM/MoO_3/Ag	17.50	0.73	67.7	8.65	53
ITO/ZnO/[BzMIM]Cl/PTB7:PC_{71}BM/MoO_3/Ag	16.97	0.72	69.5	8.49	53
	(16.09)	(0.72)	(64.8)	(7.51)	
IITO/ZnO/[BMIM]BF4/PTB7-Th:PC_{71}BM/MoO_3/Ag	17.43	0.78	70.3	9.56	53
	(17.19)	(0.78)	(66.7)	(8.94)	

Conjugated polyelectrolyte (CPE) have been reported to serve as a cathode buffer layer between the cathodic electrode and active layer in inverted PSCs to improve device performance by changing the electronic and orbital interactions at the interface.[45, 51, 88] CPE has also been employed as efficient interlayer materials to modify ZnO CBLs.[206, 207] Yang *et al*. reported the use of a thin layer (~5 nm) conjugated polyelectrolyte, poly [(9,9-bis(3'-(N,N-dimethylamino)propyl)-2,7-fluorene)-alt-2,7-(9,9-dioctylfluorene)] (PFN-Br), shown in Fig. 19b, on ZnO CBL to reengineer the interface between ZnO and PBDT-DTNT:PC_{71}BM.[252] In their study, the inverted PSCs with device architectures of ITO/ZnO/PFN-Br/PBDT-DTNT: PC_{71}BM/MoO_3/Ag showed a J_{sc} of 17.4 mA cm^{-2}, a V_{oc} of 0.75 V, a FF of 61% and an average PCE up to 8.4% was attained. The conduction band edge of ZnO was tuned from -4.46 eV to -4.08 eV (ZnO/PFN-Br) by using a PFN-Br thin layer, leading to an enhancement of the V_{oc} of the device. The enhanced J_{sc} and FF in the inverted PSCs with the PFN-Br interfacial layer were ascribed to the improved contact between PFN-Br interfacial layer and active layer, which was better than the interfacial layer formed between naked ZnO layer and active layer. As a result, over 37% enhancement in the PCE was obtained. Another conjugated polyelectrolyte (CPE), poly(9,9' –bis(6'' –N,N,N trimethylammoniumhexyl) fluorene-co-alt-phenylene) with bromide counterions (FPQ-Br, as shown in Fig. 19c) has also been successfully employed as an interlayer between ZnO and active layer to improve the electron transport and interfacial contact.[251] Compared with the device based on bare ZnO layer, the J_{sc} increased by 11% and the PCE increased from 6.37% to 7.04% for the device with ZnO/CPE layer.

Woo *et al*. report an appreciable PCE enhancement in inverted PSCs by using an electron-rich polymer nano-layer (poly(ethyleneimine) (PEI)) modified ZnO CBL (Fig. 20a).[87] The thickness of the PEI nano-layer was controlled to be only 2 nm in view of its high insulting character. It has been demonstrated that the enhanced PCEs is owning to the lowered conduction band energy of ZnO via the formation of an interfacial dipole layer at the interface between ZnO layer and PEI nano-layer (Fig. 20b). They also found that the PEI nano-layer could increase the surface roughness of ZnO, which noticeably decreases the series resistance of device. As a result, the inverted PSCs with structure of ITO/ZnO-PEI/PTB7:PC_{71}BM/MoO_3/Ag resulted in a PCE up to 8.9%, while

the devices using only ZnO or PEI buffer layer show relatively low PCEs, 6.99% and 7.49%, respectively. The enhanced PCE mainly resulting from the increased J_{sc} and FF for devices with ZnO/PEI layer was attributed to the fast electron transport.

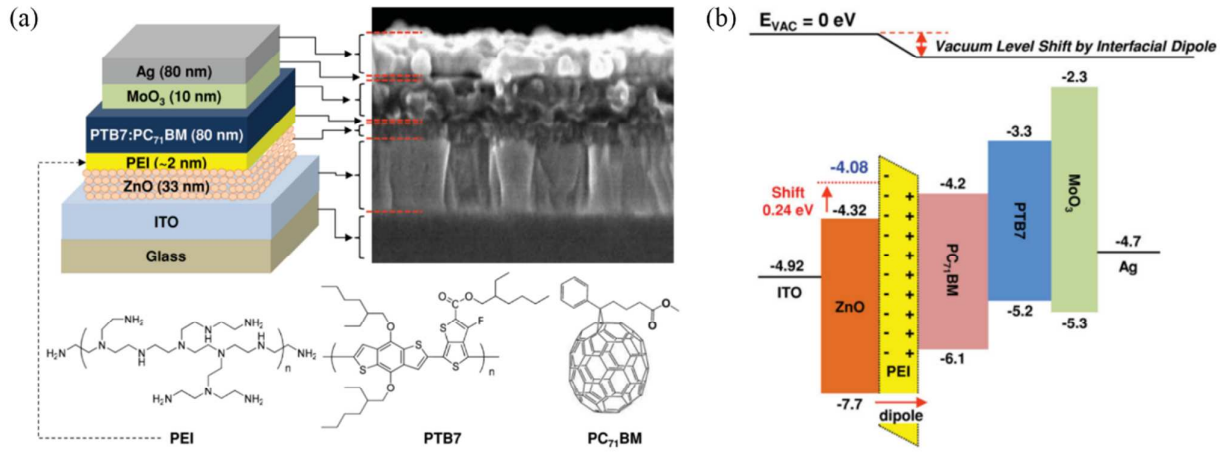

Fig. 20 (a) Inverted PSCs with PEI-coated ZnO CBL: illustration of device structure (top left), SEM image for the cross-section of the device (top right), and chemical structures of PEI, PTB7, and $PC_{71}BM$ (bottom). (b) Flat energy band diagram of the device with PEI-coated ZnO CBL where the conduction band energy of the ZnO CBL was lowered by 0.24 eV due to the dipole formation by the PEI nano-layer.[87]

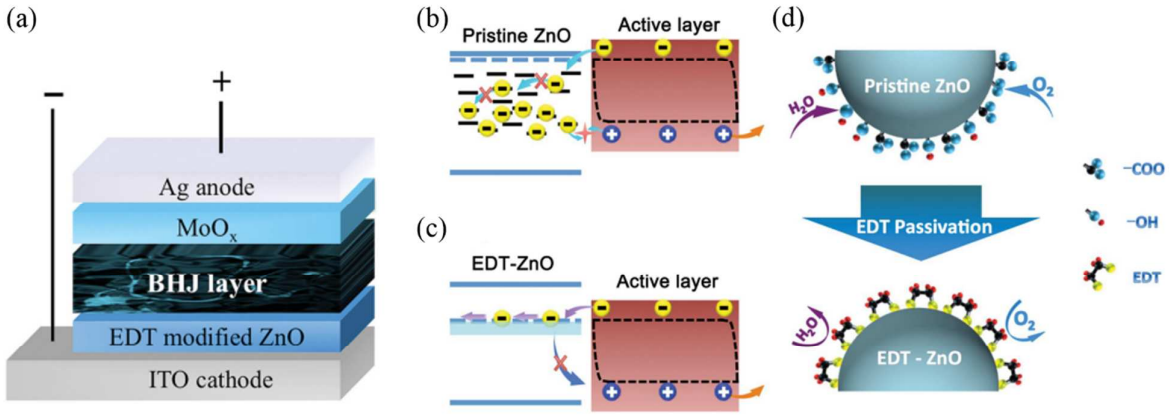

Fig. 21 (a) Schematic illustration of inverted device structure with EDT modified ZnO CBL. (b) Various intragap states of pristine ZnO layers, which act as recombination centres for photogenerated charges. (c) The intragap states are modified to a new intergap band, which facilitates electron transport in CBLs, thereby suppressing the interfacial bimolecular recombination and enhancing the charge extraction properties of the devices. (d) Schematic view showing that the various surface groups are removed and EDT molecules are covalently bound onto ZnO.[243]

Ionic liquids (ILs) have been investigated to serve as a CBL material and as a surface modification layer to modify ZnO buffer for inverted PSCs. Yu *et al*. reported a remarkable PCE exceeding 10% (10.15%) for the single-junction PTB7-Th:$PC_{71}BM$ inverted PSCs with a solution processed ZnO/[BMIM]BF4 combined CBLs.[53] The PTB7:$PC_{71}BM$ inverted PSCs with the ZnO/[BMIM]BF4 CBL achieved an average PCE pf 8.71% (champion PCE of 9.12%), which is 15.2% (champion 21.4%) increase compared to the control devices based on pure ZnO (PCE of 7.51%). The simultaneously enhanced J_{sc}, FF and PCEs were attributed to the decreased interfacial energy barrier due to the decreased work function of the cathode by forming spontaneous dipolar polarization at the interface. They demonstrated that the IL layer and the ZnO/IL combination layers with low work function, good optical transmittance, improved electron extraction and reduced resistance at the cathode interface, make an excellent and general interfacial layers for inverted PSCs. It has been found that the [BzMIM]Cl or ZnO/[BzMIM]Cl combined CBL showed a similar improvement of the device performance to the inverted devices based on [BMIM]BF4 or ZnO/[BMIM]BF4 combined CBL. Recently, Bai *et al*. developed a facial and general ethanedithiol (EDT) treatment method to passivate the surface defects and modulate the intragap states of ZnO CBLs

fabricated with solution-processing at low-temperature (Fig. 21a).[243] They demonstrated that the covalent bonding of EDT molecules onto ZnO nanocrystals could effectively remove various surface defects of ZnO nanocrystal layers by forming zinc ethanedithiolates during the EDT treatment. Due to the chemical changes through EDT-passivation, the intragap states in pristine ZnO nanocrystals were modulated and a new intragap band was introduced (Fig. 21b and 21c), resulting in enhanced electron selectivity and improved electron transport properties to EDT-treated ZnO CBL. As a result, the inverted devices with EDT-treated ZnO CBL exhibited reduced charge recombination and enhanced charge extraction property. The EDT treatment was also found to result in significantly improved of the ambient stability of the inverted PSCs. For the unencapsulated P3HT:PC61BM devices with EDT-treated ZnO CBL, the PCE remained 90% of its original value after being exposed to dark and ambient conditions for 30 days. In contrast, the PCE of control device with pure ZnO CBL degraded to around 60% of the original value under the same conditions. The improved device stability was ascribed to the well-passivated EDT-treated ZnO films, which are less susceptible to oxygen and water molecules (as shown in Fig. 21d). Furthermore, it has been demonstrated that the EDT-passivation method is suitable for both colloidal nano-crystals and sol-gel derived ZnO films.[243]

Several kinds of metal oxides and salts, such as TiO_2,[136] Cs_2CO_3,[253] hafnium dioxide [150] and even ZnO [152, 254] itself have been investigated to modify ZnO CBLs. Seo *et al*. reported that an ultrathin TiO_2 layer with a mean thickness less than 3 nm could slightly enhance the photovoltaic performance of inverted PSCs, while a thicker TiO_2 film resulted in reduced photovoltaic performance.[136] Based on the photoelectron spectroscopy study, it was suggested that the ultrathin TiO_2 layer could quench the recombination of electrons and holes on the surface of ZnO CBL. Cheng *et al*. modified ZnO NPs CBL by coating a thin layer of Cs_2CO_3, using solution process.[253] They demonstrated that the ZnO/Cs_2CO_3 bilayer presented enhanced electron-extraction and leakage-current-suppression abilities due to its modified energy level and improved surface morphology. As a result, about 40% enhancement in the PCE was obtained. More recently, Kim *et al*. reported that the wet-chemically prepared ripple-structured ZnO CBLs could be modified by depositing a very thin ZnO layer by ALD method.[152] They found that a 1~2 nm ALD-ZnO layer can effectively quench the electron-hole recombination caused by surface defects of ZnO ripples, and thus enhance the J_{sc} and PCE of inverted devices. Modifying the surface of ZnO CBL surface with a 0.6 nm ALD HfO_2 layer has been also reported to enhance the electron injection and hole-blocking, leading to the PCE increasing from 4.1% to 4.5%.[150] The R_{SH} of the devices increased significantly with the addition of the HfO_2 layer, while the R_S decreased. It was explained that the enhancement in the electron transport arose from the HfO_2 layer which passivated the ZnO CBL and reduced the defect states on ZnO surface, thereby suppressed the loss of electrons caused by charge recombination at the defect sites. It should be noted that the deteriorated performance of device with HfO_2 layer thicker than 0.6 nm indicated that the enhancement in electron transport is reduced due to the insulating effect of the HfO_2 layer, which became dominant in the case of thick HfO_2. Besides the modification of the interface between ZnO and active layer, the modification of the interface between ZnO and ITO electrode has also been investigated to achieve more efficient collection and transport of electrons from ZnO layer to ITO.[257] Yoon *et al*. reported that inserting a nanoscopic copper hexadecafluorophthalocyanine (F16CuPc) nanowire film between ZnO layer and ITO electrode of inverted PSCs can increase the performance of inverted PSCs by enhancing interfacial electron transport.[257]

6. ZnO-based nanocomposite CBLs

6.1 ZnO/polymer nanocomposite CBLs

For low-temperature solution-processed ZnO CBLs, the general presence of high density defects, such as dangling bonds and surface groups, and poor spatial distribution of nanoparticles over a large area restrict their contribution to enhancing the performance of inverted PSCs.[173, 174] The development of uniform ZnO NPs films with low density defects is essential to achieve high performance of inverted PSCs. Recently, polymer modified ZnO films, known as the so-called ZnO/polymer hybrids or nanocomposites, have been studied to meet such challenges.[174, 175, 258-261] For example, the ZnO/polymer composites, such as ZnO/poly(ethylene oxide) (PEO),[175] ZnO/poly (ethylene glycol) PEG,[259] ZnO/fullerene-end-capped poly(ethylene glycol) (C60-PEG),[262] ZnO/Polyethylenimine (PEI),[261] ZnO/polyacrylic acid (PAA),[263] ZnO/poly(zinc diacrylate) (pZA),[258] ZnO/poly (diallyldimethylammonium chloride) (PDADMAC)[260] and ZnO/Polyvinylpyrrolidone (PVP)[174, 260] have been studied to serve as the efficient CBL in inverted PSCs to further improve the device performance. The improvement of photovoltaic parameters of inverted devices using ZnO/polymer hybrids or nanocomposites CBLs is summarized in Table 6.

Table 6. Non exhaustive survey of inverted PSCs including ZnO/polymer hybrid or composite CBLs. The photovoltaic parameters are compared to those measured for a reference cell (values in parentheses), when available, made with a pristine ZnO CBL.

Device architecture	J_{sc} [mA cm^{-2}]	V_{oc} [V]	FF [%]	PCE [%]	Ref.
ITO/ZnO-PVP/PDTG-TPD:$PC_{71}BM$/MoO_3/Ag	14.0	0.86	67.3	8.1	174
ITO/ZnO-pZA/P3HT:PCBM/MoO_3/Ag	9.21 (9.02)	0.58 (0.55)	61 (52)	3.26 (2.58)	258
ITO/ZnO-pZA/PTB7:$PC_{71}BM$/MoO_3/Ag	14.03	0.73	72	7.37	258

	(13.83)	(0.72)	(67)	(6.67)	
ITO/ZnO-PEG6000/P3HT:PCBM/PEDOT:PSS/Ag	10.19	0.581	55.9	3.3	259
	(8.36)	(0.550)	(49.7)	(2.3)	
ITO/ZnO-PSS/P3HT:PCBM/MoO_3/Al	1.77	0.45	54.00	0.42	260
ITO/ZnO-PVP/P3HT:PCBM/MoO_3/Al	9.62	0.59	40.00	1.71	260
ITO/ZnO-PDADMAC/P3HT:PCBM/MoO_3/Al	10.82	0.54	33.00	1.86	260
	(0.25)	(0.59)	(58.20)	(0.10)	
ITO/ZnO-PEO/TQ1:$PC_{71}BM$/MoO_3/Ag	9.6	0.877	67	5.64	175
	(8.69)	(0.864)	(60)	(4.50)	
ITO/ZnO-PEI/P3HT:PCBM/MoO_3/Ag	11.4	0.60	67	4.6	261
	(10.3)	(0.60)	(60)	(3.7)	
ITO/ZnO-PEI/PBDTTBO:$PC_{71}BM$/MoO_3/Ag	14.7	0.85	70	8.7	261
	(13.3)	(0.85)	(65)	(7.3)	
ITO/ZnO-PAA/PBDTTPD:$PC_{71}BM$/MoO_3/Ag	12.1	0.86	54	5.6	263
	(11.9)	(0.84)	(46)	(4.6)	
ITO/ZnO-C60-PEG/PTB7:$PC_{71}BM$/MoO_3/Ag	15.86	0.733	69.1	8.0%	262
	(15.51)	(0.724)	(61.4)	(6.9)	

Shao *et al*. reported that the poly(ethylene oxide) (PEO) modification to the ZnO NPs surface could effectively passivate the surface traps, suppress the recombination loss of carriers, reduce the R_S as well as improve the electrical coupling of ZnO/active layer.[175] For the inverted devices composed of TQ1: PCBM and PCDTBT:$PC_{71}BM$ active layers, the PCE of the devices using 0.05 % PEO-modified ZnO NPs (PEO/ZnO wt%) layer increased to 5.4% and 6.59% from 4.5% and 5.39% for the reference devices based on unmodified ZnO. However, when the PEO content was increased to 1 wt%, the device performance decreased due to the very rough surface of ZnO-PEO films. To effectively hybridize ZnO with polymer, both the amount and molecular weight of the polymer should be tailored to achieve desired interface and electrical properties of ZnO/polymer nanocomposites CBLs, as well as the device performance.[175, 259] Hu *et al*. fabricated ZnO/poly (ethylene glycol) PEG hybrids as CBL to improve the performance of inverted PSCs, as shown in Fig. 22a.[259] They demonstrated that the PEG can passivate the surface traps of ZnO NPs and thus suppress the interfacial charge recombination, decrease the work function and improve the energy level alignment between the $PC_{61}BM$ and ZnO. They suggested that the PEG chains wrapped around the ZnO surface could share their lone electron pairs of oxygen in the backbone with ZnO NPs, and thus passivate the shallow surface traps of ZnO. In their study, the effect of molecular weight of PEG on the property of ZnO-PEG CBLs and the performance of inverted PSCs have been investigated. It has been found that, compared to the devices with ZnO/PEG400 CBL and ZnO/PEG20000 CBL (with average molecular weight of 400 and 20000, respectively), the devices using ZnO/PEG6000 (with averaged molecular weight of 6000) hybrids exhibited the best performance (PCE = 3.3%). This result was ascribed to the short backbone of PEG (e.g., MW = 400) containing less oxygen which could not effectively passivate ZnO surface traps. But the PEG with long backbone (e.g., MW = 20000) could lead to the formation of a charge transport barrier because of the insulating nature of PEG with long backbone.[259] Recently, by in situ grown ZnO from amphiphilic fullerene-end-capped poly(ethylene glycol) (C60-PEG) at relatively low temperatures, Hu *et al*. employed this amphiphilic fullerene/ZnO hybrids (ZnO@C60-PEG) as CBLs to improve charge selectivity of inverted PSCs.[262] They demonstrated that the C60-PEG could act as an n-dopant to the ZnO while the oxygen-rich PEG side chain of C60-PEG could passivate the defects of the ZnO. In addition, it was believed that the amphiphilic C60-PEG could facilitate the compatibility of the inorganic ZnO CBL and organic active layer. As a result, compared to the pure ZnO, they demonstrated that the ZnO@C60-PEG possessed a decreased work function, less defects, higher electron mobility, which could effectively reduce the recombination of carriers and enhance electron extraction. Consequently, the PCE of the inverted PSC based on the ZnO@C60-PEG CBL and with PTB7:$PC_{71}BM$ active layer reached 8.0%. Due to the modification of C60-PEG to ZnO with fewer defects, the inverted PSCs with ZnO@C60-PEG hybrid CBLs also exhibited a better stability than the devices with bare ZnO CBLs.

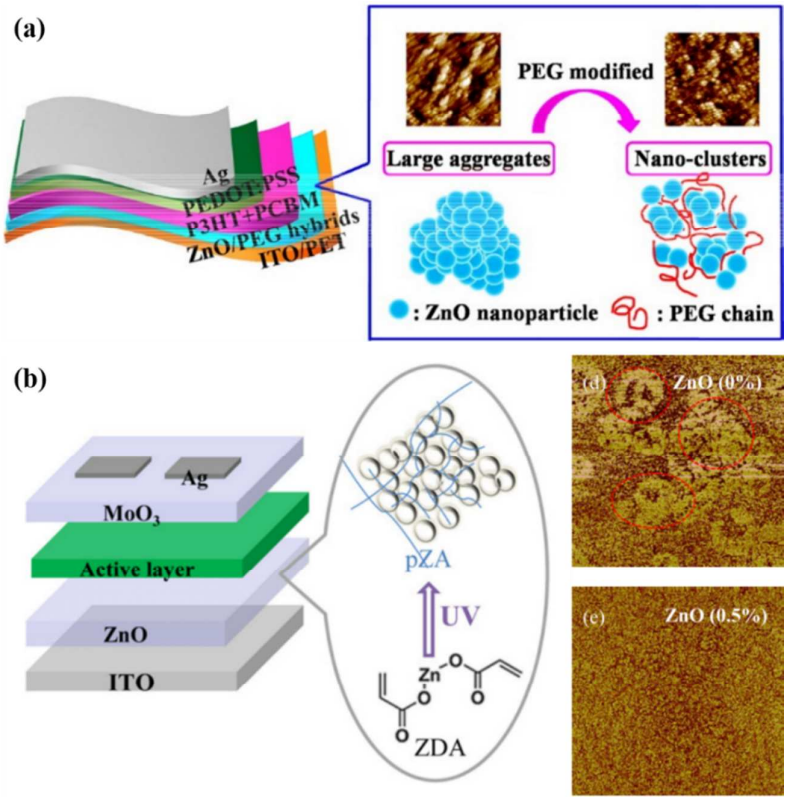

Fig. 22 (a) Schematic illustration of the inverted PSC with ZnO/PEG hybrids film as CBL. The insert is the AFM images and schematic diagrams of ZnO aggregates and PEG modified ZnO nano-clusters.[259] (b) Schematic diagram of inverted PSC with ZnO/pZA CBL (left) and a brief processes in the fabrication of pZA network (insert), and the AFM images of ZnO/pZA hybrids films with 0% and 0.5% pZA weight ratio to ZnO NPs (right), the scan size is 2 um × 2 um.[258]

The poly(zinc diacrylate) (pZA) was used to passivate the defects in ZnO CBL, as shown in Fig. 22b.[258] By in situ cross-linking poly(zinc diacrylate) (pZA) on ZnO films with a 3D network, Wu et al. demonstrated that the incorporation of pZA in ZnO NPs layer could decrease the trap-assisted recombination rather than giving better energy alignment between the active layer and the ZnO interlayer.[258] Based on the pZA cross-linked ZnO CBL derived from ZnO NPs solution containing 0.5 wt% zinc diacrylate (ZDA), the inverted PSCs composed of respective P3HT:PCBM and PTB7:$PC_{71}BM$ active layer achieved PCE of 3.26% and 7.37%, respectively, while the PCEs for the reference devices without pZA were 2.58% and 6.67% for P3HT:PCBM and PTB7:$PC_{71}BM$ active layers, respectively. The improvement in the device performance was attributed to the enhanced charge generation and transport. Polyvinylpyrrolidone (PVP) is yet another polymer studied for the preparation ZnO/polymer nanocomposite CBLs for high efficient inverted PSCs.[174, 260] Small *et al*. reported the preparation and application of ZnO-PVP nanocomposite CBL in inverted PSCs[174] and found that the ZnO-PVP nanocomposite films exhibited more uniform distribution of the ZnO nano-clusters in polymer matrix in view of suppressing ZnO aggregation. The inverted devices with UV-ozone treated (10 min) ZnO-PVP nanocomposite CBL and PDTG–TPD:$PC_{71}BM$ active layer showed a PCE of 8.1% with a J_{sc} of 14.0 mA cm^{-2} , a V_{oc} of 0.86 V, and a FF of 67.3%. It was suggested that the PVP acted as an organic capping molecule and polymeric matrix, promoting the formation of ZnO electron-transporting nanocomposite films with uniform morphology. Tiwari *et al*. compared the effects of ZnO-polyelectrolytes [poly (diallyldimethylammonium chloride) (PDADMAC), Poly (acrylic acid sodium salt) (PAS), poly (4-styrenesulfonic acid) (PSS), and Polyvinylpyrrolidone (PVP)] nanocomposites CBLs on the device performances.[260] They found that the combination of ZnO with PVP and PDADMAC gave the highest improvement in the PCEs. Besides serving as a matrix for suppressing ZnO aggregation and passivating the surface traps in ZnO films, it has also been found that the ZnO/polymer composite exhibited adjustable energy bands.[261] Chen *et al*. reported a solution processed ZnO/Polyethylenimine (PEI) nanocomposite electron transport layers for facilitating electron extraction in inverted PSCs.[261] They found that the energy bands of ZnO/PEI composite could be tuned considerably by varying the content of PEI, and thus forming a good electron transport layer. In addition, by adjusting the content of PEI, the structural order of ZnO in the ZnO/PEI films was adjusted to align perpendicular to the ITO electrode, facilitating the electron transport vertically in ZnO/PEI nanocomposite film.[261]

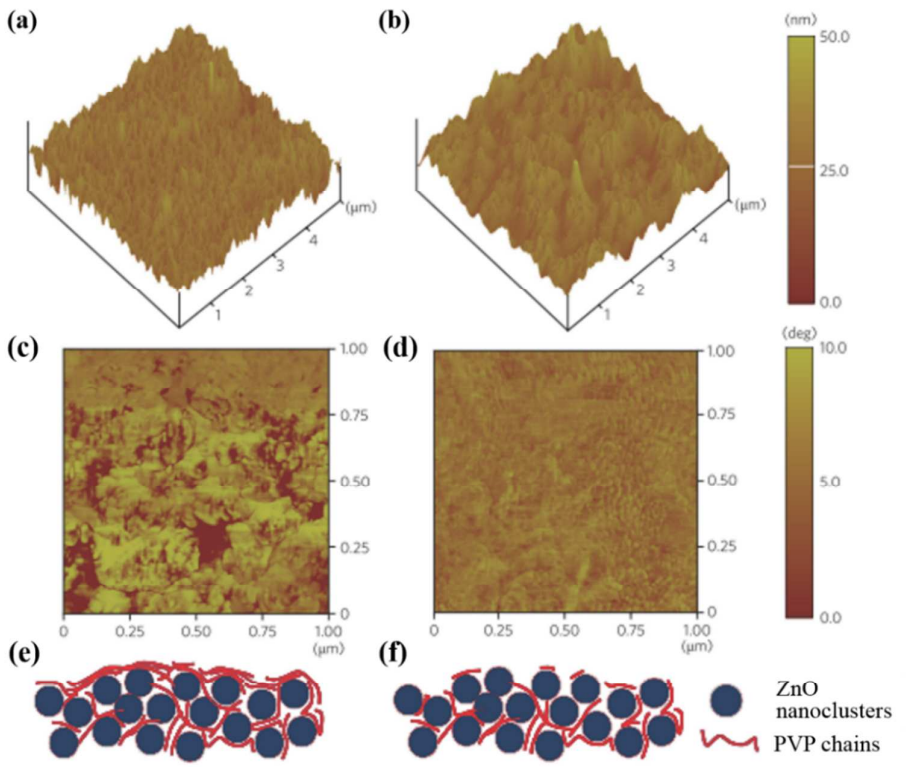

Fig. 23 Three-dimensional topography AFM images of (a) as-prepared and (b) 10 min UVO treated ZnO-PVP nanocomposite films. Phase images of (d) as-prepared and (d) 10 min UVO treated ZnO-PVP nanocomposite films. Schematic illustrations of (e) as-prepared and (f) 10 min UVO treated ZnO-PVP nanocomposite films.[174]

It is worth noting that, a crucial issue for ZnO-polymer composite or organic-stabilized ZnO NP CBLs is the removal of polymer or organic surfactant so as to improve the electrical properties of ZnO CBL as well as the device performance. This is because the insulating polymer or organic surfactant will aggravate the charge transport by introducing additional resistance.[173,174] ultraviolet-ozone (UVO) treatment is regarded as a promising approach to remove polymer from ZnO surface and to ensure a good electrical coupling between ZnO and active layer in view of the act that UVO treatment did not alter the size, shape or distribution of ZnO NPs. Cho *et al*. suggested that UVO treatment could effectively remove the residual organic stabilizer molecules on the surface of ZnO NPs films through an UV induced decomposition mechanism.[173] Small *et al*. investigated the UVO treatment duration on the performance of inverted solar cells with ZnO-PVP composite film as CBL and found that ZnO-PVP nanocomposite films with UVO treated for 10 min led to the highest enhancement in the device performance compared to the devices without UVO treatment.[174] It has been found that the UVO treatment removed the top PVP enabling the ZnO NPs to expose at the film surface, which was proven by both AFM (Fig. 23a–23d) and X-ray photoelectron spectroscopy (XPS) characterizations. The enhanced device performance with UVO treated ZNO-PVP nanocomposite films was ascribed to the modified surface composition promoting charge collection. The UVO treatment time is a crucial factor that determines the morphology and electrical property of ZNO-PVP nanocomposite films. It has been demonstrated that a too short time treatment results in an incomplete removal of the PVP from the top surface of ZnO-PVP composite films, while a too long time treatment may induces excess oxygen onto the ZnO surface, which will reduce the electron extraction efficiency.[174] Over all, polymer modified ZnO NPs/polymer hybrid or composite films are of more uniform and with low defects than the unmodified ZnO NPs films. By choosing suitable polymer or organic surfactant material, adjusting the amount and molecular weight of polymer, and employing an optimized UVO treatment process, one can expect to enhance the performance of ZnO/polymer composite CBL as well as the device performance.

6.2 ZnO and oxide or titanate composite CBLs

The composites of ZnO and other oxides or titanates have been also studied as CBLs of inverted PSCs. Lan *et al*. studied the Ta_2O_5-ZnO composite films with varied composition fabricated by sol–gel processing as the CBL for inverted polymer solar cells, and demonstrated enhanced PCE with excellent stability.[264] It was found that the CBLs incorporated with Ta_2O_5 exert two competing impacts on the solar cell performances. On one hand, the presence of Ta_2O_5 is likely to induce more positive charges around the Zn atom and form Ta-O-Zn bonding; it can reduce the surface charge recombination between the active layer and the Ta_2O_5-ZnO

composite CBL, and result in high power conversion efficiency; however, on the other hand an excessive amount of Ta_2O_5 would block the pathways of charge transport and lead to a drastic reduction in power conversion efficiency. In their results, the integration of 12% - 15% Ta_2O_5 into ZnO may result in the efficiency enhanced maximally for different active layers; the addition of excessive Ta_2O_5 would however lead to a dramatic decrease in the device performance, as the photovoltaic parameters shown in Table 7. In addition, the inverted PSCs with Ta_2O_5-ZnO nanocomposite CBLs exhibited excellent long-term stability in air. In their work, the inverted PSCs with ZnO or Ta_2O_5-ZnO nanocomposite CBLs retained almost 100% of their original PCEs after being exposed to ambient condition for 42 days without encapsulation.

Table 7. Non exhaustive survey of inverted polymer solar cells including a ZnO and oxide or titanate composite CBLs. The photovoltaic parameters are compared to those measured for a reference cell (values in parentheses) based on pristine ZnO CBL.

Device architecture	J_{sc} [mA cm^{-2}]	V_{oc} [V]	FF [%]	PCE [%]	Ref.
ITO/Ta_2O_5–ZnO/P3HT:PCBM/MoO_3/Ag	9.64	0.637	67.0	4.12	264
	(9.49)	(0.636)	(61.3)	(3.70)	
ITO/Ta_2O_5–ZnO/PSEHTT:$PC_{71}BM$/MoO_3/Ag	12.07	0.68	68.9	5.61	264
	(12.04)	(0.67)	(65.6)	(5.29)	
ITO/$SrTiO_3$:ZnO/P3HT:PCBM/PEDOT:PSS/Ag	10.08	0.63	64.7	4.10	98
	(10.16)	(0.61)	(57.0)	(3.58)	

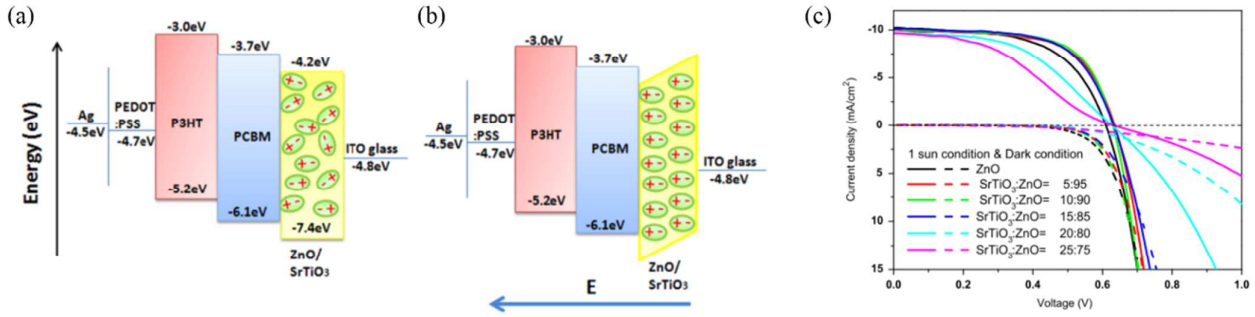

Fig. 24 Schematic energy level diagrams of inverted PSCs with $SrTiO_3$: ZnO composite CBLs. (a) The inverted device is under open circuit condition, and there is no net interface dipole. (b) The inverted device is under illumination, electron field was generated by electron and hole transfer to the opposite direction and there is a net interface dipole directed away from the CBL. (c) I–V curves of inverted PSCs with various $SrTiO_3$: ZnO composite CBLs.[98]

In another work also done by Lan *et al.*, dual phase $SrTiO_3$:ZnO nanocomposite films with varied composition ratios were fabricated by sol-gel processing and applied as CBLs in inverted PSCs, and demonstrated enhanced devices performance.[98] In their work, when the $SrTiO_3$:ZnO nanocomposite CBLs were assembled to the solar cell, the device properties including incident photon-to-current conversion efficiency (IPCE), power conversion efficiency, and electron mobility were investigated systematically. $SrTiO_3$ in CBL was found to be amorphous or quasi-amorphous. Although more detailed experiments are needed, $SrTiO_3$ is more likely to have some local ordering structure with aligned TiO_6 octohedra, i.e., quasi-amorphous phase, and thus possesses spontaneous polarization. It has been demonstrated that the localized polar molecules $SrTiO_3$ in the nanocomposite CBL are in random orientations in the dark condition or open circuit voltage condition (Fig. 24a), while a self-built electric field on the interface between the active layer and CBL was generated by electron and hole transfer to the opposite direction and there is a net interface dipole directed away from the cathodic buffer layer under illumination (Fig. 24b). It was suggested that such a spontaneous polarization is likely to induce a self-built electric field to prevent electron recombination on the interface of the active layer and CBL, which shows an enhancement of FF of device performance. As a result, an enhancement in PCE from 3.58% to 4.1% was achieved for the device with $SrTiO_3$:ZnO of 90:10 CBL and P3HT:PCBM active layer.[98] Fig. 24c shows the I-V curves of inverted devices with various $SrTiO_3$:ZnO nanocomposite CBLs. It was suggest that a further improvement of the solar cells performance could be expected by improving the crystallinity of both $SrTiO_3$ and ZnO.

Concluding remarks

PSCs is a complex device, so far high performance can only be achieved when all the following requirements are met: (1) good p-type polymer donor and n-type fullerene derivative acceptor with desired electronic structure, (2) bulk

heterojunction with desired micro and nanostructures, and (3) interfaces between different layers for efficient charge separation and transport. Inverted PSCs introduce a cathode buffer layer of electron transport but hole blocking material, and thus demand extra efforts to understand and engineer both the interface and the material in terms of chemistry, crystallinity, morphology, surface roughness and contacts, chemical and physical stability, and electrical and electronic properties.

To achieve high power conversion efficiency, long-term device stability and compatible with the low-cost roll-to-roll manufacturing, a lot of more efforts in the aspects of developing new materials, improving chemical and physical properties of interfaces, and low cost scalable processing are required. Further fundamental understanding and innovation and engineering of CBLs are an important aspect for the achievement of highly efficient inverted PSCs. ZnO is the most extensively investigated material serving as CBLs in inverted PSCs due to its relatively high electron mobility, high transparency, ease of fabrication by solution-based processing at low temperature, good chemical stability and low cost.

The role of ZnO CBL in an inverted PSC is to collect and transport electrons and block holes. The contact between ZnO CBL and the polymer active layer can significantly affect the performance of inverted polymer solar cells. The contact quality relies on both the preparation method and the post-treatment, which can influence the properties of ZnO CBL in terms of morphology, thickness and transmittance, and surface state. Doping and surface modification are effective ways to tailor the electronic, optical and chemical properties of the ZnO CBL and thus to improve the photovoltaic performance of the inverted PSCs. To further improve the efficiency of inverted PSCs, some specific considerations in regard of the ZnO-based CBL are list as follows:

(1) Development of ZnO-based CBLs with dense packing, large surface area and high transmittance. A dense and homogenous surface of ZnO CBLs favors the formation of an intimate contact between ZnO CBL and BHJ photoactive layer, and thus lower the contact resistance and decrease the series resistance (R_S) of the device. In addition, the dense surface also makes the ZnO layer having better electrical properties and higher transmittance. The large surface area of ZnO CBL can enlarge ZnO/BHJ active layer contact area, thus providing larger electron extraction interface and enabling more electrode to penetrate into the BHJ active layer so as to reduce charge transport distance and increase the J_{sc} of devices.

(2) Doping ZnO for higher conductivity and appropriate energy level. Appropriate doping can enhance the electrical conductivity of ZnO and thus improve the photovoltaic performance of inverted PSCs.

(3) Development of interfacial materials for surface modification of ZnO-based CBLs, for instance the functional fullerene based SAMs, with appropriate surface energy and improved interfacial properties. The surface modification of ZnO-based CBL helps to reduce the charge recombination and improve the charge transport at the interface by passivating the surface defects, tuning the surface energy and work function, and may thus lead to improved photovoltaic performance of the inverted devices.

Acknowledgements

This work was financially supported in part by the National Natural Science Foundation of China (21373144), Natural Science Foundation of Jiangsu Province of China (BK20140353), Natural Science Foundation of Jiangsu Province (SBK2015010299) and China Postdoctoral Science Foundation (2014M561704). The work was also supported by the National Science Foundation of the U.S. (DMR-1035196 and DMR-1505902), Intel Research Lab, and the University of Washington TGIF.

Abbreviations

AALD	atmospheric atomic layer deposition
ABL	anode buffer layer
AFM	atomic force microscopy
ALD	atomic layer deposition
AM	air mass
AZO	aluminum-doped zinc oxide
BHJ	bulk heterojunction
CBL	cathode buffer layer
C60	fullerene
C60-COOH	2-(p-carboxyphenyl)-N-methylpyrrolidino-C60
C60-PEG	fullerene-end-capped poly(ethylene glycol)
CBD	chemical bath deposition
C-PCBSD	cross-linked [6,6]-phenyl-C61-butyric styryl 32endron ester
CPE	conjugated polyelectrolyte
CuPc	copper phthalocyanine
deZn	diethylzinc
ECD	electrochemical deposition
ECL	electron collection layer (ECL)
ED	electro-deposition
EPBT	energy payback time
ESL	electron selective layer
ETL	electron transport layer
FF	fill factor
FTO	fluorinated tin oxide
GO	graphene oxide
GZO	Gallium-doped zinc oxide
HCL	hole collection layer
HOMO	the highest occupied molecular orbital
HSL	hole selective layer
HTL	hole transport layer
$IC_{60}BA$	indene-C60 bisadduct
$IC_{60}MA$	indene-C60 monoadduct
$IC_{70}BA$	indene-C70 bisadduct
$IC_{70}MA$	Indene-C70 monoadduct
ITO	indium tin oxide
IZO	indium doped zinc oxide
i-ZnO	intrinsic ZnO
J_{sc}	short circuit current density

LUMO	the lowest unoccupied molecular orbital
MEA	methoxyethoxyacetic acid
MoO_3	molybdenum oxide
MPCVD	mist pyrolysis chemical vapor deposition
NF	nanofiber
NP	nanoparticle
NR	nanorod
NW	nanowire
P3HT	poly(3-hexylthiophene)
PCE	power conversion efficiency
PCBM	methyl [6,6]-phenyl-C60-butyrate
$PC_{71}BM$	methyl [6,6]-phenyl-C70-butyrate
PCDTBT	poly[2,6-(4,4-bis-(2-ethylhexyl)-4H-cyclopenta[2,1-b;3,4 b']dithiophene)-alt-4,7-(2,1,3-benzothi-adiazole)]
PDTG–TPD	poly(thieno[3,4-c]pyrrole-4,6-dione-co-dithienogermole
PDADMAC	poly (diallyldimethylammonium chloride)
PEDOT:PSS	poly(3,4-ethylenedioxithiophene): poly(styrene sulfonic acid)
PEG	poly (ethylene glycol)
PEI	Polyethylenimine
PEN	polyethylene naphthalate
PEO	poly(ethylene oxide)
PES	polyethersulfone
PET	polyethylene terephthalate
PSC	polymer solar cell
PsiF-DBT	poly[(2,7-dioctylsi-lafluorene)-2,7-diyl-alt-(4,7-bis(2-thienyl)-2,1,3-benzothiadiaz-ole)-5,5'-diyl]
PVP	poly(vinyl pyrroli-done)
pZA	poly(zinc diacrylate)
R_S	series resistance
R_{SH}	shunt resistance
RF	radio-frequency
RMS	root-mean-square
SAM	self-assembled monolayer
SEM	scanning electron microscopy
SP	spry-pyrolysis
TiO_2	titanium oxide
T_R	relative optical transmittance
UPS	ultraviolet photoelectron spectroscopy
UV	ultraviolet
UVO	ultraviolet -ozone
UV-Vis	ultraviolet-visible
V_{oc}	open circuit voltage
XPS	X-ray photoelectron spectroscopy
XRD	X-ray diffraction
ZDA	zinc diacrylate
$Zn(OAC)_2$	zinc acetate
ZnO	zinc oxide

Notes and references

1. T. Hisatomi, J. Kubota and K. Domen, *Chemical Society reviews*, 2014, **43**, 7520-7535.
2. X. Chen, C. Li, M. Gratzel, R. Kostecki and S. S. Mao, *Chemical Society reviews*, 2012, **41**, 7909-7937.
3. H. M. Chen, C. K. Chen, R. S. Liu, L. Zhang, J. Zhang and D. P. Wilkinson, *Chemical Society reviews*, 2012, **41**, 5654-5671.
4. P. Pinel, C. A. Cruickshank, I. Beausoleil-Morrison and A. Wills, *Renewable and Sustainable Energy Reviews*, 2011, **15**, 3341-3359.
5. A. F. B. Braga, S. P. Moreira, P. R. Zampieri, J. M. G. Bacchin and P. R. Mei, *Sol Energ Mat Sol C*, 2008, **92**, 418-424.
6. Z. Zou, J. Ye, K. Sayama and H. Arakawa, *Nature*, 2001, **414**, 625-627.
7. J. Huang, Z. Yin and Q. Zheng, *Energy & Environmental Science*, 2011, **4**, 3861-3877.
8. F. He and L. Yu, *The Journal of Physical Chemistry Letters*, 2011, **2**, 3102-3113.
9. Y. J. Cheng, S. H. Yang and C. S. Hsu, *Chem Rev*, 2009, **109**, 5868-5923.
10. M. A. Green, *Physica E: Low-dimensional Systems and Nanostructures*, 2002, **14**, 65-70.
11. G. Li, V. Shrotriya, J. Huang, Y. Yao, T. Moriarty, K. Emery and Y. Yang, *Nat Mater*, 2005, **4**, 864-868.
12. S. K. Hau, H.-L. Yip and A. K. Y. Jen, *Polymer Reviews*, 2010, **50**, 474-510.
13. R. Po, C. Carbonera, A. Bernardi and N. Camaioni, *Energy & Environmental Science*, 2011, **4**, 285-310.
14. G. Li, R. Zhu and Y. Yang, *Nat Photon*, 2012, **6**, 153-161.
15. S. B. Darling and F. You, *RSC Advances*, 2013, **3**, 17633-17648.
16. S. Lizin, S. Van Passel, E. De Schepper, W. Maes, L. Lutsen, J. Manca and D. Vanderzande, *Energy & Environmental Science*, 2013, **6**, 3136-3149.
17. S. Tomoki, U. Tokiyoshi, H. Yuuki, F. Akihiko and Y. Katsumi, *Journal of Physics D: Applied Physics*, 2004, **37**, 847-850.
18. G. Yu, J. Gao, J. C. Hummelen, F. Wudl and A. J. Heeger, *Journal*, 1995, **270**, 1789-1791.
19. H. Zeng, X. Zhu, Y. Liang and X. Guo, *Polymers*, 2015, **7**, 333-372.
20. B. C. Thompson and J. M. J. Fréchet, *Angewandte Chemie International Edition*, 2008, **47**, 58-77.
21. L.-M. Chen, Z. Hong, G. Li and Y. Yang, *Advanced Materials*, 2009, **21**, 1434-1449.
22. S. Zhang, L. Ye, W. Zhao, D. Liu, H. Yao and J. Hou, *Macromolecules*, 2014, **47**, 4653-4659.
23. L. Ye, S. Zhang, W. Zhao, H. Yao and J. Hou, *Chemistry of Materials*, 2014, **26**, 3603-3605.
24. T. L. Nguyen, H. Choi, S. J. Ko, M. A. Uddin, B. Walker, S. Yum, J. E. Jeong, M. H. Yun, T. J. Shin, S. Hwang, J. Y. Kim and H. Y. Woo, *Energy & Environmental Science*, 2014, **7**, 3040-3051.
25. J. You, L. Dou, K. Yoshimura, T. Kato, K. Ohya, T. Moriarty, K. Emery, C.-C. Chen, J. Gao, G. Li and Y. Yang, *Nat Commun*, 2013, **4**, 1-10.

26. K. Kawano, R. Pacios, D. Poplavskyy, J. Nelson, D. D. C. Bradley and J. R. Durrant, *Sol Energ Mat Sol C*, 2006, **90**, 3520-3530.
27. M. P. de Jong, L. J. van Ijzendoorn and M. J. A. de Voigt, *Applied Physics Letters*, 2000, **77**, 2255-2257.
28. K. W. Wong, H. L. Yip, Y. Luo, K. Y. Wong, W. M. Lau, K. H. Low, H. F. Chow, Z. Q. Gao, W. L. Yeung and C. C. Chang, *Applied Physics Letters*, 2002, **80**, 2788-2790.
29. Y. Sun, J. H. Seo, C. J. Takacs, J. Seifter and A. J. Heeger, *Advanced Materials*, 2011, **23**, 1679-1683.
30. H. Cao, W. He, Y. Mao, X. Lin, K. Ishikawa, J. H. Dickerson and W. P. Hess, *Journal of Power Sources*, 2014, **264**, 168-183.
31. M. S. White, D. C. Olson, S. E. Shaheen, N. Kopidakis and D. S. Ginley, *Applied Physics Letters*, 2006, **89**, 143517-143513.
32. S. K. Hau, H.-L. Yip, N. S. Baek, J. Zou, K. O'Malley and A. K. Y. Jen, *Applied Physics Letters*, 2008, **92**, 253301-253303.
33. T. Yang, W. Cai, D. Qin, E. Wang, L. Lan, X. Gong, J. Peng and Y. Cao, *The Journal of Physical Chemistry C*, 2010, **114**, 6849-6853.
34. F. Zhang, X. Xu, W. Tang, J. Zhang, Z. Zhuo, J. Wang, J. Wang, Z. Xu and Y. Wang, *Sol Energ Mat Sol C*, 2011, **95**, 1785-1799.
35. C.-Y. Li, T.-C. Wen, T.-H. Lee, T.-F. Guo, J.-C.-A. Huang, Y.-C. Lin and Y.-J. Hsu, *Journal of Materials Chemistry*, 2009, **19**, 1643-1647.
36. J.-H. Huang, H.-Y. Wei, K.-C. Huang, C.-L. Chen, R.-R. Wang, F.-C. Chen, K.-C. Ho and C.-W. Chu, *Energy & Environmental Science*, 2010, **3**, 654-658.
37. H.-L. Yip and A. K. Y. Jen, *Energy & Environmental Science*, 2012, **5**, 5994-6011.
38. Z. Yin, Q. Zheng, S.-C. Chen and D. Cai, *ACS Applied Materials & Interfaces*, 2013, **5**, 9015-9025.
39. C. Girotto, B. P. Rand, S. Steudel, J. Genoe and P. Heremans, *Organic Electronics*, 2009, **10**, 735-740.
40. K. Frederik C, *Organic Electronics*, 2009, **10**, 761-768.
41. M. R. Lilliedal, A. J. Medford, M. V. Madsen, K. Norrman and F. C. Krebs, *Sol Energ Mat Sol C*, 2010, **94**, 2018-2031.
42. Z. Xu, L.-M. Chen, G. Yang, C.-H. Huang, J. Hou, Y. Wu, G. Li, C.-S. Hsu and Y. Yang, *Adv Funct Mater*, 2009, **19**, 1227-1234.
43. S. Schumann, R. Da Campo, B. Illy, A. C. Cruickshank, M. A. McLachlan, M. P. Ryan, D. J. Riley, D. W. McComb and T. S. Jones, *Journal of Materials Chemistry*, 2011, **21**, 2381-2386.
44. L.-M. Chen, Z. Xu, Z. Hong and Y. Yang, *Journal of Materials Chemistry*, 2010, **20**, 2575-2598.
45. Z. He, C. Zhong, S. Su, M. Xu, H. Wu and Y. Cao, *Nat Photon*, 2012, **6**, 591-595.
46. J. Kong, I. W. Hwang and K. Lee, *Adv Mater*, 2014, **26**, 6275-6283.
47. L. K. Jagadamma, M. Al-Senani, A. El-Labban, I. Gereige, G. O. Ngongang Ndjawa, J. C. D. Faria, T. Kim, K. Zhao, F. Cruciani, D. H. Anjum, M. A. McLachlan, P. M. Beaujuge and A. Amassian, *Advanced Energy Materials*, 2015, **5**, 1500204.
48. Z. Yin, Q. Zheng, S.-C. Chen, D. Cai, L. Zhou and J. Zhang, *Advanced Energy Materials*, 2014, **4**, 1301404.
49. S. H. Liao, H. J. Jhuo, P. N. Yeh, Y. S. Cheng, Y. L. Li, Y. H. Lee, S. Sharma and S. A. Chen, *Scientific reports*, 2014, **4**, 6813.
50. P. Li, X. Li, C. Sun, G. Wang, J. Li, T. Jiu and J. Fang, *Sol Energ Mat Sol C*, 2014, **126**, 36-41.
51. Z. He, B. Xiao, F. Liu, H. Wu, Y. Yang, S. Xiao, C. Wang, T. P. Russell and Y. Cao, *Nat Photon*, 2015, **9**, 174-179.
52. Y. Liu, J. Zhao, Z. Li, C. Mu, W. Ma, H. Hu, K. Jiang, H. Lin, H. Ade and H. Yan, *Nat Commun*, 2014, **5**, 5293.
53. W. Yu, L. Huang, D. Yang, P. Fu, L. Zhou, J. Zhang and C. Li, *Journal of Materials Chemistry A*, 2015, **3**, 10660-10665.
54. X. Ouyang, R. Peng, L. Ai, X. Zhang and Z. Ge, *Nat Photon*, 2015, **9**, 520-524.
55. M. Jørgensen, K. Norrman, S. A. Gevorgyan, T. Tromholt, B. Andreasen and F. C. Krebs, *Advanced Materials*, 2012, **24**, 580-612.
56. R. R. Søndergaard, M. Hösel and F. C. Krebs, *Journal of Polymer Science Part B: Polymer Physics*, 2013, **51**, 16-34.
57. H. Zhou, Q. Chen, G. Li, S. Luo, T.-b. Song, H.-S. Duan, Z. Hong, J. You, Y. Liu and Y. Yang, *Science*, 2014, **345**, 542-546.
58. N. J. Jeon, J. H. Noh, Y. C. Kim, W. S. Yang, S. Ryu and S. I. Seok, *Nat Mater*, 2014, **13**, 897-903.
59. Q. Lin, A. Armin, R. C. R. Nagiri, P. L. Burn and P. Meredith, *Nat Photon*, 2015, **9**, 106-112.
60. J. T. Wang, J. M. Ball, E. M. Barea, A. Abate, J. A. Alexander-Webber, J. Huang, M. Saliba, I. Mora-Sero, J. Bisquert, H. J. Snaith and R. J. Nicholas, *Nano Lett*, 2014, **14**, 724-730.
61. S. Ryu, J. H. Noh, N. J. Jeon, Y. Chan Kim, W. S. Yang, J. Seo and S. I. Seok, *Energy & Environmental Science*, 2014, **7**, 2614.
62. M. Liu, M. B. Johnston and H. J. Snaith, *Nature*, 2013, **501**, 395-398.
63. J. Burschka, N. Pellet, S. J. Moon, R. Humphry-Baker, P. Gao, M. K. Nazeeruddin and M. Gratzel, *Nature*, 2013, **499**, 316-319.
64. S. Ye, W. Sun, Y. Li, W. Yan, H. Peng, Z. Bian, Z. Liu and C. Huang, *Nano Lett*, 2015, **15**, 3723-3728.
65. C. Tao, S. Neutzner, L. Colella, S. Marras, A. R. Srimath Kandada, M. Gandini, M. D. Bastiani, G. Pace, L. Manna, M. Caironi, C. Bertarelli and A. Petrozza, *Energy & Environmental Science*, 2015, **8**, 2365-2370.
66. W. S. Yang, J. H. Noh, N. J. Jeon, Y. C. Kim, S. Ryu, J. Seo and S. I. Seok, *Science*, 2015, **348**, 1234-1237.
67. J. Shi, X. Xu, D. Li and Q. Meng, *Small*, 2015, **11**, 2472-2486.
68. J. Cao, J. Yin, S. F. Yuan, Y. Zhao, J. Li and N. F. Zheng, *Nanoscale*, 2015, **7**, 9443-9447.
69. N. Aristidou, I. Sanchez-Molina, T. Chotchuangchutchaval, M. Brown, L. Martinez, T.

Rath and S. A. Haque, *Angewandte Chemie*, 2015, **54**, 8208-8212.
70. S. Guarnera, A. Abate, W. Zhang, J. M. Foster, G. Richardson, A. Petrozza and H. J. Snaith, *The Journal of Physical Chemistry Letters*, 2015, **6**, 432-437.
71. H. Choi, C. K. Mai, H. B. Kim, J. Jeong, S. Song, G. C. Bazan, J. Y. Kim and A. J. Heeger, *Nat Commun*, 2015, **6**, 7348.
72. X. Dong, X. Fang, M. Lv, B. Lin, S. Zhang, J. Ding and N. Yuan, *Journal of Materials Chemistry A*, 2015, **3**, 5360-5367.
73. H. Choi, J. W. Cho, M.-S. Kang and J. Ko, *Chemical Communications*, 2015, **51**, 9305-9308.
74. J. Gong, S. B. Darling and F. You, *Energy & Environmental Science*, 2015, **8**, 1953-1968.
75. N. Espinosa, L. Serrano-Luján, A. Urbina and F. C. Krebs, *Sol Energ Mat Sol C*, 2015, **137**, 303-310.
76. A. K. K. Kyaw, X. W. Sun, C. Y. Jiang, G. Q. Lo, D. W. Zhao and D. L. Kwong, *Applied Physics Letters*, 2008, **93**, 221107-221103.
77. J.-p. Liu, K.-L. Choy and X.-h. Hou, *Journal of Materials Chemistry*, 2011, **21**, 1966-1969.
78. T. Z. Oo, R. D. Chandra, N. Yantara, R. R. Prabhakar, L. H. Wong, N. Mathews and S. G. Mhaisalkar, *Organic Electronics*, 2012, **13**, 870-874.
79. S. K. Hau, H.-L. Yip, O. Acton, N. S. Baek, H. Ma and A. K. Y. Jen, *Journal of Materials Chemistry*, 2008, **18**, 5113-5119.
80. T. Kuwabara, H. Sugiyama, T. Yamaguchi and K. Takahashi, *Thin Solid Films*, 2009, **517**, 3766-3769.
81. I. Sasajima, S. Uesaka, T. Kuwabara, T. Yamaguchi and K. Takahashi, *Organic Electronics*, 2011, **12**, 113-118.
82. Y.-J. Kang, C. S. Kim, D. S. You, S. H. Jung, K. Lim, D.-G. Kim, J.-K. Kim, S. H. Kim, Y.-R. Shin, S.-H. Kwon and J.-W. Kang, *Applied Physics Letters*, 2011, **99**, 073308-073303.
83. Y. Zhou, H. Cheun, J. W. J. Potscavage, C. Fuentes-Hernandez, S.-J. Kim and B. Kippelen, *Journal of Materials Chemistry*, 2010, **20**, 6189-6194.
84. O. Wiranwetchayan, Z. Liang, Q. Zhang, G. Cao and P. Singjai, *Materials Sciences and Applications*, 2011, **2**, 1697-1701.
85. Y. Zhu, X. Xu, L. Zhang, J. Chen and Y. Cao, *Sol Energ Mat Sol C*, 2012, **97**, 83-88.
86. M. Jin Tan, S. Zhong, R. Wang, Z. Zhang, V. Chellappan and W. Chen, *Applied Physics Letters*, 2013, **103**, -.
87. S. Woo, W. Hyun Kim, H. Kim, Y. Yi, H.-K. Lyu and Y. Kim, *Advanced Energy Materials*, 2014, **4**, 1301692.
88. R. Xia, D.-S. Leem, T. Kirchartz, S. Spencer, C. Murphy, Z. He, H. Wu, S. Su, Y. Cao, J. S. Kim, J. C. deMello, D. D. C. Bradley and J. Nelson, *Advanced Energy Materials*, 2013, **3**, 718-723.
89. Z. Tang, W. Tress, Q. Bao, M. J. Jafari, J. Bergqvist, T. Ederth, M. R. Andersson and O. Inganäs, *Advanced Energy Materials*, 2014, **4**, 1400643.
90. T. Kuwabara, M. Nakamoto, Y. Kawahara, T. Yamaguchi and K. Takahashi, *Journal of Applied Physics*, 2009, **105**, 124513-124516.
91. J.-J. Zhu, Z.-Q. Xu, G.-Q. Fan, S.-T. Lee, Y.-Q. Li and J.-X. Tang, *Organic Electronics*, 2011, **12**, 2151-2158.
92. J.-J. Zhu, G.-Q. Fan, H.-X. Wei, Y.-Q. Li, S.-T. Lee and J.-X. Tang, *CrystEngComm*, 2012, **14**, 8090-8096.
93. G. Li, C. W. Chu, V. Shrotriya, J. Huang and Y. Yang, *Applied Physics Letters*, 2006, **88**, 253503-253503.
94. H.-H. Liao, L.-M. Chen, Z. Xu, G. Li and Y. Yang, *Appl. Phys. Lett.*, 2008, **92**, 173303.
95. Y.-I. Lee, J.-H. Youn, M.-S. Ryu, J. Kim, H.-T. Moon and J. Jang, *Sol Energ Mat Sol C*, 2011, **95**, 3276-3280.
96. H. Bin Yang, Y. Qian Dong, X. Wang, S. Yun Khoo, B. Liu and C. Ming Li, *Sol Energ Mat Sol C*, 2013, **117**, 214-218.
97. J. W. Kim, Y. H. Suh, C. L. Lee, Y. S. Kim and W. B. Kim, *Nanoscale*, 2015, **7**, 4367-4371.
98. J.-L. Lan, Z. Liang, Y.-H. Yang, F. S. Ohuchi, S. A. Jenekhe and G. Cao, *Nano Energy*, 2014, **4**, 140-149.
99. J. Liu, S. Shao, G. Fang, B. Meng, Z. Xie and L. Wang, *Advanced Materials*, 2012, **24**, 2774-2779.
100. M. R. Rajesh Menon, M. V. Maheshkumar, K. Sreekumar, C. Sudha Kartha and K. P. Vijayakumar, *Sol Energ Mat Sol C*, 2010, **94**, 2212-2217.
101. M. R. R. Menon, M. V. Maheshkumar, K. Sreekumar, C. S. Kartha and K. P. Vijayakumar, *physica status solidi (a)*, 2012, **209**, 199-203.
102. X. Chen, J. Yang, L. Y. X. C. Haley, J. Lu, F. Zhu and K. P. Loh, *Organic Electronics*, 2010, **11**, 1942-1946.
103. K. Sun, H. Zhang and J. Ouyang, *Journal of Materials Chemistry*, 2011, **21**, 18339-18346.
104. K. Sun, B. Zhao, A. Kumar, K. Zeng and J. Ouyang, *ACS Applied Materials & Interfaces*, 2012, **4**, 2009-2017.
105. A. Li, R. Nie, X. Deng, H. Wei, S. Zheng, Y. Li, J. Tang and K.-Y. Wong, *Applied Physics Letters*, 2014, **104**, 123303.
106. Q. Zhang, D. Zhang, X. Li, X. Liu, W. Zhang, L. Han and J. Fang, *Chemical Communications*, 2015, **51**, 10182-10185.
107. C. Y. Jiang, X. W. Sun, D. W. Zhao, A. K. K. Kyaw and Y. N. Li, *Sol Energ Mat Sol C*, 2010, **94**, 1618-1621.
108. M. P. Nikiforov, J. Strzalka, Z. Jiang and S. B. Darling, *Physical Chemistry Chemical Physics*, 2013, **15**, 13052-13060.
109. X. Wan, G. Long, L. Huang and Y. Chen, *Advanced Materials*, 2011, **23**, 5342-5358.
110. J. Liu, Y. Xue, Y. Gao, D. Yu, M. Durstock and L. Dai, *Advanced Materials*, 2012, **24**, 2228-2233.
111. J. Liu, M. Durstock and L. Dai, *Energy & Environmental Science*, 2014, **7**, 1297-1306.
112. Y. W. Heo, D. P. Norton, L. C. Tien, Y. Kwon, B. S. Kang, F. Ren, S. J. Pearton and J. R. LaRoche, *Materials Science and Engineering: R: Reports*, 2004, **47**, 1-47.
113. K. Ellmer, *Journal of Physics D: Applied Physics*, 2001, **34**, 3097-3108.

114. S. H. Liao, H. J. Jhuo, Y. S. Cheng and S. A. Chen, *Adv Mater*, 2013, **25**, 4766-4771.
115. F. C. Krebs, J. Fyenbo, D. M. Tanenbaum, S. A. Gevorgyan, R. Andriessen, B. van Remoortere, Y. Galagan and M. Jorgensen, *Energy & Environmental Science*, 2011, **4**, 4116-4123.
116. F. C. Krebs, T. Tromholt and M. Jorgensen, *Nanoscale*, 2010, **2**, 873-886.
117. F. C. Krebs, J. Fyenbo and M. Jorgensen, *Journal of Materials Chemistry*, 2010, **20**, 8994-9001.
118. F. C. Krebs, T. D. Nielsen, J. Fyenbo, M. Wadstrom and M. S. Pedersen, *Energy & Environmental Science*, 2010, **3**, 512-525.
119. F. C. Krebs, S. A. Gevorgyan and J. Alstrup, *Journal of Materials Chemistry*, 2009, **19**, 5442-5451.
120. G. D. Spyropoulos, P. Kubis, N. Li, D. Baran, L. Lucera, M. Salvador, T. Ameri, M. M. Voigt, F. C. Krebs and C. J. Brabec, *Energy & Environmental Science*, 2014, **7**, 3284-3290.
121. R. Steim, F. R. Kogler and C. J. Brabec, *Journal of Materials Chemistry*, 2010, **20**, 2499-2512.
122. R. Po, M. Maggini and N. Camaioni, *J Phys Chem C*, 2010, **114**, 695-706.
123. W. Cai, X. Gong and Y. Cao, *Sol Energ Mat Sol C*, 2010, **94**, 114-127.
124. Y.-Y. Lai, Y.-J. Cheng and C.-S. Hsu, *Energy & Environmental Science*, 2014, **7**, 1866-1883.
125. F. Wang, Z. a. Tan and Y. Li, *Energy & Environmental Science*, 2015, **8**, 1059-1091.
126. I. Etxebarria, J. Ajuria and R. Pacios, *Organic Electronics*, 2015, **19**, 34-60.
127. C.-C. Chueh, C.-Z. Li and A. K. Y. Jen, *Energy & Environmental Science*, 2015, **8**, 1160-1189.
128. A. Manor, E. A. Katz, T. Tromholt and F. C. Krebs, *Sol Energ Mat Sol C*, 2012, **98**, 491-493.
129. J.-C. Wang, W.-T. Weng, M.-Y. Tsai, M.-K. Lee, S.-F. Horng, T.-P. Perng, C.-C. Kei, C.-C. Yu and H.-F. Meng, *Journal of Materials Chemistry*, 2010, **20**, 862-866.
130. J. Sun, Y. Zhu, X. Xu, L. Lan, L. Zhang, P. Cai, J. Chen, J. Peng and Y. Cao, *The Journal of Physical Chemistry C*, 2012, **116**, 14188-14198.
131. A. Moliton and J.-M. Nunzi, *Polymer International*, 2006, **55**, 583-600.
132. Z. Liang, Q. Zhang, O. Wiranwetchayan, J. Xi, Z. Yang, K. Park, C. Li and G. Cao, *Adv Funct Mater*, 2012, **22**, 2194-2201.
133. T. Kuwabara, Y. Kawahara, T. Yamaguchi and K. Takahashi, *ACS Applied Materials & Interfaces*, 2009, **1**, 2107-2110.
134. M.-Y. Liu, C.-H. Chang, C.-H. Chang, K.-H. Tsai, J.-S. Huang, C.-Y. Chou, I.-J. Wang, P.-S. Wang, C.-Y. Lee, C.-H. Chao, C.-L. Yeh, C.-I. Wu and C.-F. Lin, *Thin Solid Films*, 2010, **518**, 4964-4969.
135. H.-J. Park, K.-H. Lee, B. Kumar, K.-S. Shin, S.-W. Jeong and S.-W. Kim, *Journal of Nanoelectronics and Optoelectronics*, 2010, **5**, 135-138.
136. H. O. Seo, S.-Y. Park, W. H. Shim, K.-D. Kim, K. H. Lee, M. Y. Jo, J. H. Kim, E. Lee, D.-W. Kim, Y. D. Kim and D. C. Lim, *The Journal of Physical Chemistry C*, 2011, **115**, 21517-21520.
137. C. Zhang, H. You, Z. Lin and Y. Hao, *Japanese Journal of Applied Physics*, 2011, **50**.
138. D. C. Lim, W. H. Shim, K.-D. Kim, H. O. Seo, J.-H. Lim, Y. Jeong, Y. D. Kim and K. H. Lee, *Sol Energ Mat Sol C*, 2011, **95**, 3036-3040.
139. N. Sekine, C.-H. Chou, W. L. Kwan and Y. Yang, *Organic Electronics*, 2009, **10**, 1473-1477.
140. L. K. Jagadamma, M. Abdelsamie, A. El Labban, E. Aresu, G. O. Ngongang Ndjawa, D. H. Anjum, D. Cha, P. M. Beaujuge and A. Amassian, *Journal of Materials Chemistry A*, 2014, **2**, 13321-13331.
141. X. Bao, A. Yang, Y. Yang, T. Wang, L. Sun, N. Wang and L. Han, *Physica B: Condensed Matter*, 2014, **432**, 1-4.
142. Z. Yin, Q. Zheng, S. C. Chen and D. Cai, *ACS Appl Mater Interfaces*, 2013, **5**, 9015-9025.
143. H.-Y. Park, D. Lim, K.-D. Kim and S.-Y. Jang, *Journal of Materials Chemistry A*, 2013, **1**, 6327-6334.
144. S. K. Hau, H.-L. Yip, J. Zou and A. K. Y. Jen, *Organic Electronics*, 2009, **10**, 1401-1407.
145. S. Chen, C. E. Small, C. M. Amb, J. Subbiah, T.-h. Lai, S.-W. Tsang, J. R. Manders, J. R. Reynolds and F. So, *Advanced Energy Materials*, 2012, **2**, 1333-1337.
146. M. J. Tan, S. Zhong, J. Li, Z. Chen and W. Chen, *ACS Applied Materials & Interfaces*, 2013, **5**, 4696-4701.
147. W. Qin, X. Xu, D. Liu, C. Ma, L. Yang, S. Yin, F. Zhang and J. Wei, *Journal of Renewable and Sustainable Energy*, 2013, **5**, 053106.
148. S. Park, S. J. Tark, J. S. Lee, H. Lim and D. Kim, *Sol Energ Mat Sol C*, 2009, **93**, 1020-1023.
149. H. Cheun, C. Fuentes-Hernandez, Y. Zhou, W. J. Potscavage, S.-J. Kim, J. Shim, A. Dindar and B. Kippelen, *The Journal of Physical Chemistry C*, 2010, **114**, 20713-20718.
150. C.-Y. Chang and F.-Y. Tsai, *Journal of Materials Chemistry*, 2011, **21**, 5710-5715.
151. R. L. Z. Hoye, D. Muñoz-Rojas, D. C. Iza, K. P. Musselman and J. L. MacManus-Driscoll, *Sol Energ Mat Sol C*, 2013, **116**, 197-202.
152. K. D. Kim, D. C. Lim, J. Hu, J. D. Kwon, M. G. Jeong, H. O. Seo, J. Y. Lee, K. Y. Jang, J. H. Lim, K. H. Lee, Y. Jeong, Y. D. Kim and S. Cho, *ACS Appl Mater Interfaces*, 2013, **5**, 8718-8723.
153. N. O. V. Plank, M. E. Welland, J. L. MacManus-Driscoll and L. Schmidt-Mende, *Thin Solid Films*, 2008, **516**, 7218-7222.
154. Y.-J. Noh, S.-I. Na and S.-S. Kim, *Sol Energ Mat Sol C*, 2013, **117**, 139-144.
155. Z. Hu, J. Zhang and Y. Zhu, *Sol Energ Mat Sol C*, 2013, **117**, 610-616.
156. K.-S. Shin, H.-J. Park, B. Kumar, K.-K. Kim, S.-G. Ihn and S.-W. Kim, *Journal of Materials Chemistry*, 2011, **21**, 12274-12279.

157. S.-G. Ihn, K.-S. Shin, M.-J. Jin, X. Bulliard, S. Yun, Y. Suk Choi, Y. Kim, J.-H. Park, M. Sim, M. Kim, K. Cho, T. Sang Kim, D. Choi, J.-Y. Choi, W. Choi and S.-W. Kim, *Sol Energ Mat Sol C*, 2011, **95**, 1610-1614.
158. F. Zhu, X. Chen, L. Zhou, J. Zhou, J. Yang, S. Huang and Z. Sun, *Thin Solid Films*, 2014, **551**, 131-135.
159. F. Zhu, X. Chen, J. Zhou, Z. Lu, Y. Chen, S. Huang and Z. Sun, *Materials Research Express*, 2014, **1**, 025020.
160. J.-h. Lee, S. Yoshikawa and T. Sagawa, *Sol Energ Mat Sol C*, 2014, **127**, 111-121.
161. Y. Lare, A. Godoy, L. Cattin, K. Jondo, T. Abachi, F. R. Diaz, M. Morsli, K. Napo, M. A. del Valle and J. C. Bernède, *Applied Surface Science*, 2009, **255**, 6615-6619.
162. M. Ohyama, H. Kouzuka and T. Yoko, *Thin Solid Films*, 1997, **306**, 78-85.
163. T. Stubhan, H. Oh, L. Pinna, J. Krantz, I. Litzov and C. J. Brabec, *Organic Electronics*, 2011, **12**, 1539-1543.
164. L. Znaidi, *Materials Science and Engineering: B*, 2010, **174**, 18-30.
165. B. S. Ong, C. Li, Y. Li, Y. Wu and R. Loutfy, *Journal of the American Chemical Society*, 2007, **129**, 2750-2751.
166. C. Jiang, R. R. Lunt, P. M. Duxbury and P. P. Zhang, *RSC Advances*, 2014, **4**, 3604-3610.
167. P. Morvillo, R. Diana, A. Mucci, E. Bobeico, R. Ricciardi and C. Minarini, *Sol Energ Mat Sol C*, 2015, **141**, 210-217.
168. Z. Lin, J. Chang, C. Jiang, J. Zhang, J. Wu and C. Zhu, *RSC Advances*, 2014, **4**, 6646-6651.
169. B. A. MacLeod, B. J. Tremolet de Villers, P. Schulz, P. F. Ndione, H. Kim, A. J. Giordano, K. Zhu, S. R. Marder, S. Graham, J. J. Berry, A. Kahn and D. C. Olson, *Energy & Environmental Science*, 2015, **8**, 592-601.
170. S. K. Hau, Y.-J. Cheng, H.-L. Yip, Y. Zhang, H. Ma and A. K. Y. Jen, *ACS Applied Materials & Interfaces*, 2010, **2**, 1892-1902.
171. A. L. Roest, J. J. Kelly, D. Vanmaekelbergh and E. A. Meulenkamp, *Physical Review Letters*, 2002, **89**, 036801.
172. P. Li, T. Jiu, G. Tang, G. Wang, J. Li, X. Li and J. Fang, *ACS Applied Materials & Interfaces*, 2014, **6**, 18172-18179.
173. J. M. Cho, S.-W. Kwak, H. Aqoma, J. W. Kim, W. S. Shin, S.-J. Moon, S.-Y. Jang and J. Jo, *Organic Electronics*, 2014, **15**, 1942-1950.
174. C. E. Small, S. Chen, J. Subbiah, C. M. Amb, S.-W. Tsang, T.-H. Lai, J. R. Reynolds and F. So, *Nat Photon*, 2012, **6**, 115-120.
175. S. Shao, K. Zheng, T. Pullerits and F. Zhang, *ACS Applied Materials & Interfaces*, 2012, **5**, 380-385.
176. Y. Chen, Z. Hu, Z. Zhong, W. Shi, J. Peng, J. Wang and Y. Cao, *The Journal of Physical Chemistry C*, 2014, **118**, 21819-21825.
177. I. A. Kowalik, E. Guziewicz, K. Kopalko, S. Yatsunenko, A. Wójcik-Głodowska, M. Godlewski, P. Dłużewski, E. Łusakowska and W. Paszkowicz, *Journal of Crystal Growth*, 2009, **311**, 1096-1101.
178. S. Oh, I. Jang, S.-G. Oh and S. S. Im, *Solar Energy*, 2015, **114**, 32-38.
179. X. Yu, X. Yu, Z. Hu, J. Zhang, G. Zhao and Y. Zhao, *Materials Letters*, 2013, **108**, 50-53.
180. Z. Ma, Z. Tang, E. Wang, M. R. Andersson, O. Inganäs and F. Zhang, *The Journal of Physical Chemistry C*, 2012, **116**, 24462-24468.
181. R. B. Ambade, S. B. Ambade, R. S. Mane and S. H. Lee, *ACS Appl Mater Interfaces*, 2015, **7**, 7951-7960.
182. S. Wilken, J. Parisi and H. Borchert, *The Journal of Physical Chemistry C*, 2014, **118**, 19672-19682.
183. F. Verbakel, S. C. J. Meskers and R. A. J. Janssen, *Journal of Applied Physics*, 2007, **102**, 083701-083709.
184. A. Sharma, M. Ionescu, G. G. Andersson and D. A. Lewis, *Sol Energ Mat Sol C*, 2013, **115**, 64-70.
185. A. Sharma, J. B. Franklin, B. Singh, G. G. Andersson and D. A. Lewis, *Organic Electronics*, 2015, **24**, 131-136.
186. S. Loser, B. Valle, K. A. Luck, C. K. Song, G. Ogien, M. C. Hersam, K. D. Singer and T. J. Marks, *Advanced Energy Materials*, 2014, **4**, 1301938.
187. S. O'Brien, L. H. K. Koh and G. M. Crean, *Thin Solid Films*, 2008, **516**, 1391-1395.
188. S. Kamaruddin, K.-Y. Chan, H.-K. Yow, M. Zainizan Sahdan, H. Saim and D. Knipp, *Applied Physics A: Materials Science & Processing*, 2011, **104**, 263-268.
189. Y. Li, L. Xu, X. Li, X. Shen and A. Wang, *Applied Surface Science*, 2010, **256**, 4543-4547.
190. K. P. Bhuvana, J. Elanchezhiyan, N. Gopalakrishnan and T. Balasubramanian, *Journal of Alloys and Compounds*, 2009, **473**, 534-537.
191. X. Yu, Z.-Y. Hu, Z.-H. Huang, X.-M. Yu, J.-J. Zhang, G.-S. Zhao and Y. Zhao, *Chinese Physics B*, 2013, **22**, 118801.
192. X. Yu, X. Yu, J. Zhang, Z. Hu, G. Zhao and Y. Zhao, *Sol Energ Mat Sol C*, 2014, **121**, 28-34.
193. H. Oh, J. Krantz, I. Litzov, T. Stubhan, L. Pinna and C. J. Brabec, *Sol Energ Mat Sol C*, 2011, **95**, 2194-2199.
194. K.-S. Shin, K.-H. Lee, H. H. Lee, D. Choi and S.-W. Kim, *The Journal of Physical Chemistry C*, 2010, **114**, 15782-15785.
195. K. Aung Ko Ko, S. Xiaowei, Z. De Wei, T. Swee Tiam, Y. Divayana and H. V. Demir, *Selected Topics in Quantum Electronics, IEEE Journal of*, 2010, **16**, 1700-1706.
196. J. Alstrup, M. Jørgensen, A. J. Medford and F. C. Krebs, *ACS Applied Materials & Interfaces*, 2010, **2**, 2819-2827.
197. R. Søndergaard, M. Helgesen, M. Jørgensen and F. C. Krebs, *Advanced Energy Materials*, 2011, **1**, 68-71.
198. S. Trost, K. Zilberberg, A. Behrendt, A. Polywka, P. Görrn, P. Reckers, J. Maibach, T. Mayer and T. Riedl, *Advanced Energy Materials*, 2013, **3**, 1437-1444.

199. S.-W. Cho, Y. T. Kim, W. H. Shim, S.-Y. Park, K.-D. Kim, H. O. Seo, N. K. Dey, J.-H. Lim, Y. Jeong, K. H. Lee, Y. D. Kim and D. C. Lim, *Applied Physics Letters*, 2011, **98**, 023102-023103.
200. A. Gadisa, Y. Liu, E. T. Samulski and R. Lopez, *Applied Physics Letters*, 2012, **100**, 253903.
201. M. Thambidurai, J. Y. Kim, J. Song, Y. Ko, H.-j. Song, C.-m. Kang, N. Muthukumarasamy, D. Velauthapillai and C. Lee, *Journal of Materials Chemistry C*, 2013, **1**, 8161.
202. O. Pachoumi, C. Li, Y. Vaynzof, K. K. Banger and H. Sirringhaus, *Advanced Energy Materials*, 2013, **3**, 1428-1436.
203. T. Stubhan, M. Salinas, A. Ebel, F. C. Krebs, A. Hirsch, M. Halik and C. J. Brabec, *Advanced Energy Materials*, 2012, **2**, 532-535.
204. S. H. Tsai, S. T. Ho, H. J. Jhuo, C. R. Ho, S. A. Chen and J.-H. He, *Applied Physics Letters*, 2013, **102**, 253111.
205. J. Piris, N. Kopidakis, D. C. Olson, S. E. Shaheen, D. S. Ginley and G. Rumbles, *Adv Funct Mater*, 2007, **17**, 3849-3857.
206. B. A. MacLeod, P. Schulz, S. R. Cowan, A. Garcia, D. S. Ginley, A. Kahn and D. C. Olson, *Advanced Energy Materials*, 2014, **4**, 1400073.
207. M. Lenes, L. J. A. Koster, V. D. Mihailetchi and P. W. M. Blom, *Applied Physics Letters*, 2006, **88**, 243502.
208. D. W. Sievers, V. Shrotriya and Y. Yang, *Journal of Applied Physics*, 2006, **100**, 114509.
209. T. Kirchartz, T. Agostinelli, M. Campoy-Quiles, W. Gong and J. Nelson, *The Journal of Physical Chemistry Letters*, 2012, **3**, 3470-3475.
210. W. L. Ma, C. Y. Yang, X. Gong, K. Lee and A. J. Heeger, *Adv Funct Mater*, 2005, **15**, 1617-1622.
211. D.-H. Ko, J. R. Tumbleston, W. Schenck, R. Lopez and E. T. Samulski, *The Journal of Physical Chemistry C*, 2011, **115**, 4247-4254.
212. J. M. Lee, J. Lim, N. Lee, H. I. Park, K. E. Lee, T. Jeon, S. A. Nam, J. Kim, J. Shin and S. O. Kim, *Advanced Materials*, 2014, **27**, 1519-1525.
213. S.-H. Jeong, H. Choi, J. Y. Kim and T.-W. Lee, *Particle & Particle Systems Characterization*, 2014, **32**, 164-175.
214. C. H. Chou and F. C. Chen, *Nanoscale*, 2014, **6**, 8444-8458.
215. S.-J. Ko, H. Choi, W. Lee, T. Kim, B. R. Lee, J.-W. Jung, J.-R. Jeong, M. H. Song, J. C. Lee, H. Y. Woo and J. Y. Kim, *Energy & Environmental Science*, 2013, **6**, 1949-1955.
216. J. Li, L. Zuo, H. Pan, H. Jiang, T. Liang, Y. Shi, H. Chen and M. Xu, *Journal of Materials Chemistry A*, 2013, **1**, 2379-2386.
217. L. Müller-Meskamp, Y. H. Kim, T. Roch, S. Hofmann, R. Scholz, S. Eckardt, K. Leo and A. F. Lasagni, *Advanced Materials*, 2012, **24**, 906-910.
218. K. Takanezawa, K. Hirota, Q.-S. Wei, K. Tajima and K. Hashimoto, *The Journal of Physical Chemistry C*, 2007, **111**, 7218-7223.
219. C.-Y. Chou, J.-S. Huang, C.-H. Wu, C.-Y. Lee and C.-F. Lin, *Sol Energ Mat Sol C*, 2009, **93**, 1608-1612.
220. M. Law, L. E. Greene, J. C. Johnson, R. Saykally and P. Yang, *Nat Mater*, 2005, **4**, 455-459.
221. M. Wang, Y. Li, H. Huang, E. D. Peterson, W. Nie, W. Zhou, W. Zeng, W. Huang, G. Fang, N. Sun, X. Zhao and D. L. Carroll, *Applied Physics Letters*, 2011, **98**, 103305.
222. N. K. Elumalai, T. M. Jin, V. Chellappan, R. Jose, S. K. Palaniswamy, S. Jayaraman, H. K. Raut and S. Ramakrishna, *ACS Appl Mater Interfaces*, 2013, **5**, 9396-9404.
223. K. Takanezawa, K. Tajima and K. Hashimoto, *Applied Physics Letters*, 2008, **93**, 063308.
224. R. Thitima, C. Patcharee, S. Takashi and Y. Susumu, *Solid-State Electronics*, 2009, **53**, 176-180.
225. Y. Hames, Z. Alpaslan, A. Kösemen, S. E. San and Y. Yerli, *Solar Energy*, 2010, **84**, 426-431.
226. S. Yodyingyong, X. Zhou, Q. Zhang, D. Triampo, J. Xi, K. Park, B. Limketkai and G. Cao, *The Journal of Physical Chemistry C*, 2010, **114**, 21851-21855.
227. J.-S. Huang, C.-Y. Chou and C.-F. Lin, *Sol Energ Mat Sol C*, 2010, **94**, 182-186.
228. K. H. Lee, B. Kumar, H.-J. Park and S.-W. Kim, *Nanoscale Research Letters*, 2010, **5**, 1908-1912.
229. Z. Yuan, J. Yu, N. Wang and Y. Jiang, *Journal of Materials Science: Materials in Electronics*, 2011, **22**, 1730-1735.
230. Y.-M. Sung, F.-C. Hsu, C.-T. Chen, W.-F. Su and Y.-F. Chen, *Sol Energ Mat Sol C*, 2012, **98**, 103-109.
231. M. Ahmadi, K. Mirabbaszadeh and M. Ketabchi, *Electron. Mater. Lett.*, 2013, **9**, 729-734.
232. K. Sung Hyun, P. Sung Hwak, L. Kyoung Il, K. Seon Min and C. Jin Woo, 2010.
233. J. Ajuria, I. Etxebarria, E. Azaceta, R. Tena-Zaera, N. Fernandez-Montcada, E. Palomares and R. Pacios, *Physical Chemistry Chemical Physics*, 2011, **13**, 20871-20876.
234. H. Woo Choi, K.-S. Lee, N. David Theodore and T. L. Alford, *Sol Energ Mat Sol C*, 2013, **117**, 273-278.
235. D. C. Olson, J. Piris, R. T. Collins, S. E. Shaheen and D. S. Ginley, *Thin Solid Films*, 2006, **496**, 26-29.
236. Z. Hu, J. Zhang, Y. Liu, Y. Li, X. Zhang and Y. Zhao, *Synthetic Metals*, 2011, **161**, 2174-2178.
237. Z. Hu, J. Zhang, Y. Liu, Z. Hao, X. Zhang and Y. Zhao, *Sol Energ Mat Sol C*, 2011, **95**, 2126-2130.
238. Z. Liang, R. Gao, J.-L. Lan, O. Wiranwetchayan, Q. Zhang, C. Li and G. Cao, *Sol Energ Mat Sol C*, 2013, **117**, 34-40.
239. Y.-C. Ho, P.-Y. Ho, H.-C. Lee, S.-K. Chang, Y.-R. Hong and C.-F. Lin, *Sol Energ Mat Sol C*, 2015, **132**, 570-577.
240. P. P. Boix, J. Ajuria, I. Etxebarria, R. Pacios, G. Garcia-Belmonte and J. Bisquert, *The Journal of Physical Chemistry Letters*, 2011, **2**, 407-411.
241. A. Manor, E. A. Katz, T. Tromholt and F. C. Krebs, *Advanced Energy Materials*, 2011, **1**, 836-843.

242. X. Bulliard, S.-G. Ihn, S. Yun, Y. Kim, D. Choi, J.-Y. Choi, M. Kim, M. Sim, J.-H. Park, W. Choi and K. Cho, *Adv Funct Mater*, 2010, **20**, 4381-4387.
243. S. Bai, Y. Jin, X. Liang, Z. Ye, Z. Wu, B. Sun, Z. Ma, Z. Tang, J. Wang, U. Würfel, F. Gao and F. Zhang, *Advanced Energy Materials*, 2015, **5**, 1401606.
244. J. J. Intemann, K. Yao, Y.-X. Li, H.-L. Yip, Y.-X. Xu, P.-W. Liang, C.-C. Chueh, F.-Z. Ding, X. Yang, X. Li, Y. Chen and A. K. Y. Jen, *Adv Funct Mater*, 2013, **24**, 1465-1473.
245. S. K. Hau, H.-L. Yip, H. Ma and A. K. Y. Jen, *Applied Physics Letters*, 2008, **93**, 233304-233303.
246. H.-L. Yip, S. K. Hau, N. S. Baek, H. Ma and A. K. Y. Jen, *Advanced Materials*, 2008, **20**, 2376-2382.
247. C.-H. Hsieh, Y.-J. Cheng, P.-J. Li, C.-H. Chen, M. Dubosc, R.-M. Liang and C.-S. Hsu, *Journal of the American Chemical Society*, 2010, **132**, 4887-4893.
248. S. Cho, K. D. Kim, J. Heo, J. Y. Lee, G. Cha, B. Y. Seo, Y. D. Kim, Y. S. Kim, S. Y. Choi and D. C. Lim, *Scientific reports*, 2014, **4**, 4306.
249. T. Tromholt, M. V. Madsen, J. E. Carlé, M. Helgesen and F. C. Krebs, *Journal of Materials Chemistry*, 2012, **22**, 7592.
250. Y.-J. Cheng, C.-H. Hsieh, Y. He, C.-S. Hsu and Y. Li, *Journal of the American Chemical Society*, 2010, **132**, 17381-17383.
251. J. Jo, J. R. Pouliot, D. Wynands, S. D. Collins, J. Y. Kim, T. L. Nguyen, H. Y. Woo, Y. Sun, M. Leclerc and A. J. Heeger, *Adv Mater*, 2013, **25**, 4783-4788.
252. T. Yang, M. Wang, C. Duan, X. Hu, L. Huang, J. Peng, F. Huang and X. Gong, *Energy & Environmental Science*, 2012, **5**, 8208-8214.
253. G. Cheng, W.-Y. Tong, K.-H. Low and C.-M. Che, *Sol Energ Mat Sol C*, 2012, **103**, 164-170.
254. K.-D. Kim, D. C. Lim, M.-G. Jeong, H. O. Seo, B. Y. Seo, J. Y. Lee, Y. Song, S. Cho, J.-H. Lim and Y. D. Kim, *Bulletin of the Korean Chemical Society*, 2014, **35**, 353-356.
255. S. I. Yoo, T. T. Do, Y. E. Ha, M. Y. Jo, J. Park, Y.-C. Kang and J. H. Kim, *Bulletin of the Korean Chemical Society*, 2014, **35**, 569-574.
256. Y. E. Ha, M. Y. Jo, J. Park, Y.-C. Kang, S.-J. Moon and J. H. Kim, *Synthetic Metals*, 2014, **187**, 113-117.
257. S. M. Yoon, S. J. Lou, S. Loser, J. Smith, L. X. Chen, A. Facchetti and T. Marks, *Nano Letters*, 2012, **12**, 6315-6321.
258. Z. Wu, T. Song, Z. Xia, H. Wei and B. Sun, *Nanotechnology*, 2013, **24**, 484012.
259. T. Hu, F. Li, K. Yuan and Y. Chen, *ACS Appl Mater Interfaces*, 2013, **5**, 5763-5770.
260. J. P. Tiwari, S. Pillai, S. Parakh, F. Ali, A. Sharma and S. Chand, *Applied Physics Letters*, 2014, **104**, 041114.
261. H. C. Chen, S. W. Lin, J. M. Jiang, Y. W. Su and K. H. Wei, *ACS Appl Mater Interfaces*, 2015, **7**, 6273-6281.
262. T. Hu, L. Chen, K. Yuan and Y. Chen, *Nanoscale*, 2015, **7**, 9194-9203.
263. M. Eita, A. E. Labban, F. Cruciani, A. Usman, P. M. Beaujuge and O. F. Mohammed, *Adv Funct Mater*, 2015, **25**, 1558-1564.
264. J.-L. Lan, S.-J. Cherng, Y.-H. Yang, Q. Zhang, S. Subramaniyan, F. S. Ohuchi, S. A. Jenekhe and G. Cao, *J. Mater. Chem. A*, 2014, **2**, 9361-9370.

Energy & Environment Science

ARTICLE

Broader context

Photovoltaic technology converting sunlight into electricity has been acknowledged as a promising way to meet the growing energy needs and the increasing concerns about carbon dioxide emission from the consumption of fossil fuel. In recent years, inverted polymer solar cells (PSCs) have attracted considerable attention due to their combined advantages of high power conversion efficiency, good stability, rapid energy payback time (EPBT), low-cost, and compatible with flexible substrate and roll-to-roll manufacturing. For the inverted PSCs, the device performance is strongly dependent on the optical and electric properties of cathode buffer layer (CBL) as well as the condition of the interface between the CBL and active layer. Engineering the CBL and the interface thereof has been considered as an essential issue for the next-stage development of PSCs towards high efficiency and good long-term stability. In this review, we focus on the rapid progress of the most widely used CBLs constructed with ZnO. The fabrication and characterization of CBLs with pristine ZnO, doped-ZnO, and ZnO-based composites and the surface modification of ZnO-based CBLs were described in detail, with the attempt to reach suggestions in regard of the strategies for fabricating inverted PSCs with high efficiency and long term device stability of inverted PSCs, so as to pave ways for their practical application.